

Adsorption of charged diblock copolymers

effect on colloidal stability



CENTRALE LANDBOUWCATALOGUS

0000 0576 3145

Promotor: dr. G. J. Fler
hoogleraar op persoonlijke gronden werkzaam in de
vakgroep Fysische en Kolloïdchemie

Co-promotor: dr. ir. F. A. M. Leermakers
universitair docent bij de
vakgroep Fysische en Kolloïdchemie

Rafel Israëls

Adsorption of charged diblock copolymers

effect on colloidal stability

Proefschrift
ter verkrijging van de graad van
doctor in de landbouw- en milieuwetenschappen
op gezag van de rector magnificus,
dr. C. M. Karssen,
in het openbaar te verdedigen
op woensdag 13 april 1994
des namiddags te half drie in de aula
van de Landbouwuniversiteit te Wageningen.

BIBLIOTHEEK
LANDBOUWUNIVERSITEIT
WAGENINGEN

CIP-DATA KONINKLIJKE BIBLIOTHEEK, DEN HAAG

Israëls, Rafel

Adsorption of charged diblock copolymers : effect on
colloidal stability / Rafel Israëls. - [S.E. : s.n.]

Thesis Wageningen. - With summary in Dutch.

ISBN 90-5485-231-3

Subject headings: polyelectrolyte adsorption / colloidal stability

-1-

Het regime voor geladen brushes dat gekenmerkt wordt door een afwezigheid van tegenionen in de brush, zoals beschreven door Pincus, bestaat niet.

P. Pincus 1991 *Macromolecules* 24, 2912.

-2-

In de limiet dat de zoutsterkte naar nul gaat gedraagt een brush met zwak zure groepen zich als een ongeladen brush.

-3-

Indien de lading op het boeiblok een belangrijke rol speelt in het stabiliseren van een kolloïdale suspensie door adsorptie van een ankerboei diblok-copolymeer, dan neemt het stabiliserend effect toe bij afnemende lading op het boeiblok.

-4-

In een forceprofiel op een log-lineaire schaal is het niet de afsnijding van de horizontale as, maar de helling van de curve, die gerelateerd is aan de dikte van de geadsorbeerde laag.

-5-

De overeenkomst die Van de Steeg et al. menen te vinden tussen voorspellingen van Muthukumar en berekeningen met het Scheutjens-Fleer model ten aanzien van de desorptie van polyelektrolieten, bestaat niet.

H. G. M. van de Steeg, M. A. Cohen Stuart, A. de Keizer, B. H. Bijsterbosch 1992 *Langmuir*, 8, 2538.

M. Muthukumar 1987 *J. Chem. Phys.*, 86, 7230.

-6-

De theorie voor de adsorptie van zwakke polyelektrolieten van Böhmer et al. is niet sterk.

M. R. Böhmer, O. A. Evers, J. M. H. M. Scheutjens 1990 *Macromolecules*, 23, 2288.

-7-

Het door Barneveld beschreven "lattice-artefact" wordt veroorzaakt door de gemiddeld veld benadering.

P. A. Barneveld 1991 Proefschrift Landbouwniversiteit Wageningen

-8-

Vrouwenemancipatie is een modeverschijnsel.

-9-

Als gevolg van het afnemende belang van de landbouw voor Nederland, en door het feit dat de grootte van een universiteit in toenemende mate belangrijk is, wordt het voortbestaan van de Landbouw Universiteit kritiek. In deze situatie zou zij zelf actief moeten zoeken naar verregaande samenwerkingsverbanden en is het zeer de vraag of het opeisen van een penvoerderschap van een onderzoekschool een strategisch juiste keuze is.

-10-

Het door veel vliegtuigmaatschappijen gehanteerde systeem dat "punten" verdiend kunnen worden door het maken van een zakenreis is een vorm van corruptie.

-11-

In een door de Nederlandse overheid gefinancierde milieuspot pleit Hans Böhm ten onrechte voor het verminderen van het aantal verschillende schoonmaakmiddelen in een huishouden. Het milieu is zeker niet gebaat bij een gebruik van specifieke middelen, omdat daarvan meer gebruikt moet worden voor eenzelfde effect.

Adsorption of charged diblock copolymers,
effect on colloidal stability.

Rafel Israëls

13 april 1994

Contents

1	Introduction	3
1.1	Subject	3
1.2	Models	6
1.2.1	Scheutjens-Fleer model	6
1.2.2	Monte Carlo method	7
1.2.3	Scaling	8
1.2.4	Evaluation of SF model	10
1.3	Systems	12
1.3.1	Adsorption of charged diblock copolymers	12
1.3.2	Homopolymer adsorption	12
1.3.3	Polyelectrolyte adsorption	13
1.3.4	Uncharged brush	14
1.3.5	Adsorption of uncharged diblock copolymer	14
1.3.6	Charged brush	15
1.4	Outline of the thesis	15
2	Charged brushes	17
2.1	Introduction	17
2.2	Analytical model	18
2.3	Self-consistent-field lattice model	25
2.4	Results	28
2.5	Conclusions	35
3	Grafted polyacid brushes	39
3.1	Introduction	39
3.2	Numerical model	40
3.3	Scaling-type approach	41
3.4	Results	44
3.5	Conclusions	49

4	Adsorption of charged diblock copolymers	51
4.1	Introduction	51
4.2	Self-consistent-field lattice model	53
4.3	Scaling model	56
4.4	Parameters	58
4.5	Results	59
4.6	Discussion	65
4.7	Conclusions	66
5	Stabilization by charged diblock copolymers	69
5.1	Introduction	69
5.2	SCF model	71
5.3	Scaling	74
5.4	Results	75
5.5	Conclusion	82
6	Summary	83
7	Samenvatting	87
A	Parabolic potential profile	91
B	Twostate model for monomers	93
C	curriculum vitae	95

Chapter 1

Introduction

1.1 Subject

This thesis deals with the adsorption of charged block copolymers and their effect on colloidal stability. We discuss the relevance of such an investigation for a number of technical applications below. First, however, we introduce the most important terms that we are going to use throughout the text: colloidal stability, adsorption, and diblock copolymers.

To begin with, a colloidal system can be introduced as any system containing structures, such as particles, droplets, bubbles, etc., that are much larger than simple molecules (i.e. $\gg 1\text{ nm}$) but, on the other hand, still very small ($\lesssim 1\mu\text{m}$). At least two different components are needed to form a colloidal system. One of the components forms a continuous phase, while the other one is dispersed in this continuum. Colloidal systems are ubiquitous in daily life. Examples can be found high in the sky, where we know clouds to be ice crystals in air, or down in the soil, where we may find mixtures of clay particles and water. In the human body, blood is a colloidal suspension of cells in plasma, and if we mix pigment particles in a solvent, the colloidal suspension we get is generally known as a paint.

If the particles, droplets, or bubbles at-

tracted one another, they would lump together, forming bigger and bigger particles, until two separate phases have been formed. Colloidal stability means that such a phase separation – in the case of solid particles called flocculation or coagulation – does not take place. Thus, all systems listed above exist by virtue of their colloidal stability: a lack of colloidal stability in blood would cause it to coagulate, in clouds it actually causes rain to fall down from the sky.

Colloidal systems necessarily contain a large amount of interface: the surface of the solid particles, for example. If a third species is present in a colloidal system, it turns out that very often this component accumulates at these interfaces. This preferential accumulation is called adsorption.

Adsorption is a common phenomenon in colloidal systems. We may understand why from the well-known physical principle "like prefers like", indicating that apolar molecules dissolve more readily in apolar than in polar solvents, and vice versa. From this principle, it follows that molecules with a polarity intermediate to that of the two components in a colloidal system will favor the interface between the two. Bipolar molecules such as surfactants may adsorb even more strongly to the interface, where they can arrange their polar head to be in con-

tact with one, and their apolar tail to mix with the other phase.

Now the third keyword can be introduced: polymers. Polymers are big molecules. They can be visualized as a string of beads, in which a single bead is called a monomer. We may distinguish homopolymers, in which all monomers are identical, and copolymers in which there are different types of monomers. Block copolymers are a specific class of copolymers. These molecules consist of several (usually two or three) different homopolymeric blocks. Within these blocks all monomers are identical.

Polymers are special in many ways. A well-known feature of polymeric material is that it can have special mechanical properties. Thus, polymers are commonly used in protective layers, both in nature and in synthetic products. Examples include keratine in skin, synthetic clothes, paint, coatings, etc. Alternatively, polymers may be used to impart structure, as myosin does in muscles, cellulose in plant cell walls, and carbon fibre in tennis rackets. The large choice in different polymers makes it possible to optimize chemical and physical properties, such as chemical inertness, heat capacity, and melting point, to specific applications.

A second feature of polymers is that often they adsorb at interfaces much more strongly than the disconnected free monomers. In order to understand why, we have to introduce an abstract thermodynamic quantity: translational entropy.

Translational entropy can be seen as "freedom to move". Free monomers can translate through a solution and thus have a relatively high amount of translational entropy. The segments in a polymer have lost much of their freedom: one might say that a polymer has little translational entropy per segment. This has important implications for many processes, be-

cause whether or not a process takes place depends on its energetic as well as its entropic effect. It is widely known that processes in which energy is liberated take place readily. Also the fact that entropy is gained in a process makes it more likely to happen. For processes in which the energetic and entropic driving forces are antagonistic (e.g., when energy is liberated and entropy lost), the relative magnitudes of the two effects determine whether or not the process takes place. Adsorption is one of these processes: it is driven by the liberation of adsorption energy, and more or less strongly hindered by an entropy loss. Because of their low translational freedom, polymers have little entropy to lose. Consequently, they do adsorb to interfaces more easily than small molecules.

Applications that rely on adsorption include the use of polymers in adhesives and paints. Specific groups can be included in the adsorbing polymer to modify the properties of a surface. Polymers are used in this way in biosensors, and in preventing immunoreactions against artificial implants. The major effect that most polymers have on colloidal stability is also related to adsorption. For example, a long polymer can adsorb simultaneously to two particles and drag the particles together and thus induce flocculation. For obvious reasons, this is called bridging flocculation. On the other hand, adsorbing polymer may also stabilize colloidal suspensions. We will return to this point below.

Another consequence of their low translational entropy is that polymers do not mix easily. Mixing two species increases translational entropy, while according to the "like prefers like" principle it is often energetically unfavorable. Polymers, compared to small molecules, do not have much entropy to gain, and generally dissolve only reluctantly in low-molecular-weight solvents; in this case, at least the solvent

gains a considerable amount of entropy. With other polymers they mix only if the energetic interactions are favorable, which is hardly ever the case.

The translational freedom of molecules is directly related to the osmotic pressure of a solution. That is why storage forms in living cells, such as starch (poly-glucose) and polyphosphate, are polymers. A large number of monomers can be stored in this way without creating too high an osmotic pressure in the cell.

As explained above, polymers have little entropy, compared to a collection of free monomers. However, they have much more entropy than a rigid rod of the same length: a polymer is flexible and has the conformational freedom to move the relative positions of its segments. A polymer in solution continuously changes its conformation, resulting in an average shape that is somewhat like a coil. Now suppose we squeeze such a coil between two surfaces. This would restrict the conformational freedom of the polymer, an unfavorable situation as we have seen above, and a repulsive force on the surfaces is expected. Although an adsorbed polymer generally has lost some of its coil shape, it still has a considerable amount of conformational entropy. Thus, thick adsorbed polymer layers may prevent flocculation, because of the potential loss of conformational entropy. The latter phenomenon is generally referred to as steric stabilisation.

The combination of more than one type of monomer in a copolymer makes it possible to combine functionalities within a single molecule. This is exploited optimally in biology, as in enzymes, which may contain several sites to which different substrates can bind as well as one or more other sites to which regulator molecules bind. Note that a single site generally consists of at least two or three chem-

ical groups. It is only the combination of these groups which makes an active site, and it is only the combination of these sites in one molecule that makes the enzyme useful to the cell.

An noteworthy application of the combination of functionalities is the function of copolymers in information storage and transfer. In DNA, for example, four different monomers combine in a specific sequence to archive the structures of all the proteins in a cell. Compared to a microchip, we would find DNA to be an extremely compact storage form.

Man-made applications of copolymers do not approach this level of sophistication. One of the most complicated synthetic molecules that can be made so far is a block copolymer, in which the features of two or more homopolymers may be combined. For example, the mixing of two incompatible polymers A and B may be enhanced by adding a diblock copolymer consisting of an A block and a B block. Such a molecule may stabilize the A-B interface and thus improve the mixing by assuming a conformation in which the A block extends in the A phase, and the B block in the B-phase. This application is very similar to the solubilization of oil in water by surfactant molecules.

A second application of diblock copolymers is in improving colloidal stability. As explained above, polymers may either induce flocculation due to bridging, or prevent it through steric stabilization. The problem with the use of (homo)polymers as stabilizers is that bridging can not be avoided rigorously. The so-called anchor-buoy diblock copolymers do not have this problem. In these molecules, a strongly adsorbing anchor block is connected to a non-adsorbing buoy block. Upon adsorption, the molecules assume a specific conformation: the anchor block is flatly adsorbed to the surface, while the buoy block extends in the solution and

forms a dense layer, sometimes called a "brush". These molecules, and their application as stabilizers, are the subject of this thesis. Why we are interested in these specific molecules may be illustrated by discussing a possible application.

In paints, for example, polymers are mainly used (i) to improve the colloidal stability of the pigment particles, (ii) to regulate the viscosity of the paint and (iii) to form a network in the paint when it has been applied. These properties affect, respectively, the shelf life of the paint, its ease of application and the strength/resistance of the ultimate coating. For environmental reasons, organic solvents in paints will probably have to be replaced by water in the near future. Hence, water-based paints containing charged copolymers are being developed. The charge is helpful in improving the solubility of these additives. That is why we are interested in an evaluation of the stabilizing effect of charged block copolymers in aqueous systems. We compare this with the effect of the corresponding uncharged block copolymers. A prediction of the effect of important parameters, such as molecular architecture and salt concentration, may help in the development of new water-based paint systems.

1.2 Models

One of our models is the Scheutjens-Fleer (SF) theory. An introductory overview of this theory, its background, elaboration, and application to a number of different systems can be found in a recent book by Fleer et al.²⁷ In this section we briefly present its basic concepts (Section 1.2.1), as well as those of two other approaches: "Scaling" (1.2.2) and "Monte Carlo" (1.2.3). This collection of models is by no means complete; scaling and Monte Carlo are simply two methods that are often applied to the problems that

also the SF theory can handle. In our opinion, the three models should be viewed upon as complementary: only a combination of results from the three approaches gives a reliable picture of polymeric systems.

In the last part of this section (1.2.4) we list the strong, as well as the weak points of the SF theory. A clear understanding of at least the shortcomings of any model is crucial to a meaningful interpretation of the results that were obtained with it.

1.2.1 Scheutjens-Fleer model

The SF theory is actually a combination of two distinct parts. A Self-Consistent mean-Field or SCF approach is used to handle the energetic interactions. The conformations of the polymers are calculated using a first-order Markov approximation.

The SCF approximation can be illustrated in terms of a well-known representative, the Gouy-Chapman model. The latter describes the distribution of salt ions in the vicinity of a charged surface. A rigorous description of such a system would require a specification of the exact location of every single ion, as well as its interaction with each of the other ions and with the surface. According to the mean-field approximation, all these interactions sum up to a potential of mean force $y(z)$ which, due to the symmetry of the problem, depends only on the distance z to the surface. The probability to find an ion at a certain location can easily be obtained from this potential. According to Boltzmann's law it is (for a cation with a unit charge) proportional to $\sim \exp[-y(z)]$. The crucial point in SCF models is that the potential field depends on the distribution of the species which, in turn, depends itself on the potential field. Thus, a self-consistent solution must be

found. In the case of the Gouy-Chapman model an analytical solution is available (if the volume of the ions is neglected). In most other cases, as in the SF model, it has to be found numerically.

The SCF part of the Scheutjens-Fleer theory differs only in a few respects from the Gouy-Chapman model. Firstly, in the SF model space is discretized in a finite number of lattice layers. The Gouy-Chapman model, on the other hand, is a continuous model in which the positions of species are not discretized. This is not a fundamental point, as can easily be seen: when we take the spacing between neighboring lattice layers infinitely small, the continuous model is recovered.

A more important difference is formed by the types of interactions incorporated in the potential field. The Gouy-Chapman approach considers only Coulombic forces, summing up to an electrostatic potential of mean force $y(z)$, denoted as $u^{\text{el}}(z)$. Two additional interactions are included in the SF theory. Excluded volume interactions, arising from the physical interaction of two hard spheres, are included in a hard-core potential denoted $u'(z)$. This potential is determined by the demand that each lattice layer is exactly filled. In this way the volume of the ions (and the polymer segments) can be accounted for. Short range interactions such as Van der Waals and dipole-dipole interactions are included in an interaction potential $u^{\text{int}}(z)$. The total potential ($u^{\text{el}}(z) + u'(z) + u^{\text{int}}(z)$) is determined self-consistently by the distribution of all species, in the same way as in the Gouy-Chapman model, where only the electrostatic contribution is taken into account.

If the SF model is applied to monomers, this is all there is to it. In most cases, however, we wish to apply it to systems containing chain molecules. To do so, we need the second part of the SF model: the chain propagation part. The

basic assumption used for calculating the conformations of polymers in the system is the first order Markov approximation. In this approximation the analogy between the conformation of a polymer and the trajectory followed by a diffusing particle is exploited. Basically it says that the set of all conformations of a chain of N segments with the first segment located at position z , may be approximated by the set of all walks of $N-1$ steps starting at this location z . In such a walk each step is made without any "memory" about previously visited positions. Consequently, the walk may occasionally turn back on one of its previous steps. Thus in a Markov approximation it is not rigorously prohibited that two segments of one chain occupy the same lattice site. Note, however, that excluded volume interaction *are* included in the SF model, although only in the mean field approximation.

1.2.2 Monte Carlo method

A problem in computer simulations on systems containing long polymers is the huge number of possible conformations that the chain molecules can assume. For example, on a cubic lattice a (Markov) polymer of 100 segments can have $6^{100} \approx 10^{78}$ different conformations. In SCF-models indeed *all* these conformations are taken into account, at the cost, however, that interactions have to be averaged into a mean-field potential. The obvious alternative is to sample only a limited number of different conformations. In this case there is no need for a mean field approximation and *all* individual interactions can be explicitly accounted for. This approach is adopted in a co-called Monte-Carlo simulation. The big issue in this approach, as may be expected, is to make sure that the set of sampled states is representative of the complete

set. To obtain this, (i) the set should be big enough, (ii) it should contain the more probable states, and (iii) the correct statistical weight for each set should be computed.

In the most straightforward Monte Carlo implementation, different ways to distribute molecules in the system are chosen completely at random and weighted with the proper Boltzmann factor according to the total energy of that state. This approach is very inefficient due to two related problems. Firstly, there is no bias towards the more probable states, so that the size of the sampled set must be very big in order to ensure that a large enough number of most-probable states is included. Secondly, since states are sampled randomly, also a (usually large) number of disallowed states will be chosen. These have to be discarded right away, since they do not contribute to the total sum of states. Although the sampling of forbidden conformations (leading to loss of efficiency) may be avoided, it should be done with great care: any special way to generate new states should not favor certain states over other ones.

Alternatively, in a method described by Metropolis et al.,⁴⁹ states are obtained sequentially from one another. A new state is obtained from a randomly chosen operation (called "move") on a previous state. Typical moves are flipping or rotating one bond or translating a molecule. This may be done quite efficiently, since only the difference in energy between two similar states need be calculated. On the other hand, a large number of these basic movements have to be performed before a new uncorrelated state is found: for example in Refs. 77 and 78, which describe the first Monte Carlo simulations on block copolymer adsorption, only one out of every 10^4 moves is included in the summation from which the average properties of the system are obtained.

Nevertheless, efficiency is gained in this way, not because of the simpler calculation, but from the fact that the sampling of less probable or even forbidden states is avoided. As mentioned above, this biasing of the sampling towards more probable states may easily lead to incorrect statistics. In the Metropolis scheme, which has been shown to lead to correct results, a move is always accepted when it leads to a decrease of the total energy. If the energy increases by an amount ΔU (in kT units), a random number α ($0 < \alpha < 1$) is generated and the new configuration is accepted only when $e^{-\Delta U} > \alpha$. Otherwise the old conformation is counted again.

In principle, with Monte Carlo only equilibrium properties of a system may be evaluated. The demands placed on the basic moves are related to the soundness of the statistical analysis. Specifically, the moves need not reflect the actual dynamics of the system and may be chosen such that the efficiency of the method is optimized. It is tempting, however, to try and choose indeed those moves that are expected to take place in reality. Possibly, dynamic properties of the system may then be obtained.

1.2.3 Scaling

The scaling approach is not a clear-cut model or theory, but more like a general route that can be recognized in a collection of studies. Some people prefer to restrict the title scaling only to those models that incorporate the blob concept pioneered by de Gennes,²² or those leading to a description in terms of power laws. Here we define scaling more loosely as any model in which physical insight, possibly combined with known experimental dependencies, leads to an analytical description of a system. Representatives that we will refer to in this thesis include

the description of uncharged brushes by Milner et al.⁵¹ or Zhulina et al.,⁸¹ the adsorption of uncharged block copolymers by Marques and Joanny,⁴⁷ charged brushes by Pincus⁵⁷ and by Borisov et al.,⁹ and the adsorption of charged block copolymers by Argillier and Tirrell² and by Wittmer and Joanny.⁷⁶ All these studies follow an approach that can be summarized as follows:

1. visualise a picture of the structure under investigation
2. distinguish the most important interactions
3. find expressions for each of them
4. distinguish different regimes based on the relative importance of these interactions and find expressions for measurable quantities in each of those regimes.

Although this seems a pretty straightforward approach, it should be noted that it is fundamentally different from either the SF or Monte Carlo model. We will illustrate this approach with an example: the adsorption of uncharged block copolymers from a non-selective solvent as studied by Marques and Joanny⁴⁷ (MJ).

(1) The adsorbing block is assumed to stick to the surface and to form a layer of A segments, the buoy block extends in the solution and forms a brush of B segments. Depending on the relative size of the two blocks N_A and N_B , the A layer can be expected to be either continuous or to have the structure of isolated pancakes. Depending on the density in the B layer, it is either a brush, or consists of isolated mushrooms. Different analyses are needed for each of these situations. We will repeat below the analysis for a dense and continuous brush

layer, combined with a low-density and discontinuous A layer. Note that the structure of the polymer layer is preassumed.

(2) The equilibrium adsorbed amount has been reached when the energetic and entropic effects of further adsorption exactly cancel. In thermodynamic language: the change in free energy of the adsorbed layer upon adsorption or desorption of one molecule should be equal in magnitude (but opposite in sign) to the change in free energy of the bulk solution.

$$\frac{\partial F_{\text{layer}}}{\partial \sigma} = - \frac{\partial F_{\text{bulk}}}{\partial \sigma} \quad (1)$$

where σ denotes the number of adsorbed molecules per unit of surface area. The most important contributions to the free energy of the adsorbed layer are the adsorption energy, the two-dimensional translational entropy of the adsorbed molecules, and the elastic energy stored in the brush. The free energy of the bulk solution contains contributions such as mixing energy and translational and conformational entropy.

(3) According to the physical picture, all A segments contact the surface and the adsorption free energy per surface area is given by $-kTN_A\chi_s\sigma$, where χ_s is the (positive) adsorption energy gain per A segment. For the elastic energy stored in the B brush several expressions are available. The one that correctly incorporates the excluded volume interactions in a good solvent is the one following from the blob picture: $kTN_B\sigma^{11/6}$. The translational entropy of an adsorbed chain is, according to standard thermodynamics, given by $k \ln \sigma$. Thus, we arrive at the following expression for the free energy of the adsorbed layer per unit area:

$$\frac{F_{\text{layer}}}{kT} = -N_A\chi_s\sigma + N_B\sigma^{11/6} + \sigma \ln \sigma \quad (2)$$

For a full expression of the free energy in the bulk we refer to the original article by MJ.

An important contribution is the translational entropy $k \ln \phi^b$ per molecule, where ϕ^b is the volume fraction of copolymer in the bulk solution.

(4) As mentioned before, the driving force for adsorption is the energetic interaction, which is counteracted by the loss of translational and conformational entropy. However, if the block lengths N_A and N_B are long, the translational entropy of adsorbed and free molecules can be neglected compared to the contributions of the adsorption energy and the conformational entropy (= elastic energy). Thus, we may write Eq. 1 as:

$$\frac{\partial (-N_A \chi_s \sigma + N_B \sigma^{11/6})}{\partial \sigma} = 0 \quad (3)$$

leading immediately to:

$$\sigma \sim \left(\frac{N_A \chi_s}{N_B} \right)^{6/5} \quad (4)$$

This expression can be combined with the well known scaling law for the brush thickness $H \sim N_B \sigma^{1/3}$ to give:

$$H \sim N_B^{3/5} (N_A \chi_s)^{2/5} \quad (5)$$

Several other regimes are described by MJ. For example, when $N_A \gg N_B$, the picture that all A segments are in contact with the surface is no longer valid and a different expression must be used for F_{layer} . The interested reader is referred to the original paper.

1.2.4 Evaluation of SF model

The value of a model depends on the amount of information it gives and the validity of its assumptions. Concerning the amount of information provided, the SF model is intermediate between scaling and Monte Carlo. From a Monte Carlo calculation the exact positions of all molecules may be obtained for a given state.

From a collection of such snapshots, averaged properties like segment density profiles, as well as the fluctuations thereof may be obtained. However, a physical explanation for these results is not easily obtained. For example, collecting thermodynamic quantities such as the free energy or a chemical potential is extremely difficult and the values obtained are usually not very accurate. In this respect, a scaling analysis is fully complementary: by definition a physical explanation is provided, but detailed information about distributions or conformations can not be obtained.

The kind of information provided by SF calculations is almost as detailed as that given by Monte Carlo: segment density profiles and the probabilities of individual conformations can be obtained. Moreover, also thermodynamic quantities can easily be calculated. However, the physical insight is not as immediate as from a scaling analysis. It has to be obtained from interpreting a large amount of numerical data.

We now discuss the assumptions and simplifications we use in our model. Firstly, we assume that a thermodynamic equilibrium has been reached. It should be noted that this shortcoming is shared with nearly all other models: the application of Monte Carlo to dynamics is questionable, and most scaling analyses are based on standard thermodynamics, which, by definition, is concerned only with equilibrium properties. However, non-equilibrium aspects play an important role in polymer adsorption,¹⁶ and probably even more so in block copolymer adsorption.^{44,66}

Secondly, in the calculations we assume that the polymers are homodisperse, and that the solution contains no impurities. Actually, this is not connected to the SF model. Indeed, the effect of impurities can easily be incorporated, and also polydispersity effects have been stud-

ied with the SF model.²⁷ However, in the calculations described in this thesis, as well as in most calculations published so far, such effects are neglected. It should be noted that even small amounts of impurities can have very big effects in colloidal systems, especially when these compounds are surface active. Also polydispersity effects are generally very important: even for a relatively homodisperse polymer they may lead to qualitatively different behaviour.

A third and most severe approximation, the mean-field one, is necessarily present in all SF calculations. The problem with this approximation is that it has numerous implications, each of which is difficult to explain rigorously. We will give a few examples below.

Fluctuations induced by excluded volume interactions are neglected in the mean field picture. This has an important consequence for the "correlation length" or "blob size" of a semidilute polymer solution. This length has been shown by Edwards¹⁷ to scale with the polymer concentration ϕ as $\xi \sim \phi^{-1/2}$ in a mean field, whereas experiments have proved that in good solvents it should scale as $\xi \sim \phi^{-3/4}$. The wrong mean-field scaling leads, for example, to an incorrect shape of the segment density profile of homopolymers adsorbed from a good solvent, as discussed recently by van der Linden and Leermakers.⁷¹

Also fluctuations resulting from electrostatic and/or contact interactions are neglected. If two components A and B attract one another, it may be expected that the number of $A-B$ contacts increases, leading to some clustering. In the mean-field approximation, this clustering is not taken into account. Several models exist to incorporate charge-induced fluctuations in a mean-field model.⁴ It turns out that qualitative effects can be observed only when divalent or trivalent ions are present in high concentra-

tions.³⁵ The effect of fluctuations induced by contact interactions can be studied using the quasi chemical approximation.³³ Preliminary results seem to indicate that again only in concentrated systems these fluctuations are important.

The first-order Markov approximation, which is connected with the mean-field approximation, implies that once the chains have been placed on the lattice, the connectivity information is lost: a segment does not "know" to which chain it belongs. This has important consequences for dilute systems, e.g., for the conformation of an isolated coil. The average dimension of a Markov chain scales as $R \sim N^{0.5}$, whereas if the segments within a chain do feel one another, a higher exponent $R \sim N^{0.6}$ is found. This breakdown of the mean-field approximation is also illustrated by its failure to describe correctly the system of dilute brushes, also called mushrooms, as discussed in Chapter 2. For charged molecules even stronger effects can be expected. Mutual repulsion among charged segments in a polyelectrolyte increases the chain stiffness considerably. At very low salt concentrations, isolated polyelectrolytes may even behave as rigid rods. In our current mean-field model, these intramolecular stiffening effects are neglected.

One might easily conclude from the above that our approach is useless: important aspects of polymer behaviour such as polydispersity effects and adsorption dynamics are not taken into account, and we use a mean-field approximation, which may cause severe errors. We would not agree with such a conclusion. If the results of SF calculations are interpreted with care, they may give valuable information on many aspects of polymer adsorption. Preferably, information obtained by SF calculations should be combined with results from other

models to arrive at a more complete picture.

1.3 Systems

1.3.1 Adsorption of charged diblock copolymers

The adsorption of charged block copolymers is the central issue in this work. The type of block copolymer we consider is an anchor-buoy diblock copolymer. The anchor block, consisting of N_A segments, is uncharged and adsorbs to the surface. The buoy block, on the other hand, consists of N_B segments that do not adsorb and carry a charge which is specified by an average segment valency α . The interaction of A and B block segments with the solvent (0) is specified by Flory-Huggins interaction parameters χ_{A0} and χ_{B0} , which are taken to be identical (non-selective solvent). We consider the adsorption of these molecules from a dilute solution to a flat, homogeneous, and uncharged surface.

Very little is known about such systems. To our knowledge, only three other theoretical papers, using the "scaling" approach, have been published.^{2,15,76} Below, we give a brief overview of available information on some related systems for which at least a partial similarity may be expected. Several of those systems may be considered as limiting cases of the adsorption of charged diblock copolymers. For example, if we take the buoy block length to be zero, the problem reduces to homopolymer adsorption (Section 1.3.2), for which a wealth of information is available. Choosing $\alpha = 0$ leads to the case of uncharged block copolymer adsorption (1.3.3). The resemblance to a third system, that of the terminally anchored chains or brushes, is obvious: it follows automatically when desorption is disregarded (1.3.4 and 1.3.5). Strictly speaking, the adsorption of charged homopoly-

mers can not be obtained as a limiting case of (charged) diblock copolymer adsorption. Nevertheless, it shares some of its characteristics and will be discussed as well (1.3.3). We will discuss each of these systems below and refer, where appropriate, to existing literature. All these systems are discussed in more detail in two reviews on polymer adsorption that have appeared recently.^{27,41}

1.3.2 Homopolymer adsorption

The affinity of polymers for interfaces results usually from Van der Waals forces. Also dipolar and hydrogen-bonding forces may play a role. The adsorbed amount may be expressed as a mass per unit of surface area. A typical value for homopolymers is of order of 1 mg/m^2 .

It has been mentioned before that polymers adsorb strongly due to their size. One of the consequences is that the adsorbed amount hardly depends on the polymer concentration in the bulk phase. This is illustrated in Figure 1, where we plot the adsorbed amount Γ as a function of this bulk concentration ϕ^b , for a polymer and for a small molecule. Such a curve is known as an adsorption isotherm. The initial part of the isotherm for the small molecule is called the Henry-region: Γ increases linearly with the concentration. For a polymer the adsorbed amount rises very steeply at low concentrations, and reaches a semi-plateau. For obvious reasons, this kind of curve is called a high-affinity isotherm. Strictly speaking, the difference is only a matter of scale. A Henry-type isotherm is also found for polymers, but only at extremely low concentrations.

The conformations of adsorbed homopolymers are often discussed in terms of loops, tails,

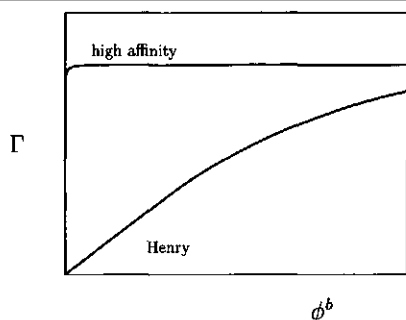


Figure 1 Schematic illustration of a high-affinity and a low-affinity adsorption isotherm

and trains. Trains are defined as sequences of segments in contact with the surface, loops have no contacts with the surface and connect two trains, and tails are non-adsorbed chain ends. For relatively short chains, most segments can be found in trains. Hence, the adsorbed layer is relatively thin in this case. For longer chains and in poor solvents, the number of segments in loops increases, while the number of train segments remains roughly constant. This leads to an increase of both the adsorbed amount and the thickness of the adsorbed layer.

Detailed information on the structure of the adsorbed layer has been obtained by scaling analyses,^{19,20} SF calculations,^{61,62} and MC simulations.^{23,43} For an evaluation of the results, and a comparison with experimental results, we refer to two reviews mentioned above.

1.3.3 Polyelectrolyte adsorption

The most important observation that we wish to make on the adsorption of charged homopolymers is that it is much more complicated than the adsorption of uncharged polymers. Since either the surface, or the polymer, or both may be charged, there are several additional parameters. Moreover, also the salt concentra-

tion is an important variable now. Despite its complexity, one general principle can be formulated for this system: charge compensation is an important factor in determining the adsorbed amount. Consequently, for polyelectrolytes adsorbing to an oppositely charged surface, the adsorbed amount increases with increasing surface charge. Moreover, also a decreasing polymer charge leads to higher adsorbed amounts. However, when this charge becomes too small, the driving force for adsorption disappears: the adsorbed amount decreases again and the salt ions take over in compensating the surface charge. Thus, a maximum in the adsorbed amount can be found as a function of polymer charge. Adsorption of polymers to equally charged or uncharged surfaces counteracts electroneutrality. Consequently, adsorbed amounts are low in this case; adsorption occurs only if there is a non-electrostatic contribution to the segmental adsorption energy. The salt concentration is very important in both cases: if it is increased, the adsorption at uncharged surface increases strongly, whereas the adsorption at oppositely charged surfaces decreases.

A number of important questions are still open. For example, experimentally determined adsorption isotherms appear to be of the low-affinity type, which is unexpected. Furthermore, extremely thick, as well as very thin layers have been measured; theoretical treatments almost always predict thin layers. Generally, non-equilibrium aspects seem to play an even more important role than they seem to do for the adsorption of uncharged polymers.

Overviews of experimental work on the adsorption of polyelectrolytes can be found in the two previously mentioned reviews and in a third one by Cohen Stuart.¹² Almost all theoretical studies employ the Self Consistent Field method, leading either to analytical^{56,58,69,74} or

numerical^{8,25,32,70,72} solutions. Some calculations based on the Monte Carlo method have been published,^{5,50} but we are not aware of any scaling analyses.

1.3.4 Uncharged brush

Chemical procedures exist to attach the end of a polymer to a surface. Such a "terminally-attached", or "grafted" molecule cannot desorb: the adsorbed amount is constant, determined by the way in which the system was synthesized. The question that needs to be answered in these systems is: how does the thickness and structure of the adsorbed layer depend on three parameters: grafting density, chain length, and solvent quality. Depending on the grafting density, two regimes may be distinguished. At low density the grafted molecules do not feel one another and each molecule forms an isolated "mushroom". The brush regime is found at higher coverages. This is one of the subjects on which agreement has been reached between different theories and experiments: the segment density profile of a brush has a parabolic shape, and the thickness H is given by:

$$H \sim N(v\sigma)^{1/3} \quad (6)$$

where N is the chain length, σ the anchoring density, and v the excluded volume parameter of brush segments.

Several scaling approaches, based on two different physical pictures, have been applied to the brush problem. Firstly, the blob model was used by Alexander and de Gennes.^{1,18,21} In this early model the volume fraction profile was assumed to be a step-function. Several years later, a strong-stretching model was employed independently by two different groups.^{51,81} Monte Carlo results are due to Cosgrove et al.¹³ who also compared them to SF calculations. The

first SF calculations on this system, however, are due to Hirz.³⁴ The theoretical approaches and results of SANS experiments on these systems have been reviewed recently by Halperin²⁹ and Milner.⁵²

1.3.5 Adsorption of uncharged diblock copolymer

Characteristics of both homopolymer adsorption and end-grafted polymers are combined in the adsorption of diblock copolymers. The anchoring block adsorbs in trains and loops, similar to a homopolymer, whereas the buoy block extends into the solutions, forming a brush.

The big difference with a brush of grafted molecules is that the adsorbed amount is now determined by the adsorption/desorption equilibrium and thus depends on both block lengths as well as the surface affinity of the anchor. At least two regimes may be distinguished. When $N_A \gg N_B$ the amount of free surface space is the determining factor and the adsorbed amount decreases with increasing anchor block length N_A ; when $N_A \ll N_B$ the affinity of the anchor is more important and the adsorbed amount increases with N_A . Consequently, the adsorbed amount passes a maximum with increasing N_A .

This system has been studied only very recently with the Monte Carlo technique.^{77,78} The calculations are limited to systems containing relatively short chains. Still, they confirm roughly the picture described above, which was obtained from a number of scaling studies,^{44,47,54,55} two independent SF calculations,^{24,73} and several experimental results.^{42,46,55,67}

1.3.6 Charged brush

Charged brushes have been described by several groups.^{9,10,50,53,57,60} The most extensive results are due to Pincus et al.^{57,60} and Borisov et al.^{9,10} Both groups, employing a scaling approach, agree that several regimes can be identified. At high salt concentration, low charge density, or extremely high grafting density, electrostatic interactions can be neglected and the brush behaves as a quasi-neutral brush. For the case that electrostatic interactions are important, at least two additional regimes have been described. In the absence of external salt the *Osmotic Brush* is found, of which the thickness is independent of the grafting density and scales as:

$$H \sim N\alpha^{1/2} \quad (7)$$

In the *Salted brush* regime electrostatic interactions are partly screened by the addition of salt and the scaling behaviour is very similar to that of an uncharged brush:

$$H \sim N(v_{\text{eff}}\sigma)^{1/3} \quad (8)$$

where the rescaled excluded volume parameter is given by:

$$v_{\text{eff}} = v + \alpha^2/\phi_s \quad (9)$$

The various scaling analyses begin to reveal a consistent and highly interesting picture of these charged brushes. Monte Carlo and SF results have not yet been described, though. A start with the investigation of these system is made in the present thesis: Chapters 2 and 3 are devoted to charged brushes.

1.4 Outline of the thesis

The principal aim of this thesis is an evaluation of the effect that the adsorption of charged

diblock copolymers has on colloidal stability. However, this specific issue is addressed explicitly only in Chapter 5. First, we study in Chapters 2 - 4 three related issues that will serve as building blocks for our final conclusion.

We start with investigating the related system of charged brushes. In Chapter 2 we present SCF calculations for a wide variety of different parameter choices in this system and compare the results to existing scaling theory. The scaling approaches for charged brushes are also based on the mean-field approximation and, as expected, our numerical results roughly confirm their predictions.

In Chapter 3 we study brushes of weak polyacids. We show that the acid-base equilibrium may be incorporated very straightforwardly into the model, analogous to the two-state approach as developed independently by Björling et al.⁷ and van Lent et al.⁶⁸ The results are very surprising indeed: the brush thickness is shown to pass a maximum as a function of salt concentration. This at first sight anomalous behaviour can be fully accounted for in terms of a simple scaling model.

The next two chapters are devoted to the adsorption of charged diblock copolymers. First we concentrate on the adsorbed amount and layer thickness in Chapter 4. The numerical results show the adsorption of charged copolymers to be fundamentally different from that of uncharged block copolymers. The adsorbed amounts are very low, and the maximum that was described for uncharged diblock copolymers is not found. Nevertheless, the system can be described with a few very simple scaling expressions, adapted from the scaling behavior of charged brushes.

The consequences of those results for the effect of diblock copolymers on colloidal stability are discussed in Chapter 5. We are indeed able

to formulate a simple law predicting which systems will be stable and which not.

Each of the four Chapters 2 - 5 may be read independently. Those who are interested in the

most important conclusions only, may proceed directly to the summary given in Chapter 6, or to the dutch "samenvatting" in Chapter 7.

Chapter 2

Charged brushes

2.1 Introduction

During the last decade, a considerable amount of effort has been spent on the theoretical analysis of polymer brushes, i.e., layers of polymer chains fixed by one end at impermeable surfaces of various geometries. Typical examples of such systems are the supermolecular structures that are formed in melts and solutions of block copolymers with incompatible blocks. Brush-like structures are also present in the adsorption layers formed by block copolymers with selectively adsorbing blocks. The practical relevance of these systems is that the brush forms a stabilizing coating on colloid particles, preventing aggregation.

The behaviour of neutral polymer brushes under various conditions is rather well understood. Not only the scaling dependences for the average brush characteristics, but also the fine details of the intrinsic brush structure predicted theoretically are in reasonable agreement with experimental observations (see e.g., the review by Halperin et al.²⁹).

Charged brushes, i.e., brushes formed by polymer chains containing ionizable groups, have been investigated to a lesser extent than neutral ones. This is due to the complexity of the system, which arises from the appear-

ance of long-range electrostatic interactions in a charged brush. Scaling analyses of a planar polyelectrolyte brush^{9,57,81} revealed a much more complex behaviour than that of neutral brushes.

Pincus was the first to show that, depending on the degree of charge of the chain and the grafting density, a polyelectrolyte brush can exhibit two different types of behaviour:⁵⁷ it can be either strongly charged, loosing its mobile counterions (*Pincus regime*), or conserve the counterions mainly inside the brush and, thus, be practically electroneutral (*Osmotic regime*). Borisov et al.¹⁰ argued that at high grafting densities the volume interactions between non-charged units dominate over electrostatic interactions, leading to the *quasi-neutral regime*.

If the salt concentration in solution exceeds by far the concentration of counterions in the brush, the so-called salt-dominance regime (*Salted Brush*) is found.^{9,57} The scaling dependences of the brush thickness in this regime are similar to those in the uncharged brush: the interactions in the brush can be described by an *effective* second virial coefficient incorporating both non-electrostatic and electrostatic interactions.

Some attempts have been carried out to analyze the intrinsic brush structure, the distribu-

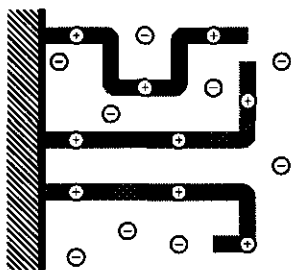


Figure 1 Schematic picture of a charged brush. The positively charged chains are grafted to a flat interface. Co- and counterions are free to move inside the brush or in the bulk phase.

tion of counterions and that of the electrostatic field. Based on the solution of the Poisson-Boltzmann equation for the electrostatic field in a brush, segment density profiles were calculated numerically.^{50,53} An asymptotical analytical solution for brush characteristics was obtained by Zhulina et al.⁸¹ under the simplifying assumption of local electroneutrality in the brush. It was shown that, contrary to the case of a neutral brush, where the shape of the segment density profile is sensitive to the solvent quality (parabolic under the conditions of athermal solvent, sharpening gradually with decreasing solvent quality¹¹), the distribution of segments in a polyelectrolyte brush is described by a Gaussian function over a wide range of solvent qualities. Only at solvencies that are worse than that of a θ -solvent ($\chi > 0.5$), the brush collapses abruptly.

In the present paper we present the analysis of polyelectrolyte brushes, using the self-consistent-field approach developed originally by Scheutjens and Fleer^{61,62} to describe the adsorption of uncharged homopolymers. It was extended to describe brushes by Cosgrove et

al.¹³ and to electrostatically charged systems by Evers et al.^{8,25} With this lattice model, it is possible to obtain a rigorous numerical solution (within the self-consistent mean-field approximation) for the equilibrium characteristics of a polyelectrolyte brush. Thus, a detailed comparison of (asymptotical) analytical predictions with a more exact numerical solution of the brush is possible over a wide range of conditions.

This chapter is organized as follows: In Section 2.2 we present the main results of the analytical theory for a polyelectrolyte brush. Section 2.3 outlines the numerical lattice model. Section 2.4 contains the results of comparisons between the two models, and in Section 2.5 we summarize the main conclusions.

2.2 Analytical model

Definitions We consider a planar layer formed by long flexible polyelectrolyte chains consisting of N units of size a (with $N \gg 1$). The chains are grafted at one end onto an impermeable surface with an average area per chain denoted by $a^2\sigma$ (Figure 1). Each polymer chain contains $Q = N/m$ ionizable groups, with am being the average distance along the chain between two neighboring charged units. We assume that all polymer chains are positively charged and that each ionizable group carries a charge $+e$. Only weakly charged chains are considered ($m \gg 1$), so that direct electrostatic repulsion along the chain does not lead to electrostatic stiffening.

The grafted layer is in equilibrium with a bulk solution, which contains only solvent (water), and sometimes salt. We take the salt to be symmetrical. Consequently, the concentrations of both (monovalent) ions in the bulk are equal and denoted by ϕ_s (expressed as a volume

fraction). In theory, one can distinguish chain-counterions and salt-counterions. In this paper we assume both types of counterion to be identical. Thus, in the grafted layer, we distinguish only the concentration of co-ions (ϕ_+) and the (total) concentration of counterions (ϕ_-).

Below we will introduce four different measures of brush thickness, which we summarize here for quick reference. The thickness H is defined as the upper boundary of the brush, i.e., the distance where the segment density profile drops to zero. A gaussian profile extends infinitely far: $H = \infty$. Therefore we define h_0 to be the characteristic length of the (Gaussian) profile for a salt-free brush. H_{rms} is defined as the second moment of a segment density profile. Finally, we will use the rescaled thickness $z = H/h_0$

Scaling-type relations In addition to long-range electrostatic interactions, conventional short-range interactions between non-charged units are also present in the system. The equilibrium structure of a brush is determined by the balance of all intermolecular interactions. Ignoring all numerical coefficients, a rough scaling-type picture of a polyelectrolyte brush has been constructed.¹⁰ In Figure 2 we summarize the main results of this treatment. The figure shows a "diagram of states" for a grafted polyelectrolyte brush in (m, σ) coordinates on a logarithmic scale. The brush is assumed to be immersed in a salt-free solution under the conditions of a marginal solvent.

Several different regimes are distinguishable in Figure 2. At high σ (loose grafting), individual coils can behave either as quasi-neutral Non-overlapping Chains (*NC*) at low charge densities (high m) or, if the charge density $1/m$ is high enough, as Isotropically distributed Sticks (*IS*). In this *IS* regime, chains are stretched

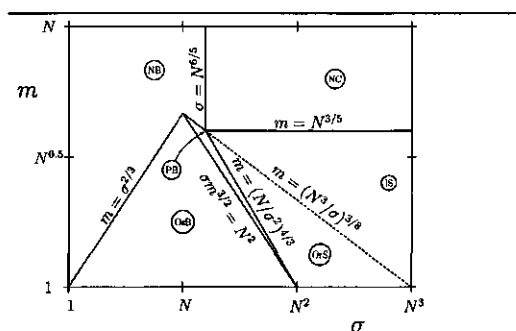


Figure 2 Diagram of states for a charged brush in the absence of external salt. At fixed chainlength N , six different regimes may be found, depending on the distance m between charges on the chain and the area σ per grafted molecule: *NB* (quasi-Neutral Brush), *NC* (Neutral Coils), *OsB* (Osmotic Brush), *PB* (Pincus Brush), *OrS* (Oriented Sticks), and *IS* (Isotropically distributed Sticks). The scaling behavior for the boundaries is given in the figure.

due to *intramolecular* electrostatic repulsion. *Intermolecular* orientational effects in charged coils appear with decreasing σ , leading to the Oriented Sticks regime (*OrS*).

Below the conventional threshold of laterally overlapping chains, three main regimes are possible. Weakly charged ($m \gg 1$) and densely grafted ($\sigma \lesssim N$) brushes exhibit *quasi-neutral* behaviour, where non-electrostatic interactions between units dominate over electrostatic interactions; we call this the quasi-Neutral Brush (*NB*). For more highly charged brushes ($m \ll N$), we find either the *Osmotic Brush* (*OsB*) or *Pincus Brush* (*PB*) regime. In the osmotic regime, the mobile counterions are located inside the layer and the brush is swollen by the osmotic pressure of the counterions. In the Pincus regime practically all counterions leave the brush and the chains are stretched by the unscreened electrostatic repulsion among units.

NB	$v^{1/3} N \sigma^{-1/3}$
NC	$v^{1/5} N^{3/5}$
OsB	$N m^{-1/2}$
PB	$N^3 \sigma^{-1} m^{-2}$
<i>OrS, IS</i>	$N m^{-2/3}$
G	$N^{1/2}$
SB	$N \sigma^{-1/3} m^{-2/3} \phi_s^{-1/3}$

Table 1 Scaling relations for the brush thickness H/a in various regions of the diagrams in Figures 2 and 3.

The scaling dependences of the brush thickness H in the various regimes, are collected in the first five rows of Table 1 (the last two rows will be discussed later). The parameter v in the table is the dimensionless second virial coefficient. The boundaries between any two regimes (indicated in the figure) are obtained by equating the expressions for the brush thickness in those two regimes, except for the *OrS/IS* boundary, which is obtained from the condition that the orientational energy of a polyion is of the order kT .¹⁰ In the expressions given in the figure, v was omitted.

Above we described the scaling behaviour of a brush (I) using the Gaussian expression for the stretching energy, (II) neglecting ternary and higher order interactions, and (III) using the mean-field approximation. In order to make a comparison with the numerical model, we have to simplify the picture slightly more, as we will do in Figure 3a. The limitations of the numerical approach used in the present paper, in par-

ticular the fact that it collects *inter-* as well as *intramolecular* interactions into one (averaged) mean field, cause it to break down at low densities. Here intermolecular interactions are negligible; as a consequence, also intramolecular interactions are neglected. The behaviour of a single Gaussian coil with $H \simeq \sqrt{N}$ is recovered. In Figure 3a a modified diagram of a salt-free brush is shown, where the three regimes at low density: (NC), (OrS), and (IS) are substituted by this *Gaussian* regime (G). This is the diagram that may be expected to agree with calculations from our numerical calculations. As is seen from Figure 3a, such a substitution makes the PB regime wider than in Figure 2. Correspondingly, the boundaries PB/G and NB/G are also shifted to higher values of σ .

So far we only considered brushes that are in contact with a salt-free solution. The effects of added salt have been described before.^{9,57} We will summarize the main points of this analysis. The addition of electrolyte increases the screening of electrostatic interactions, and as a consequence a new regime appears between the OsB and PB regimes. This *salted brush* (SB) regime and the evolution of its boundaries upon further increase of the salt concentration are shown in Figures 3b-c. Below we will first describe the interactions in the SB regime and then discuss the location of its boundaries.

We adopt here the simple picture of a salted brush suggested in Ref. 57. According to this picture, when the concentration of salt ions exceeds by far the concentration of brush counterions, the brush characteristics are similar to those of a neutral brush. As mentioned before, we describe non-electrostatic interunit interactions using a mean-field approximation and introduce $a^3 v = a^3(1/2 - \chi)$ as the second virial coefficient of pair interactions. As will be derived below (Eq. 23), screened electrostatic

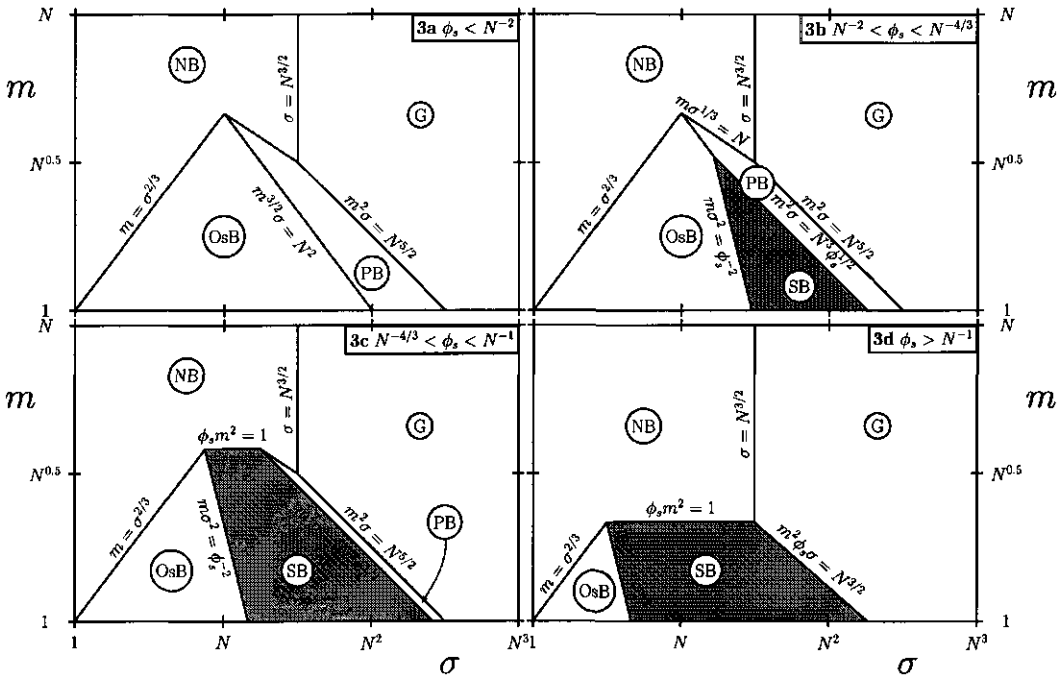


Figure 3 Diagram of states for a charged brush in a mean field model at fixed N for different salt concentrations $\phi_s < N^{-2}$ (3a), $N^{-2} < \phi_s < N^{-4/3}$ (3b), $N^{-4/3} < \phi_s < N^{-1}$ (3c), and $\phi_s > N^{-1}$ (3d). The SB regime (Salted Brush) is shaded, the expressions for the boundaries are indicated.

interactions in the (SB) regime can be described by an *electrostatic* second virial coefficient:^{9,57}

$$v_{el} \cong \frac{a^3}{4\phi_s m^2} \quad (1)$$

and scaling relations can be obtained by substituting v_{el} for v in the expressions for a neutral brush (see Table 1).

We now turn to the size and shape of the SB regime. Upon increasing the salt concentration, beginning at $\phi_s = 0$, the SB regime will first appear next to the PB regime. The threshold salt concentration ϕ_s^0 above which salt ef-

fects become noticeable, is given by the demand that the Debye screening length $\kappa^{-1} \simeq a\phi_s^{-1/2}$ is of the order of the brush thickness H . Since the maximal stretching of chains in the PB regime is attained at $m \simeq 1$, near the boundary with the OsB regime ($\sigma \simeq N^2$), one obtains $H/a \simeq N \simeq \phi_s^{-1/2}$ or $\phi_s^0 \simeq N^{-2}$. At $\phi_s < \phi_s^0$ the diagram of a brush coincides with that for a salt-free brush (Figure 3a). Increasing the salt content ($\phi_s > \phi_s^0$) results in the appearance of the SB regime as indicated in Figure 3b; the highest point of this regime, located at the intersection

of the lines $\sigma^2 m = \phi_s^{-2}$ and $\sigma m^{3/2} = N^2$, moves up along the latter line until the NB regime is reached at $\sigma = N$, $m = N^{2/3}$. At that point $\phi_s = N^{-4/3}$, which is the upper limit for Figure 3b.

If the salt concentration is further increased (Figure 3c), the horizontal boundary between the SB and NB regimes, at $m = \phi_s^{-1/2}$, moves down, thereby diminishing and narrowing the PB and OsB regimes. When m has decreased to the intersection of the lines $\sigma = N^{3/2}$ and $\sigma m^2 = N^{5/2}$, at $m^2 = N$ or $\phi_s = N^{-1}$, the PB regime has disappeared altogether. The effect of a further increase of ϕ_s (Figure 3d) is to enlarge the NB regime (to higher values of the charge density $1/m$), at the expense of the OsB and SB regimes.

Segment density profiles The remainder of this section is devoted to a detailed description of the brush in the three high density brush regimes: OsB, SB, and NB. First we derive a general description of the segment density profile, then we solve these equations neglecting excluded volume interactions, and in the final part we derive an implicit equation for the profile without neglecting excluded volume interactions.

In the OsB regime mobile counterions of charged chains are located mainly inside the brush. In the SB regime salt ions provide the screening of electrostatic repulsion between polycations. In both cases, the characteristic scale of smoothening of the counterion distribution in the brush and outer solution is given by the Debye-Hückel screening length:

$$\kappa^{-1} \simeq \begin{cases} am^{1/4}\sigma^{1/2} & (\text{OsB}) \\ a\phi_s^{-1/2} & (\text{SB}) \end{cases} \quad (2)$$

The expression for κ^{-1} in the OsB regime can be obtained from the conventional relation

$\kappa \sim \phi_s^{1/2}$, realizing that the screening of electrostatic interactions in this regime is carried out by the chain-counterions with a concentration $N/(m\sigma H) \simeq \sigma^{-1}m^{-1/2}$. In the SB regime (where $\phi_s \gg m^{-1/2}\sigma^{-1}$), the Debye length is determined by the external concentration ϕ_s .

If $\kappa^{-1} \ll H$, we can use the approximation of local electroneutrality. This results in a considerable simplification of the description of the system, because it permits us to reduce all electrostatic interactions (if we neglect free energy contributions due to correlation effects^{9,81}) to the translational entropy of (counter-)ions only. Following the scheme of Ref. 81, we first generalize the results of Ref. 9, and take non-electrostatic volume interactions between units as well as the own volume of salt ions into account. For simplicity we assume that the own volume of an ion coincides with that of a polymer unit, a^3 . Denoting by $\phi_p(x)$ the volume fraction of polymer segments at distance ax from the grafting surface and with $\phi_+(x)$ and $\phi_-(x)$ the corresponding profiles of co- and counterions, respectively, we write the condition of local electroneutrality in the brush as:

$$\frac{\phi_p(x)}{m} + \phi_+(x) = \phi_-(x) \quad (3)$$

We keep in mind that all concentrations are a function of the position in the brush and omit x from the equations. Note that both ϕ_+ and ϕ_- converge to the bulk solution concentration ϕ_s outside the brush ($x \rightarrow \infty$). Assuming that contact interactions are identical for solvent and ions, we can write the local free energy density in a brush as:

$$\begin{aligned} \frac{f[\phi_+, \phi_p]}{kT} &= \phi_+ \ln[\phi_+] + \phi_- \ln[\phi_-] \\ &+ \phi_0 \ln \phi_0 + \chi \phi_p (1 - \phi_p) \end{aligned} \quad (4)$$

where ϕ_- can be expressed in ϕ_+ and ϕ_p through

Eq. 3. The volume fraction of solvent, ϕ_0 , follows from:

$$\sum_i \phi_i = \phi_p + \phi_+ + \phi_- + \phi_0 = 1 \quad (5)$$

The first two terms in Eq. 4 take into account the translational entropy of salt co- and counter-ions, respectively, the third term represents the translational entropy of solvent molecules (i.e. excluded volume effects), and the last term accounts for the solvent quality (χ is the familiar Flory Huggins parameter²⁸). In the bulk solution, where $\phi_p = 0$ and $\phi_+ = \phi_- = \phi_s$, the free energy is given by:

$$\frac{f^b[\phi_s]}{kT} = 2\phi_s \ln \phi_s + (1 - 2\phi_s) \ln(1 - 2\phi_s) \quad (6)$$

Following the scheme of Ref. 81 the conditions for equilibrium in a brush are given by:

$$\frac{\delta f[\phi_+, \phi_p]}{\delta \phi_+} = \mu_s = \frac{\partial f^b[\phi_s]}{\partial \phi_s} \quad (7)$$

$$\frac{\delta f[\phi_+, \phi_p]}{\delta \phi_p} = \Lambda - \frac{3\pi^2}{8N^2} x^2 \quad (8)$$

where μ_s is the chemical potential of salt and Λ is an undetermined constant providing normalization of the profile of polymer units. Eq. 7 reflects the constancy of the salt chemical potential in- and outside the brush, while Eq. 8 is analogous to that for a one-component brush.¹¹ The derivation of Eq. 8 was obtained along the lines of Ref. 82 from a first approach by Semenov.⁶⁴ It is briefly outlined in Appendix A. The two approximations used are, that the elastic free energy of stretching is given by a Gaussian expression, and that the full set of conformations is reduced: all conformations having their endsegments at the same distance x' from

the surface are represented by only one conformation. After some algebra one obtains:

$$\frac{(\phi_+ + \phi_p/m)(\phi_+)}{[1 - 2\phi_+ - \phi_p(1 + 1/m)]^2} = \frac{(\phi_s)^2}{[1 - 2\phi_s]^2} \quad (9)$$

$$\frac{(\phi_+ + \phi_p/m)}{[1 - 2\phi_+ - \phi_p(1 + 1/m)]^{1+m}} = \frac{\phi_s \exp[(H^2 - x^2)/h_0^2 + 2\chi\phi_p m]}{[1 - 2\phi_s]^{1+m}} \quad (10)$$

where H is the upper boundary of the brush, determined by the normalization condition:

$$\sigma \int_0^H \phi_p(x) dx = N \quad (11)$$

and $h_0 a$ is the decay length of the (Gaussian) segment density profile of the corresponding salt-free brush, given by:

$$h_0^2 = \frac{8}{3\pi^2} \frac{N^2}{m} \quad (12)$$

Simultaneous solution of eqs. 9, 10 and 11 provides the equilibrium parameters of a polyelectrolyte brush: its height, H , the profile $\phi_p(x)$ of polymer units, and the distributions of salt co-ions $\phi_+(x)$, and counterions $\phi_-(x) = \phi_+(x) + \phi_p(x)/m$.

Profiles – no excluded volume If non-electrostatic excluded volume effects are totally neglected, these equations transform into the corresponding equations of ref. 81:

$$\phi_+(x) = \phi_s \exp[-(H^2 - x^2)/h_0^2] \quad (13)$$

$$\phi_p(x) = m(\phi_s^2/\phi_+(x) - \phi_+(x)) \quad (14)$$

The upper boundary of the layer, H , is determined by the normalization condition (14):

$$\gamma = e^{z^2} \int_0^z e^{-t^2} dt - e^{-z^2} \int_0^z e^{t^2} dt \quad (15)$$

with:

$$z = H/h_0 \quad (16)$$

$$\gamma = \frac{Na^3}{m\sigma h_0 \phi_s} \quad (17)$$

Here we introduce two dimensionless parameters that will prove to be convenient: a rescaled layer thickness $z = H/h_0$ and γ , which is the ratio between the concentration of counterions in the corresponding salt-free brush $N/(m\sigma h_0)$, and the counterion concentration ϕ_s in the actual bulk solution. In a salt-free brush γ is large, decreasing as ϕ_s becomes higher. For a salted brush γ is smaller than unity. The analysis of Eq. (15) shows that, depending on the value of γ , several regimes can be distinguished, which will be discussed shortly. Starting at low salt concentrations, where the second term in Eq. 15 may be neglected, it can be easily seen that, when ϕ_s goes to zero, $z = H/h_0$ must go to infinity as

$$z \approx \sqrt{\ln\left(\frac{2}{\sqrt{\pi}}\gamma\right)} \quad (18)$$

In the limit of a salt-free case, $\phi_s = 0$ (*Osmotic Brush*), the distribution of polymer units in a brush is given by⁸¹

$$\phi_p(x) = \frac{2}{\sqrt{\pi}} \frac{N}{\sigma h_0} e^{-x^2/h_0^2} \quad (19)$$

Introducing the weight-averaged brush thickness, defined as:

$$H_{\text{rms}}^2 = \frac{\int_0^H \phi_p(x) x^2 dx}{\int_0^H \phi_p(x) dx} \quad (20)$$

as a convenient measure of brush thickness, we find that it is given by:

$$H_{\text{rms}}^2 = \frac{1}{2} h_0^2 \quad (21)$$

Now let us consider the case of a considerable amount of salt in solution, leading to $z \ll 1$ (*Salted Brush*). The expansion of the integrals in Eq. 15 with respect to small parameters z transforms it into

$$\gamma \approx \frac{4}{3} z^3 \quad (22)$$

Substitution of h_0 from Eq. 12 into the definition of γ (Eq. 17) then gives:

$$H \approx N \left(\frac{8v_{\text{el}}}{\pi^2 \sigma} \right)^{1/3} \quad (23)$$

where v_{el} , given by Eq. 1, is the electrostatic excluded volume parameter. Other characteristics are given by:

$$\phi_p(x) \approx \frac{3}{2} \frac{N}{\sigma H} (1 - x^2/H^2) \quad (24)$$

$$H_{\text{rms}}^2 \approx \frac{1}{5} H^2 \quad (25)$$

$$\begin{aligned} \phi_+(x) &\approx \phi_s [1 - (H^2 - x^2)/h_0^2] \\ &\approx \phi_s \end{aligned} \quad (26)$$

Thus, in a salt dominance regime ($\gamma \ll 1$) the electrostatic interactions in a brush can be described by an electrostatic excluded volume parameter v_{el} and the brush characteristics are similar to those of a neutral brush, with v_{el} substituted for v .

Profile – excluded volume In the previous paragraph all non-electrostatic excluded volume effects in the system were ignored. As was already mentioned above, expression 4 takes into account the volume of all ions and polymer units through the mixing entropy. However, in many practical cases, the volume of the ions can be neglected with respect to the volume of the polymer units. Neglecting the contribution of the ions in expression 5 and using once again the conditions of equilibrium 7 and 8, one obtains:

$$\begin{aligned} \phi_+(x) &= \phi_s \exp\{-(H^2 - x^2)/h_0^2\} \\ &+ m[\ln(1 - \phi_p) + 2\chi\phi_p] \end{aligned} \quad (27)$$

$$\begin{aligned} \frac{\phi_p(x)}{m\phi_s} &= \exp\{(H^2 - x^2)/h_0^2 + \\ &m[\ln(1 - \phi_p) + 2\chi\phi_p]\} \\ &- \exp\{-(H^2 - x^2)/h_0^2 - \\ &m[\ln(1 - \phi_p) + 2\chi\phi_p]\} \end{aligned} \quad (28)$$

Under the conditions of salt dominance ($z \ll 1$) and for not too dense layers ($\phi_p \ll 1$), a virial expansion of the mixing entropy in z and ϕ_p is justified and an approximate solution of Eq. 28 is available. We arrive at the same expressions that were derived for the Osmotic Brush (Eq. 23 and 24) although now we have to substitute an *effective* excluded volume parameter v_{eff} for v_{el} , given by

$$v_{\text{eff}} = v + v_{\text{el}} \quad (29)$$

Hence, v_{eff} consists of the excluded volume part $v = 1/2 - \chi$ for uncharged units, and an electrostatic part v_{el} , given by Eq. 1. At considerable salt contents $v_{\text{el}} \ll v$ and the non-electrostatic interactions between units dominate over electrostatic ones: the polyelectrolyte brush passes into the quasineutral regime. The structure of a neutral brush is well known:^{51,65,75} in a good solvent, the segment density profile and the brush thickness are given by relation 24 and 25, where H is obtained from Eq. 23 with v_{eff} substituted for v_{el} .

For relatively dense brushes, when the virial expansion of the mixing entropy breaks down and the own volume of salt ions can be essential, the equation for the profile $\phi_p(x)$ can be obtained implicitly only. Solving Eq. 9 for ϕ_+ and substituting the result into 10, one obtains for the good solvent case ($\chi = 0$):

$$\exp\left(\frac{H^2 - x^2}{h_0^2}\right) = \frac{(1 - 2b)^m}{2b[1 - \phi_p - c]^{m+1}} \times [\phi_p(1 - 4b^2)/m - 4b^2(1 - \phi_p) + c] \quad (30)$$

where:

$$b = \phi_s/(1 - 2\phi_s) \\ c^2 = \frac{\phi_p}{m^2}(1 - 4b^2) + 4b^2(1 - \phi_p)^2$$

The right-hand part of Eq. 30 can be viewed on as a rescaled volume fraction $\mathcal{F}(x)$. It follows

from the left-hand side that, if we plot $\mathcal{F}(x)$ on a logarithmic scale as a function of x^2/h_0^2 , we may expect to find a straight line with slope -1 and intercept H^2/h_0^2 . We shall use Eq. 30 later for a detailed comparison of the analytical predictions with results of the numerical SCF theory.

Note that in the limit of a non-charged brush ($m \rightarrow \infty$) Eq. 30 reduces to

$$\phi_p(x) = 1 - e^{-K^2(H^2 - x^2)} \quad (31)$$

where $K^2 = 3\pi^2/(8N^2)$ and H is obtained from Eq. 11, which has to be solved numerically. Expression 31 has been derived before⁶⁵ and is slightly more precise than the more well known parabola given by Eq. 24. It reduces to the parabola at low densities.

2.3 Self-consistent-field lattice model

General The self-consistent-field (SCF) lattice model initially developed by Scheutjens and Fleer for the adsorption of homopolymers^{61,62} serves as the starting point of our numerical analysis. The model contains a number of simplifying assumptions. Firstly, the mean-field approximation implies the replacement of the local potential $u(x, y, z, t)$ of a segment at position (x, y, z) and time t by a time-independent potential $u(x)$ for a segment at a distance x from the surface. Hence, a pre-averaging over the variables y, z , and t is carried out. Secondly, for the generation of conformations a first order Markov approximation is used: the position of any segment is restricted by the position of its immediate neighbors along the chain only (i.e., backfolding is allowed). The electrostatic interactions are handled using the multilayer Stern-model,⁸ which is a straightforward modification

of the Poisson-Boltzmann equation to the case of a lattice containing an arbitrary mixture of molecules, taking into account the own volume of polymer, solvent and salt molecules. The introduction of a lattice, finally, is convenient to define and count conformations.

A major drawback of the model is the fact that the resulting equations can only be solved numerically; exact analytical expressions can not be obtained. Despite these shortcomings, there are two very important reasons to use the model. Firstly, many characteristics of the system, including profiles of all molecules and all thermodynamic properties of the system may be obtained. Secondly, these properties are calculated without any presupposition as to the conformations of the polymers.

Potential field We divide the half-space next to a surface in parallel layers, numbered $x = 1, \dots, M$ where M is sufficiently large. The potential experienced by a segment depends on its position x only. In the absence of chemical interactions ($\chi = 0$), the potential energy of a segment of type A in layer x is given by^{8,25}

$$u_A(x) = u'(x) + eq_A\psi(x) \quad (32)$$

where $u'(x)$ is a Lagrange multiplier for layer x , introduced to meet the constraint that the lattice is completely filled:

$$\sum_A \phi_A(x) = 1 \quad [x = 1, \dots, M] \quad (33)$$

This summation runs over all segment types in the system: the brush segments (p), co-ions (+), counterions (−), and solvent molecules (0).

The last term of Eq. 32 represents the electrostatic contribution to the potential energy of a segment. In this term, e is the elementary charge, q_A the valence of a segment A (zero for the solvent, +1 for the cations, −1 for the anions, and $1/m$ for the polymer segments). A

variation of m could, in principle, be carried out by inserting uncharged segments between the fully charged segments. This would preclude, however, a continuous variation of m . Therefore we choose to give every segment a charge qe , where $0 \lesssim q \lesssim 1$. Note that, as a consequence, the brush molecules are homopolymers. The electrostatic potential $\psi(x)$ in each layer x is obtained from the set of equations:

$$\frac{\partial^2 \psi(x)}{\partial x^2} = \frac{\rho(x)}{\epsilon(x)} d^2 \quad [x = 1, \dots, M] \quad (34)$$

In this equation the lattice spacing d is needed to keep x dimensionless. In our lattice calculations we use a discrete analogue of Eq. 34, taking into account the changes in dielectric permittivity between different layers.⁸ The space charge density $\rho(x)$ in layer x and the dielectric permittivity $\epsilon(x)$ of layer x are obtained from the following mean field expressions, in which ϵ_A is the dielectric permittivity of pure A and $V_{cell} = d^3$ (cubic lattice) is the volume of one lattice cell:

$$\rho(x) = \frac{\sum_A q_A \epsilon_A \phi_A(x)}{V_{cell}} \quad (35)$$

$$\epsilon(x) = \sum_A \epsilon_A \phi(x) \quad (36)$$

The electroneutrality of the system is ensured by setting the field strength at the boundaries zero:

$$\left. \frac{\partial \psi}{\partial x} \right|_{x=0} = \left. \frac{\partial \psi}{\partial x} \right|_{x=M} = 0 \quad (37)$$

Again, in the lattice model a discrete version of these expressions is used.⁸

Segment density profile In order to calculate the volume fraction profile, we introduce a function $G_A(x, s|x', s')$, which is the combined statistical weight of all conformations of chain parts of molecules of type A starting with segment s' in layer x' and ending with segment s in layer x . Summation of $G_A(x, s|x', 1)$ over all x' leads to the end-point distribution function $G_A(x, s|1)$ of a sequence $1, 2, \dots, s$. It is convenient to define a weighting factor for species A as

$$G_A(x) = e^{-u_A(x)/kT} \quad (38)$$

Now we have for grafted chains, which have their first segment restricted to the first layer:

$$G_p(x, 1|1) = \begin{cases} G_p(x) & [x = 1] \\ 0 & [x > 1] \end{cases} \quad (39)$$

and similarly :

$$G_p(x, N|N) = G_p(x) \quad \text{for any } x \quad (40)$$

where N is the number of segments of the molecule. The solvent and salt molecules are assumed to consist of only one segment ($N_0 = N_- = N_+ = 1$). Thus we have, e.g. for the co-ions: $G_+(x, 1|1) = G_+(x, N|N) = G_+(x)$ for all values of x .

The first-order Markov approximation allows us to obtain a simple recurrence relation to compute the distribution function $G_p(x, s+1|1)$ from its predecessor $G_p(x, s|1)$ by taking into account all possible steps from segment s to $s+1$, regardless of the positions of all segments 1 to $s-1$:

$$G_p(x, s+1|1) = G_p(x) \langle G_p(x, s|1) \rangle \quad (41)$$

where $\langle G_p(x, s|1) \rangle$ is a shorthand notation for $G_p(x, s|1)$ averaged over the neighbors (in layers $x-1$, x , and $x+1$) of a lattice site in layer x . Applying expression 41 recursively $N-1$ times to the starting relation 39 and also $N-1$

times to expression 40, two sets of N distribution functions are generated. From these sets many characteristics of the adsorbed layer can be calculated. For the brush molecule, the volume fraction profile is given by:

$$\phi_p(x) = C_p \sum_{s=1}^{N_p} \frac{G_p(x, s|1) G_p(x, s|N)}{G_p(x)} \quad (42)$$

where $C_p = \theta_p / N_p G_p(N_p|1)$ is the proper normalization factor to fix the total amount θ_p of polymer on the surface, where θ_p is defined as $\theta_p = \sum_x \phi_p(x)$ and

$$G_p(N|1) = \sum_{x=1}^{x=M} G_p(x, N|1) \quad (43)$$

The area σ per chain, used in the analytical model (section 2.2), is obtained as $\sigma = N/\theta$.

The volume fraction profile for the salt and solvent molecules, which are in full equilibrium with those far away from the surface (the bulk solution), is simply given by:

$$\phi_A(x) = \phi_A^b G_A(x) \quad (44)$$

where $A = +$ (coion), $-$ (counterion), or 0 (solvent).

Numerical solution We now have for any monomer type A in every layer x two unknowns $\phi(x)$ and $G(x) = e^{-u(x)/kT}$ and two corresponding equations: 32 and 42 or 44. Additionally we have for every layer two unknowns $\psi(x)$ and $u'(x)$ with corresponding Eqs. 33 and 34. This set of equations can be solved numerically.

2.4 Results

Parameters In this section we present numerical results from the lattice model (section III) and discuss them in terms of the analytical model (section II). We vary the chain length N , the area per chain σ (= the inverse anchoring density), the average distance m between two charges on the brush molecules (= the inverse charge density), and the salt concentration ϕ_s , and examine the effect on the brush (root-mean-square) thickness H_{rms} as well as the segment density profiles. Variation of m is carried out by giving every segment a charge qe , where $0 \lesssim q \lesssim 1$. A chain, for which $q = 0.1$ is equivalent to a chain with $m = 10$. We use a cubic lattice with a lattice constant $d = 0.6$ nm. The relative permittivity of the solvent (water) is chosen $\epsilon_r = 80$, the permittivity of the other substances (surface, polymer and salt molecules) is taken as $\epsilon_r = 5$. The solvent is taken to be a good solvent for the polymer ($\chi = 0$).

Scaling picture Figure 4a shows the diagram of states for a charged brush with $N = 500$, in a low concentration of salt ($\phi_s = 10^{-4}$). This salt concentration corresponds to $N^{-1.48}$, which is in between the limits $N^{-4/3}$ and N^{-2} , and so Figure 3b applies. To compare Figure 4a with the results of the lattice model, we calculated the dependence of the brush thickness H_{rms} on each of the parameters σ , m , and N throughout the parameter space, denoting the exponents with α_σ , α_m , and α_N respectively ($H \sim \sigma^{\alpha_\sigma} m^{\alpha_m} N^{\alpha_N}$). For example, assuming a power law dependence of H on σ , the exponent α_σ of this power law is found from:

$$\alpha_\sigma = \frac{\partial \log H}{\partial \log \sigma} \quad (45)$$

Obviously, we use a discrete version of this equation, $\frac{\Delta \sigma}{\sigma}$ being of the order of 10%. In this

way exponents are calculated for the power law dependence of the thickness on the area σ per chain (Figure 4b), the charge separation m (4c), and the chain length N (4d). The exponents are displayed using contour plots, where the isolines connect points of equal values. These values may be compared with the analytical predictions for the various regimes (Table I), which are indicated in the rectangular boxes in the four diagrams of Figure 4.

Inspection of Figure 4b reveals the four major regimes in Figure 4a: $\alpha_\sigma = 0$ for G and OsB, $\alpha_\sigma = -1/3$ for SB and NB. At extremely low σ and high m (upper left corner in Figure 4b) an even lower exponent $\alpha_\sigma < -0.40$ is found. This is due to the onset of ternary and higher interactions, which were neglected in the derivation of the $-1/3$ power law.

The slope of the contour lines should follow roughly the slope of the corresponding boundaries between the two neighbouring regimes. This seems to be the case for the NB/G, OsB/SB and SB/G boundary, but a deviation can be seen for the NB/OsB boundary at low σ . Probably this is due to the onset of higher order interactions as well.

In Figure 4c the correct power law exponent $\alpha_m = 0$ for the NB and G regimes can be recognized, and an exponent close to $\alpha_m = -2/3$ for the SB regime is found. For the OsB regime the numerical model seems to give a somewhat too low exponent, around $\alpha_m \approx 0.40$.

For the dependence of σ on N (shown in Figure 4d) we find the correct exponent $\alpha_N = 0.5$ in the Gaussian and $\alpha_N = 1.0$ in the Osmotic and Neutral Brush regimes, but an exponent slightly above unity (≈ 1.1) at the transition between the SB and G regimes. This small deviation may be reminiscent of the Pincus regime (where α_N should be 3).

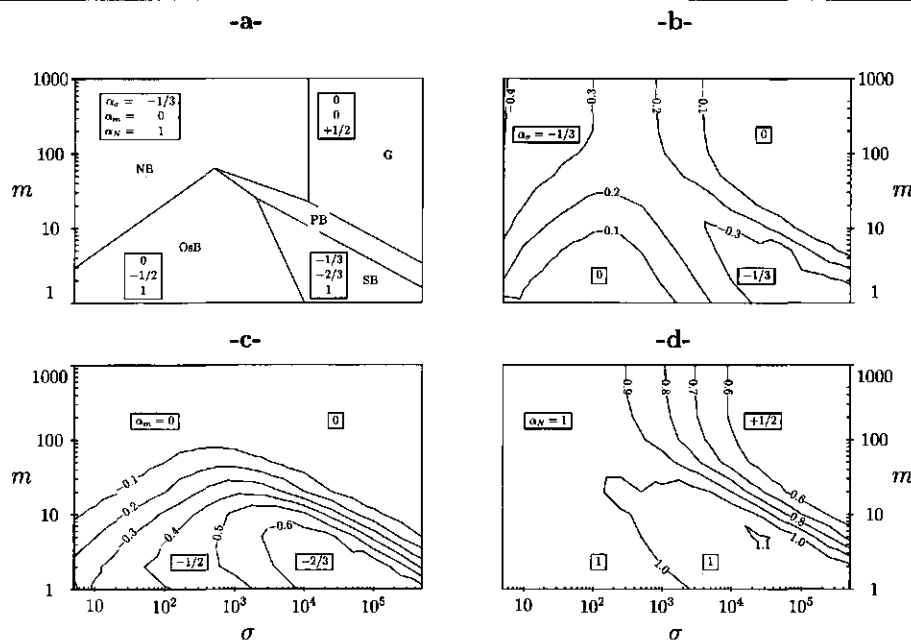


Figure 4 Diagram of states for a polymer with chain length $N = 500$ at a salt concentration $\phi_s = 10^{-4}$ (a), and two dimensional contour plots calculated using the SCF model giving the value of the exponent α_σ for the power law dependence of H on σ (b), the exponent α_m (c), and α_N (d). Values of the isolines are indicated, as well as the analytical predictions for the exponents in each of the regimes (in the rectangular boxes).

In the results of Figure 4 as discussed above, we find good agreement between the numerical and analytical predictions on the power law behaviour in OsB, NB, SB, and G regimes. The one regime that is not easily recognized in these diagrams is the Pincus regime (PB). This is not quite unexpected, since for our choice of chain length $N = 500$ the transitions between the various regimes are relatively broad, and at the salt concentration $\phi_s = 10^{-4}$ the PB regime is very narrow. To make this transition sharper, the chain length should be increased, and to make

the PB regime wider, a lower salt concentration is needed. However, due to convergence problems, there is a lower limit on salt concentrations that can be reached. For our present software this limit is located around $\phi_s \approx 10^{-5}$.

To illustrate the difficulties encountered when trying find the PB regime, we present in Figure 5 results of calculations that were aimed specifically at investigating this peculiar regime. We consider a system at $m = 1$, where the PB regime is widest, and plot α_σ as a function of σ . The salt concentration was adjusted to the

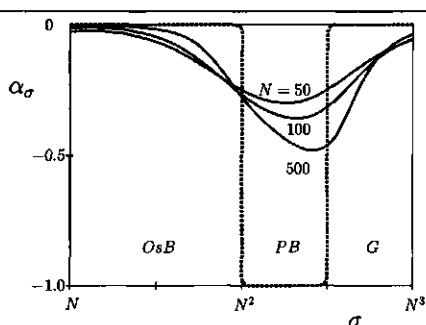


Figure 5 The exponent α_σ for the dependence of the brush thickness on the area σ per chain (i.e., $H_{rms} \sim \sigma^{\alpha_\sigma}$), as a function of σ for three different chain lengths (indicated) at salt concentrations $\phi_s = N^{-2}$. The calculations with the SCF theory are represented by the continuous curves, the prediction of the analytical theory is shown as the dashed curve.

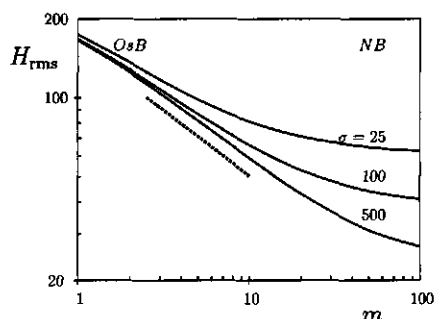


Figure 6 The brush thickness H_{rms} as a function of the inverse charge density m , for three different values of the area σ per chain. Parameters: $N = 500$, $\phi_s = 10^{-5}$. The slope $-1/2$ on the double-logarithmic plot, as expected in the OsB regime, is indicated by the dashed line.

chain length according to $\phi_s = N^{-2}$, so that Figure 3a should apply. Thus we may expect the SB regime to be absent and any deviation from $\alpha_\sigma = 0$, which is valid in the neighbouring OsB and G regimes, must be due to the onset of the PB regime, where a value $\alpha_\sigma = -1.0$ is

expected. This analytical prediction for α_σ is indicated by the dashed curve in Figure 5. The three continuous curves correspond to numerical calculations for three different chain lengths (length indicated).

The minimum in α_σ decreases with N , and is already for $N = 500$ clearly lower than the value $\alpha_\sigma = -1/3$, which is the lowest value in any of the other theoretical regimes. In other words, a regime with $\alpha_\sigma \ll -1/3$, probably corresponding to a kind of PB regime, can be predicted with a mean field theory. The exact power law for this regime cannot be found with our present computer program, since it requires calculations at very high chain lengths and extremely low salt concentrations. Note, however, that the present numerical limits of the SCF model are of the same order as physical limits in real systems. Therefore the existence of the PB regime, although interesting for theoreticians, will be hard to prove experimentally as well. Note that our mean-field assumption already causes the Pincus regime to be wider than in more exact treatments (compare Figures 2 and 3).

Above we considered the general scaling behaviour of the thickness in the full parameter space. Below we will inspect more carefully the OsB/NB transition (upon increasing m) and the OsB/SB/NB transition (upon increasing ϕ_s).

The transition from the OsB to the NB regime is illustrated in Figure 6, where we plot the brush thickness as a function of m for three anchoring densities (indicated), using $\phi_s = 10^{-5}$ and otherwise the same parameters as used in Figure 4. Actually, Figure 6 can be compared to a vertical cross section in Figure 4 at the indicated values for σ . At high charge density ($m < 10$), we find the OsB regime with hardly any

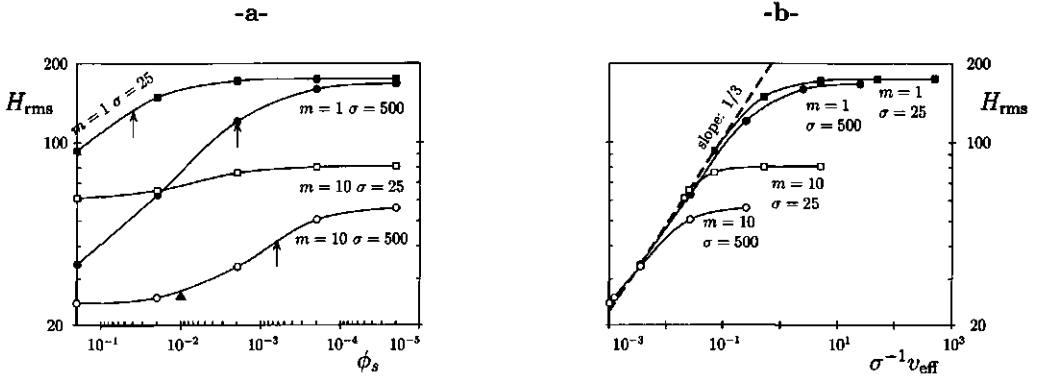


Figure 7 (a) The brush thickness H_{rms} as a function of the salt concentration ϕ_s , for four different combinations of σ and m (indicated) and $N = 500$. The salt concentrations $\phi_s = \sigma^{-1}m^{-1/2}$, corresponding to the OsB/SB transitions, are indicated by the upward arrows; the concentration $\phi_s = m^{-2}$, representative for the SB/NB transition of the $m = 10, \sigma = 500$ brush, is given as a small triangle. (b) The same data as in Figure 7a, plotting $\sigma^{-1}v_{eff}$ (see Eqs. 1 and 29) instead of ϕ_s on the horizontal axis. Such a plot leads to a linear dependence with slope $1/3$ (dashed line) for the part of the curve corresponding to the SB regime, followed by a plateau in the OsB regime.

dependence on σ and a power law dependence on m with almost the analytically predicted exponent $\alpha_m = -0.5$ (indicated by the dashed line). Careful inspection shows the slope (and thus the exponent) to decrease slightly at extremely high charge densities ($m < 2$). This may be attributed to the finite extensibility of the chains, i.e., the breakdown of the Gaussian expression for the chain elasticity. At low charge density ($m > N^{4/3}\sigma^{-2/3}$), on the other hand, we find the NB regime with little or no dependence on m but with a big effect of the anchoring density.

As an introduction to Figure 7, let us take a look at Figures 3a-d again and consider specifically a brush corresponding to one σ, m coordinate e.g., ($\sigma = N, m = N^{0.5}$). At low ϕ_s

(Figures 3a and 3b), such a brush finds itself in the OsB regime. Upon increasing the salt concentration above $\phi_s = \sigma^{-1}m^{-1/2}$, it will be located first in the SB regime (Figure 3c) and finally, above $\phi_s = m^{-2}$ in the NB regime (Figure 3d). This OsB \rightarrow SB \rightarrow NB transition is illustrated in Figures 7a and b. First we plot the thickness of a brush as a function of the salt concentration (increasing from right to left) for two charge densities ($m = 1$ and 10), each at two different anchoring densities ($\sigma = 25$ and 500). At low salt concentrations, the systems for $\sigma = 500$ and that for $m = 1, \sigma = 25$ are in the OsB regime. As the salt concentration is increased, these three systems enter the SB regime, crossing the OsB/SB boundary around

$\phi_s = \sigma^{-1}m^{-1/2}$, which value is indicated in Figure 7a by the upward arrows. Indeed around these points H_{rms} starts to decrease with the salt concentration, and for the system with $m = 10$ eventually the *SB/NB* boundary is crossed at $\phi_s = 1/m^2$ (indicated by a triangle), leading to a thickness that should not depend on either ϕ_s or m .

The fourth curve in Figure 7a represents the system $m = 10$, $\sigma = 25$. This brush is located at the *OsB/NB* boundary at low ϕ_s and passes directly into the *NB* regime with increasing salt concentration. Consequently, its thickness is hardly effected by any change in ϕ_s .

When we substitute $v_{eff} = v + v_{el}$ (Eq. 29) for v_{el} in Eq. 23, we have an equation that incorporates electrostatic as well as non-electrostatic excluded volume interactions. Consequently, this equation should describe the effect of increasing ϕ_s in the *SB* regime, as well as in the *SB/NB* transition region. This is checked in Figure 7b, where we plot the same data as in Figure 7a, rescaled according to these equations in such a way that a straight line with slope $1/3$ is expected for the points corresponding to the *SB* regime. Indeed we find that the data for different charge- and anchoring densities can be collected onto one master curve, as long as they describe a system in the *SB* or *NB* regime (low v_{eff} , high ϕ_s). Each of the four curves eventually branches off as, for high v_{eff} or low ϕ_s , it reaches the *OsB* regime, where Eq. 23 is no longer valid and the brush thickness becomes independent of ϕ_s (see Table 1). The level of this plateau at high v_{eff} (which is the same plateau as that for low ϕ_s in Figure 7a) scales as $m^{-1/2}$, as expected from Table 1.

Segment density profiles In Figures 4, 5, 6, and 7 we checked the scaling dependencies for the brush thickness. Now we turn to the shape

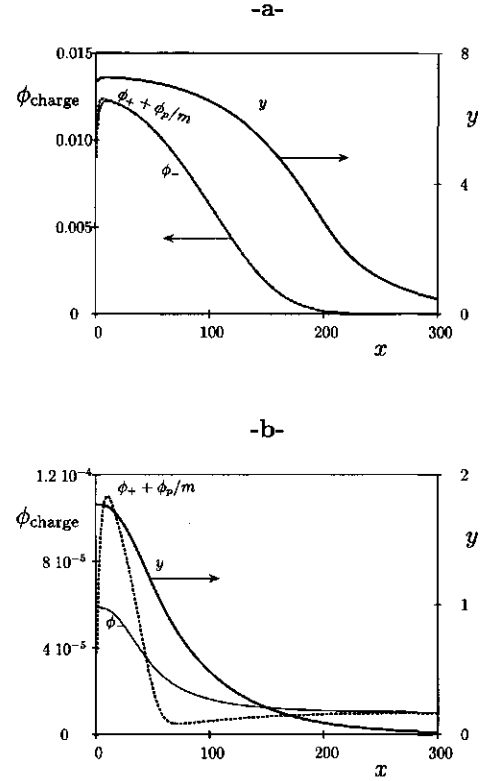


Figure 8 Density profiles of positive charge ($\phi_p/m + \phi_+$), and negative charge (ϕ_-), and the profiles of the dimensionless electrostatic potential ($y = e\psi/kT$) for an Osmotic Brush (a) and a Pincus Brush (b). Parameters: $N = 500$, $\sigma = 40$, $m = 10$, $\phi_s = 10^{-5}$ (8a) and $N = 500$, $\sigma = N^{1.4} \approx 6000$, $m = N^{-0.5} \approx 0.045$, $\phi_s = 10^{-5}$ (8b)

of the segment density profiles. Analytical predictions for the profile of a polyelectrolyte brush are based on the assumption of local electroneutrality in the *OsB* and *SB* regimes. Figure 8a shows the profile of total positive charge $\phi_+ + \phi_p/m$ as a function of x for a brush in the

OsB regime. The dotted curve corresponds to the profile ϕ_- of mobile counterions. Both profiles coincide nearly completely, thus confirming Eq. 3 (i.e., the assumption of local electroneutrality).

Figure 8a presents also the dependence of the dimensionless electrostatic potential $y(x)$, defined as $e\psi(x)/kT$. As can be seen from Figure 8, $\psi(x)$ is evidently a non-linear function of x within the brush. This non-linearity of the potential-profile enforces (through Poissons law, Eq. 34) deviations from the local electroneutrality. However, this differential charge density is much smaller than the absolute value of positive (or negative) charge in the brush. It is not seen on the scale of Figure 8 except for a small region close to the surface. Thus, the condition (3) of local electroneutrality is, indeed, a reasonable approximation for describing the internal brush structure in the OsB regime. The deviations are even smaller (not shown) in the SB regime.

A complete breakdown of the local electroneutrality is expected outside the OsB and SB regimes. This is illustrated in Figure 8b, where we plot the same three quantities as in Figure 8a, but now for a brush that is (according to the analytical theory) located in the PB regime. We find, indeed, a considerable difference between the profiles of positive and negative charge. Note that only at the intersection point of these charge profiles ($x \approx 50$) the system is locally electroneutral. Consequently, at this point the curve representing the electrostatic potential y shows an inflection point. While illustrating the breakdown of local electroneutrality, this diagram also shows why the PB scaling relations are not recovered. The basic assumption leading to the PB regime is that all counterions leave the brush. This is clearly not the case in this example: more than 50% of

the brush charge is compensated by counterions that are located within the brush.

Since the local electroneutrality condition is fulfilled in the OsB and SB regimes, we expect the segment density profiles to obey the predicted dependences as discussed above. In Figure 9a we plot the segment density profiles for a charged brush ($N = 500$, $\sigma = 40$, $m = 10$) at high ($\phi_s = 10^{-2}$), intermediate ($\phi_s = 10^{-3}$), and low ($\phi_s = 10^{-5}$) salt concentrations. According to the diagrams of Figure 3, at the high salt concentration the brush is in the quasi-Neutral Brush regime (NB), at the lower salt concentration in the Osmotic Brush regime (OsB), whereas at the intermediate concentration the Salted Brush regime (SB) applies.

In the quasineutral NB regime, the profile of a polyelectrolyte brush is expected to coincide with that for a neutral brush. In a good solvent and at low grafting density, when only pair contacts between units are significant, the segment density profile is parabolic.⁷⁵ However, in order to make the comparison with the numerical results more precise, we use the more general expression Eq. 31, which takes into account also higher order interactions. Thus, plotting the calculated distribution of polymer segments in the brush as $\ln[1 - \phi_p(x)]$ vs. $(x/H)^2$, one expects a straight line. As is seen from Figure 9b, the profile corresponding to the highest salt concentration turns indeed into a straight line in such a representation. However, the thickness is still slightly higher than that of an uncharged chain, which reaches $\phi_p = 0$ exactly at $x = H$.

For a charged brush in the OsB regime, an analytical expression for the density profile is given by Eq. 19, provided that all non-electrostatic interactions are neglected. From this equation a straight line is expected, when the profile is plotted as $\ln \phi_p$ vs. $(x/h_0)^2$. This plot is shown in Figure 9c, where, to a first ap-

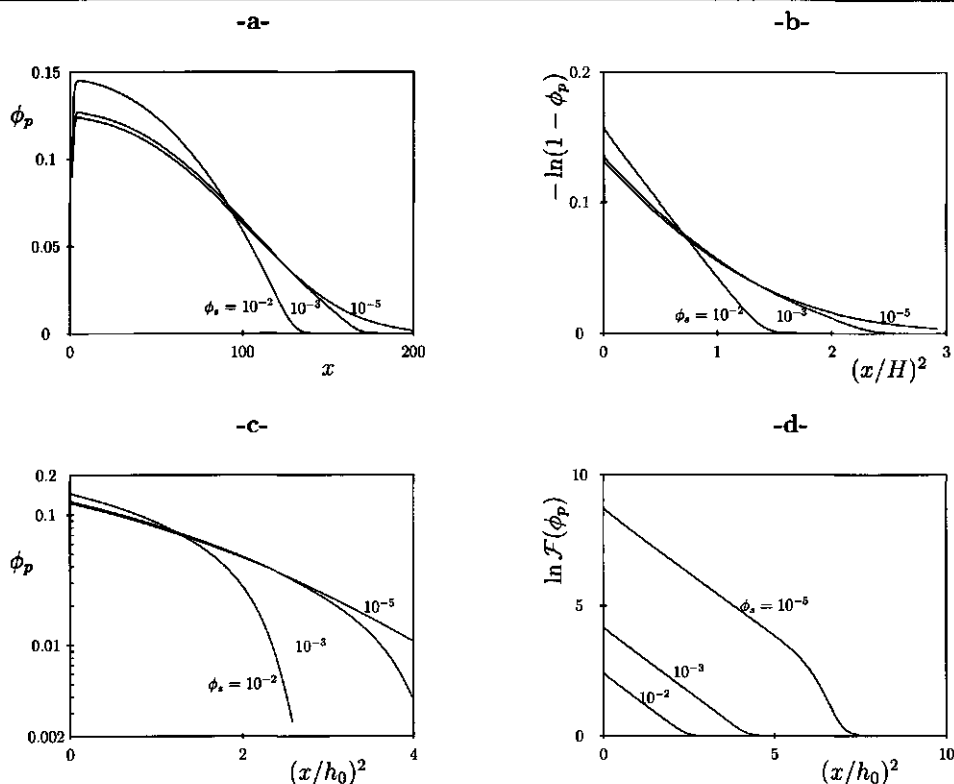


Figure 9 Volume fraction profiles ϕ_p of a charged brush at different salt concentrations ϕ_s (indicated), for $N = 500$, $\sigma = 40$, and $m = 10$. In diagram (a) ϕ_p is plotted against x on a linear scale, in diagram (b) $-\ln(1 - \phi_p)$ is plotted against $(x/H)^2$. In such a plot a profile of a neutral brush would become a straight line. Diagram (c) gives $\ln \phi_p$ against $(x/h_0)^2$, so that the curves would become straight lines if only electrostatic interactions were present. Finally, diagram (d) shows profiles that have been rescaled according to eq. 30, i.e., $\ln \mathcal{F}(\phi_p)$ against $(x/h_0)^2$, which should lead to straight lines irrespective of the dominance of either electrostatic or non-electrostatic interactions.

proximation, a more or less straight line is seen for the profile corresponding to the lowest salt concentration. The substantial deviation from the straight line must be attributed to the ne-

glect of non-electrostatic excluded-volume interactions.

Finally, we use the general Eq. 30 for the representation of the profiles. Doing so, we

take into account both electrostatic and non-electrostatic interactions between grafted polycations, salt co-ions, and all counterions. Plotting the profiles as $\mathcal{F}(\phi_p)$ vs. $(x/h_0)^2$, where $\mathcal{F}(\phi_p)$ is given by the RHS of Eq. 30, we obtain straight lines for all three (NB, SB, and OsB) profiles with the same slope -1 . The intercept $\mathcal{F}(x=0)$ can, according to Eq. 30, be used to calculate the brush thickness H :

$$H^2 = h_0^2 \ln[\mathcal{F}(x=0)] \quad (46)$$

This thickness increases to infinity when the salt concentration goes to zero (compare Eq. 18).

Thus, in spite of the fact that an exact analytical expression for the segment density profile is not available from Eq. 30, it does predict rescaled coordinates in which the density profiles of polyelectrolyte brushes with various values of N , σ , m , and ϕ_s are transformed into straight lines with a slope -1 .

Deviations from these straight lines, however, are noticeable. In the OsB regime ($\phi_s = 10^{-5}$), the downward deviation of the actual density profile from the analytical prediction is due to the finite extensibility of grafted chains.

At higher salt concentrations deviations appear in the opposite direction: the numerical SCF theory predicts a more extended profile than that predicted by the analytical theory. This deviation is due to fluctuations at the edge of the brush. These fluctuations are not found in the analytical theory due to the replacement of all conformations having the free end at $x = x'$ by one (the most probable) conformation. This replacement effectively discards conformations that turn back in the direction of the surface. The deviation (smoothing of the profile near the periphery of the brush) is expected to increase with diminishing brush thickness (increasing salt content). However, on the scale of Figure 9d, this increase is hardly noticeable.

2.5 Conclusions

In this paper we compare the analytical predictions on the structure and scaling relations of a charged brush^{9,81} with a numerical lattice model.¹³ Both models are self consistent field (SCF) methods. The analytical model classifies a system, based upon theoretical considerations, to be in a particular regime and then gives (analytical) expressions for brush thickness and segment density profiles. The numerical SCF model, on the other hand, is based upon a limited set of basic assumptions (such as Poisson's law, Boltzmann's law and the demand that the lattice be filled), but does not make presuppositions about the conformations; however, it needs to be solved numerically.

Obviously, a comparison of both methods cannot judge the validity of SCF methods in general. It does give, however, an independent proof of the validity of additional assumptions in the analytical model. On the other hand, it provides the numerical model with a framework to interpret the results of the calculations. Without such a framework, a numerical model is of limited value.

One fundamental difference between the two models is the fact that *intramolecular* and *intermolecular* interactions are distinguished explicitly in the analytical theory, whereas they are collected into one mean field in the numerical model. The latter mean-field approximation breaks down at low densities, more precisely: the OrS (oriented sticks) and IS (isotropically distributed sticks) regimes, where individual brush molecules are stretched due to intramolecular electrostatic repulsion, cannot be found from the numerical model. In addition, the NC (quasi-neutral non-overlapping

coils) regime, where chains behave as isolated uncharged coils and the size scales as $N^{3/5}$, is treated as a Gaussian regime, the size scaling with an (incorrect) mean-field exponent $1/2$.

Despite these minor (and expected) differences, we find excellent agreement in the three most important regimes. For the scaling of the brush thickness with either N (chain length), m (inverse charge density), σ (inverse grafting density), or ϕ_s (salt concentration), in each of the NB (quasi neutral), OsB (osmotic brush), and SB (salted brush) regimes complete agreement between the two theories is found. Even the exponents of the expressions giving the boundaries between the various regimes predicted by the analytical model are fully recovered in the numerical calculations.

A special remark is due on what may be called the *Pincus brush* regime^{9,57} (PB). The very peculiar scaling $H \sim N^3/(\sigma m^2)$ in this regime is not found from the numerical calculations. Closer investigation, using relatively short chain lengths, shows, however, that we can find a regime that is reminiscent of the PB regime. Moreover, with increasing chain length, calculated exponents change in the direction of the predicted values. To find the proper PB regime, we might have to go to very large chain lengths, but (in order to stay in the PB regime) also to lower salt concentrations, with ϕ_s scaling as $1/N^2$. Our conclusion is that, even though the theoretical considerations leading to this regime are probably correct, the numerical model will never show the typical PB behaviour, since salt concentrations cannot be chosen arbitrarily low. The lower limit on salt concentrations in the numerical model is set by numerical convergence problems. Although these numerical problems have no physical relevance, a lower limit on the salt concentration does exist in real systems as well. We therefore expect that PB

behaviour will be very hard to find experimentally.

A second remark must be made on the transition regions. We find the transition regions to be relatively large: in major parts of the parameter space the behaviour should be classified as intermediate between two limiting cases: the analytical power law behaviour is recovered for relatively extreme values of charge and anchoring density only. Consequently, we do not expect the analytical model to predict the exact value of exponents to be found experimentally, nor do we even expect experiments to reveal true power law behaviour. What it can predict is a range in which exponents may be expected to fall, as well as the direction in which they will change. In short, the primary gain of the analytical theory is not the exact prediction of experimental results, but the provision of a qualitative physical interpretation for them.

A convincing proof of the agreement between the two theories can be obtained by a rescaling of the segment density profiles. Although the analytical model cannot give a closed expression for the density profile in each of the regimes, it does provide a rescaling procedure, transforming each profile into a straight line when plotted in the appropriate way. If we apply this procedure to profiles calculated using the numerical model, we find indeed lines with the correct slope in the three most important regimes: NB, OsB, and SB.

From a theoretical point of view, the conclusion is that the assumptions leading to the OsB, NB, and SB expressions in the analytical model are evidently correct. More specifically: (i) the charge in a brush may be assumed to be fully compensated by counterions in the OsB and SB regimes (equivalent to the local electroneutrality assumption), and (ii) the elasticity of the chain can be described by a Gaussian expres-

sion over a wide range of parameters. As shown before,⁷⁵ the confinement of chain molecules to a lattice, as is done in the numerical model, does

not seem to lead to a significantly deviating behaviour.

Chapter 3

Grafted polyacid brushes

3.1 Introduction

Over the last few years, the properties of brushes have received a great deal of attention (see ref.29 for a review). It is now well established that the thickness of a brush is proportional to the chain length,¹ and that the segments in an uncharged brush experience a potential which is a parabolic function of the distance from the surface. In a good solvent, where this potential is proportional to the volume fraction of brush segments, this leads to a parabolic segment density profile,^{51,79} whereas in poorer solvents a more condensed volume fraction profile is predicted.⁸⁰

Much less work has been done on brushes where the polymers carry charges.^{9,57} In a recent contribution³⁸ the structure of a brush in which the segments carry a constant, invariable charge was investigated in detail, both in the absence and in the presence of salt. When the brush is in equilibrium with a salt-free solution, it can be described as a so-called *Osmotic Brush* (OsB) at relatively low grafting densities and as a *Quasi-Neutral Brush* (QNB) at high coverage. At higher concentrations of external salt a *Salted Brush* (SB) may be found, which can be described as a neutral brush with a (high) *effective* excluded volume parameter. In excess

of electrolyte, the charges are largely screened, even inside the brush, and the QNB regime can be found down to relatively low grafting densities.

In this paper we extend this treatment to brushes carrying *weak* groups (e.g., carboxylic groups), for which the degree of dissociation is a function of the local pH. One important consequence is that, at low ionic strength, the segments in the brush are much more weakly charged than in a brush with fixed charges. Under salt-free conditions most of the segments associate with a proton in order to minimize the free energy of the brush in the high electrostatic potential generated by the few remaining charges. Hence, paradoxically, a brush of a weak polyacid becomes a neutral brush in the absence of salt.

We are not aware of any theory that predicts how the properties of these brushes depend on the important system parameters. In many practical applications local regulation of charges in brushes is important. For example, in biological systems, where (charged) brush-like structures are frequently found, the local salinity and pH are carefully maintained and the extension of the brush might be under active control.

Another example where the subject of this

paper is of relevance is the stability of core-shell lattices. Often, polyelectrolyte shells are used to make hydrophobic lattices water-compatible. The extension of the shell layer can then be controlled by ionic strength and, when the charges are weak, by the pH of the solution. Detailed predictions on how these parameters determine the brush properties is of considerable importance and will help to tune these brushes for specific applications.

We analyze brushes by scaling-type relations and a numerical self-consistent-field (SCF) model. In the numerical model, we employ the so-called two-state approach, which was developed by Björling et al.⁷ to describe the anomalous phase behaviour of poly(ethylene-oxide) (PEO) molecules. We apply this model to (weakly) acidic segments, that may be either charged or uncharged. The relative statistical weight of these two states is a function of the local electrostatic potential. We start by giving a number of relevant details of the two theoretical approaches in sections 3.2 and 3.3. Subsequently, in section 3.4 we compare the outcome of the results of the two approaches, and in section 3.5 we end up with a summary of the main conclusions.

3.2 Numerical model

For the present case of weak polyacid groups, the charge of which is a function of the local pH, we adopt the two-state model as derived by Björling⁷ to describe the anomalous phase behaviour of PEO chains. This phase behavior is explained in terms of an equilibrium between two states that are assumed to have a different solvency. We apply the two-state model to seg-

ments that may either be charged or uncharged in order to model the acid-base equilibrium of these segments. The two-state model as derived by Björling can be simplified considerably, as has been shown by Hurter.³⁶ In appendix B we show this approach to be valid if monomers are considered. Actually, the validity for the monomeric case is a rigorous proof for the polymeric case as well, since in our SCF model the energetic interactions can be separated from the chain statistics. In the following we will give the most important arguments for the two-state polyelectrolyte system.

The average segment weighting factor $G_A(z)$ of a polyacid group A in layer z with respect to the bulk solutions* may be defined as

$$G_A(z) = \alpha^b G_{A^-}(z) + (1 - \alpha^b) G_{HA}(z) \quad (1)$$

where α^b is the degree of dissociation of the groups in the bulk solution, and $G_{A^-}(z)$ and $G_{HA}(z)$ are the weighting factors of charged and uncharged groups, respectively, in layer z . These weighting factors are defined with respect to the bulk solution: $G^b \equiv G(\infty) = 1$ for both the charged and uncharged states. The degree of dissociation of the acid groups is determined by the intrinsic dissociation constant K_a according to the equilibrium



with $K_a = [H^+(z)][A^-(z)]/[HA(z)]$, where the square brackets denote a (local) concentration. Since $\alpha(z)$ is defined as $[A^-(z)]/([A^-(z)] + [HA(z)])$, the equilibrium condition can be written as $K_a = [H^+(z)] \alpha(z)/(1 - \alpha(z))$ or:

$$\alpha(z) = \frac{K_a}{K_a + [H^+(z)]} \quad (3)$$

*Obviously, for the presently modeled brush system, the concentration of A segments in the bulk equals zero. Still, the weighting factor can be defined with respect to the bulk as $G_A(z) = \exp(u_A(z) - u_A^b)$, where u_A^b is the reference potential for A segments. Similarly, α^b gives the (virtual) degree of dissociation in this reference state.

which shows explicitly the dependence of α on the local pH, defined as $pH(z) \equiv -\log([H^+(z)])$.

In Eq. 1 the bulk value α^b is determined by the pH in the bulk solution:

$$\alpha^b = \frac{K_a}{K_a + [H^+]} \quad (4)$$

Here $[H^+] \equiv [H^+(\infty)] = 10^{-pH}$ is the bulk solution concentration of protons.

In the two-state model, $\alpha(z)$ is given by²⁷

$$\alpha(z) = \alpha^b G_{A^-}(z)/G_A(z) \quad (5)$$

where $G_A(z)$ is the average weighting factor defined in Eq. 1. If all non-electrostatic contributions such as solvency and (non-electrostatic) adsorption energy are taken to be identical for HA and A^- , then the ratio $G_{A^-}(z)/G_{HA}(z)$ is simply expressed as a Boltzmann factor of the local potential $y(z)$:

$$G_{A^-}(z)/G_{HA}(z) = e^{y(z)} \quad (6)$$

where $y(z)$ is expressed in units kT per elementary charge e to make it dimensionless. For a polyacid brush, this electrostatic potential $y(z)$ is negative with respect to the bulk solution, and $G_{A^-}(z)$ is smaller than $G_{HA}(z)$. By substitution of eqs. 1, 4, and 6 into eq. 5, $\alpha(z)$ is found as

$$\alpha(z) = \frac{K_a}{K_a + [H^+]e^{-y(z)}} \quad (7)$$

Comparison of eqs. 3 and 7 shows that the two-state model is fully consistent with the mass action law, whereby the local concentration $[H^+(z)]$, which exceeds the bulk solution concentration, is written as $[H^+]e^{-y(z)}$.

Using the average weighting factor $G_A(z)$ for the polyacid segments, the end-point distributions of the chains can be evaluated numerically along the lines of the Scheutjens-Fleer

theory.^{24,61,62} In this method all allowed conformations of chain molecules are generated in a first order Markov approximation (direct chain backfolding is permitted). In this paper we only allow chain conformations which have their first segment in layer $z = 1$ next to the surface and fix the total number of polymer units in the system (i.e., grafting condition¹³). In addition, monomeric components (water, positively and negatively charged ions) are allowed in each lattice layer. The monomeric components are free to leave the brush. Consequently, for these compounds the concentration in the bulk solution is an input parameter.

The electrostatic potential can be expressed in the local concentrations using the multilayer Stern model. For the details and the numerical procedure to solve the equations, we refer to the literature.^{3,8,40}

3.3 Scaling-type approach

In a previous contribution,³⁸ the structure of a polyelectrolyte brush in which the segments have a fixed charge was analyzed in detail along the lines originally proposed by Borisov et al.^{9,11} In that work m is the number of bonds between two charges along the chain. The charge density $1/m$ can thus be identified as a partial charge per segment. Below the symbol $\alpha_0 \equiv 1/m$ will be used to denote this constant degree of dissociation. We summarize some main conclusions for a constant-charge brush, concentrating on the effects of the salt concentration, expressed as the volume fraction ϕ_s of the cations. Unlike in Refs. 9 and 38, we use the symbol σ for the grafting density (number of chains per area d^2), which is the inverse of the area per chain.

When the Debye screening length κ^{-1} is much smaller than the brush thickness H , then the mobile counterions of the charged groups

are trapped within the brush, which is swollen by the osmotic pressure of these counterions. At low ϕ_s , this leads to the *Osmotic Brush* (OsB) regime. In this regime H is independent of σ and ϕ_s and proportional to the chain length and the square root of the charge density:³⁸

$$H \sim N\alpha_0^{1/2} \quad (\text{OsB}) \quad (8)$$

where H is expressed in bond lengths and N is the number of segments per chain.

As ϕ_s increases, salt penetrates into the brush and screens the electrostatic interaction. At a certain ϕ_s there is a transition from an osmotic brush to a *Salted Brush* (SB). Here the brush characteristics are similar to those of neutral brushes with, however, a larger excluded volume parameter v_{eff} . In the neutral case the excluded volume parameter $v = (\frac{1}{2} - \chi)$ is of order unity. As shown in Ref. 38, the salted brush may be described by

$$H \sim N(\sigma v_{\text{eff}})^{1/3} \quad (\text{SB, QNB}) \quad (9)$$

where

$$v_{\text{eff}} = v + \alpha_0^2/\phi_s \quad (10)$$

The value of ϕ_s at the transition from OsB to SB is found by equating the expressions for H given in Eqs. 8 and 9: $\alpha_0^{1/2} \sim (\sigma\alpha_0^2/\phi_s)^{1/3}$ or $\phi_s \sim \sigma\alpha_0^{1/2}$.

If ϕ_s is further increased, v_{eff} decreases. Eventually the ratio α_0^2/ϕ_s becomes of order unity, so that at $\phi_s \approx \alpha_0^2$ the Salted Brush becomes a Quasi Neutral brush (QNB), where $v_{\text{eff}} \approx v$ and Eq. 9 reduces to the well-known expression for a neutral brush; in this regime the electrostatic interactions are fully screened by the excess of salt.

Let us now consider what modifications on this picture become necessary for a weak brush, where α is a function of the (local) pH. We consider the brush as a homogeneous region (i.e.,

we assume a block profile) with degree of dissociation α , in equilibrium with a bulk solution where the (imaginary) degree of dissociation is α^b . By comparison with the two-state approximation (Eqs. 1, 5, and 6), we may write α as:

$$\alpha = \frac{\alpha^b}{\alpha^b + (1 - \alpha^b)e^{-y}} \quad (11)$$

where y is now the (z independent) electrostatic potential in the brush with respect to the bulk solution. It may be expressed in the ratio ϕ_+/ϕ_s between the counterions inside the brush and those in the bulk solution through the simple Boltzmann relation

$$e^{-y} \approx \phi_+/\phi_s \quad (12)$$

In the SB and QNB regimes, y is close to zero and $\alpha \approx \alpha^b$. In these regimes Eqs. 9 and 10 apply, where α_0 has to be replaced by α^b . The only difference with the constant charge brush is that α and α^b are determined by the external pH of the solution.

In contrast to this, there is a major difference between brushes with constant and variable charge in the OsB regime. We may then approximate Eq. 12 by:

$$e^{-y} \sim \sigma\alpha^{1/2}/\phi_s \quad (13)$$

where we used the electroneutrality condition (for a block profile) $\phi_+ = \alpha\sigma N/H$, and substituted $H/N \sim \alpha^{1/2}$ according to Eq. 8. The counterion concentration inside the brush is now much higher than in the bulk solution, which goes along with a highly negative electrostatic potential. Under the action of this potential the acid groups associate with protons to minimize their free energy, and α decreases.

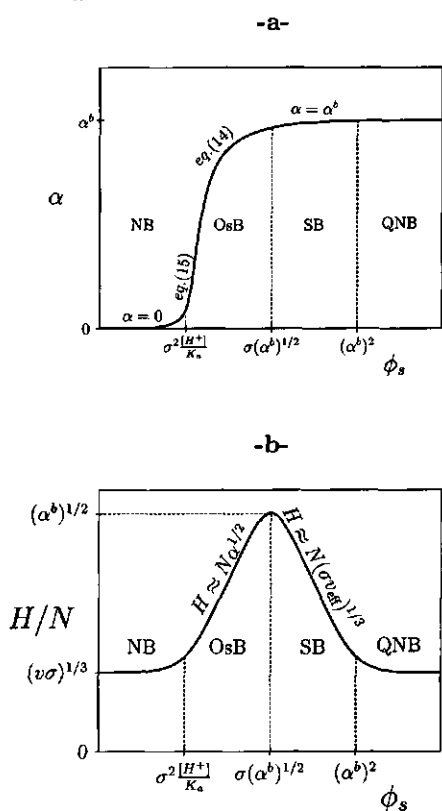


Figure 1 Schematic picture of the degree of dissociation α within the brush (a) and the brush thickness H (b) as a function of the salt concentration ϕ_s . In the NB regime α is close to zero, it increases in the OsB regime, and reaches the constant (bulk) level α^b in SB and QNB regimes. In the OsB regime, the dependence $\alpha(\phi_s)$ is given by Eq. 14; for low α the approximate Eq. 15 applies. The thickness, plotted as H/N , passes through a maximum as a function of the salt concentration. This maximum is located at the OsB/SB boundary.

$\alpha^b/(1 - \alpha^b)$ by $K_a/[H^+]$ this equation reads

$$\alpha^{-1} \sim 1 + \frac{[H^+]}{K_a} \frac{\sigma}{\phi_s} \alpha^{1/2} \quad (14)$$

This is an implicit equation for α and can not easily be solved analytically. An approximation for high y (hence, low ϕ_s and low α) is found by neglecting the term 1 in Eq. 14, resulting in

$$\alpha^{3/2} \approx \frac{K_a}{[H^+]} \sigma^{-1} \phi_s \quad (\text{low } \alpha) \quad (15)$$

The dependence of α on ϕ_s in the various regimes is summarized in Figure 1a. The QNB/SB and SB/OsB transitions are the same as discussed for the constant-charge brush (with α_0 replaced by α^b). Upon further decreasing ϕ_s and thus reducing the screening of charges, a new transition takes place from the osmotic brush to a neutral brush (NB). In this regime the electrostatic potential is so high that virtually all the groups are in the uncharged HA state, and the brush properties are essentially the same as for a fully neutral brush. As shown before for a brush with fixed charges,³⁸ the NB/OsB transition occurs at $\alpha \sim \sigma^{2/3}$ or, with Eq. 15, at $\phi_s \sim \sigma^2[H^+]/K_a$.

Figure 1b shows schematically how the brush thickness H depends on ϕ_s . In the NB and QNB regimes, the thickness is given by $H \sim N(\sigma v)^{1/3}$, where v is of order unity in a good solvent. In the OsB regime $H \sim N\alpha^{1/2}$, where α increases with ϕ_s because the addition of salt facilitates the dissociation of the acid groups. In the SB regime $H \sim N(\sigma v_{\text{eff}})^{1/3}$ according to Eq. 9, where $v_{\text{eff}} \sim 1/\phi_s$ so that the brush thickness decreases with increasing salt content, due to the screening of the charged groups. Hence, a maximum brush thickness is found at the transition between the OsB and SB regimes, at:

$$\phi_s^{\text{max}} \sim \sigma(\alpha^b)^{1/2} \quad (16)$$

This decrease is expressed quantitatively by Eq. 11. After substitution of Eq. 13 and replacing

At this maximum, the thickness equals the thickness of an osmotic brush with $\alpha = \alpha^b$:

$$H^{\max} \sim N(\alpha^b)^{1/2} \quad (17)$$

3.4 Results

In this section we present numerical SCF results for the brush characteristics, and we compare them with the analytical predictions given in the previous section.

The numerical results were obtained for a hexagonal lattice with a lattice spacing $d = 0.6$ nm, using the two-state formalism discussed in the theory section. The relative dielectric permittivities were chosen as 80 for the solvent and 5 for all other substances. All calculations were performed for athermal systems. In the language of the Flory-Huggins model,²⁸ all χ parameters were taken to be zero. The value of K_a was fixed at 10^{-7} M ($pK_a = 7$) in order to be able to vary the salt concentration over a wide range; if the pK_a had been chosen much lower, e.g., $pK_a = 4$, no computations for salt concentrations below 10^{-4} M would have been possible. The salt concentration ϕ_s is expressed as a volume fraction; if desired, this value may be converted to a molarity by multiplying ϕ_s by $\sim 7.7M$. In the present implementation of the lattice model all monomers have an equal volume $v_{\text{cell}} = d^3$. Consequently, the molarity of pure water (-clusters), pure salt, or pure polymer (on monomer basis) equals $10^{-3}/(v_{\text{cell}}N_{\text{av}}) \approx 7.7$ M.

Figure 2a shows volume fraction profiles for a polyacid with chain length $N = 500$, grafted onto a surface with a density $\sigma = 0.002$, in equilibrium with a bulk solution at $pH = 8$ (equivalent to $[H^+]/K_a = 0.1$), at three widely different salt concentrations. For these parameters, the NB regime would be found below $\phi_s \approx 4 \times 10^{-7}$,

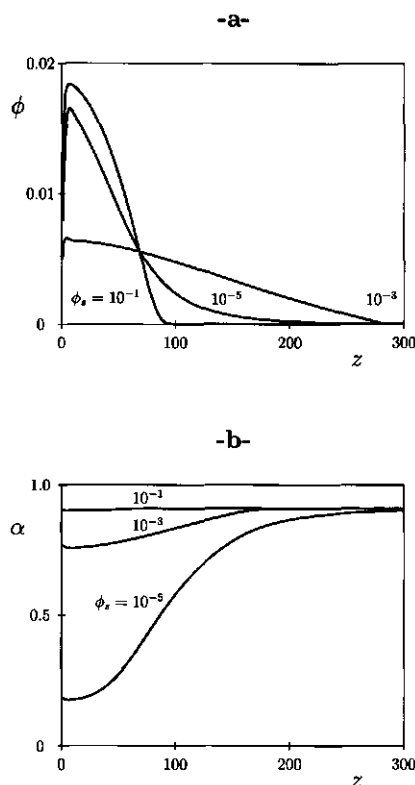


Figure 2 (a) Volume fraction profiles of a terminally anchored polyacid at three different salt concentrations (indicated) and the degree of dissociation $\alpha(z)$ of brush segments as a function of the distance to the surface (b). Parameters: $N = 500$, $pH = 8$, $pK_a = 7$, $\sigma = 0.002$.

the transition between OsB and SB is expected around $\phi_s \approx 2 \times 10^{-3}$, and the QNB regime would be reached only above $\phi_s \approx 0.8$. Hence, $\phi_s = 10^{-5}$ is in the lower end of the OsB-regime, 10^{-3} is close to the OsB/SB transition, and 10^{-1} is in the upper end of the SB-regime. In the latter case, the profile resembles the parabolic profile for a neutral brush. Despite the low an-

choring density, the polymer is already fairly stretched: the profile extends over ~ 90 layers, as compared to $\sqrt{500} \approx 22$ for its radius of gyration. A fully screened brush would give a thickness of $500(0.001)^{1/3} \approx 50$ layers, so that at $\phi_s = 10^{-1}$ the screening is not yet complete.

At a lower salt concentration $\phi_s = 10^{-3}$ the increased electrostatic interaction causes a much stronger stretching and a much more dilute profile. However, a further decrease of ϕ_s to 10^{-5} causes the profile to shrink again because of a decreasing α . This at first sight unexpected behaviour is in full agreement with the scaling predictions in section 3.3. Since $\phi_s = 10^{-5}$ is still located in the OsB regime, the chains extend further into the solution than in the QNB or NB regimes, and the profile shape still deviates from a parabola. Nevertheless, Figure 2a shows clearly that with decreasing ϕ_s the brush characteristics approach again those of a neutral brush.

In Figure 2b we plot the degree of dissociation of brush segments as a function of their distance to the surface, for the same set of parameters as in Figure 2a. The degree of dissociation tends to the bulk value $\alpha^b = 0.9$ at large distances from the surface, irrespective of ϕ_s . In the Salted Brush (upper curve), virtually all brush segments have the maximum degree of dissociation α^b , as expected. The Neutral Brush ($\phi_s = 10^{-5}$), on the other hand, consists mainly of segments that have a much lower degree of dissociation. The curve for $\phi_s = 10^{-3}$ corresponds to the most extended brush. In the scaling section we assumed that up to this point the segments in the brush remain maximally dissociated. The figure shows this to be true to a first approximation only. The observed deviation of α from α^b is expected to lead to a lower value for the maximum thickness than predicted by Eq. 17, as we will show below.

The next two figures illustrate the behaviour of the average degree of dissociation in the brush and of the brush thickness as a function of the salt concentration ϕ_s . These figures may be compared with the qualitative picture of Figure 1. Since it is not unambiguous to locate the boundary of a continuous brush profile, we use the root-mean-square thickness H_{rms} as a measure of H . It is defined as

$$H_{\text{rms}}^2 = \frac{1}{\theta} \sum_z z^2 \phi(z) \quad (18)$$

where $\theta = N\sigma = \sum_z \phi(z)$ is the grafted amount per surface site. Although H_{rms} is expected to be lower than H as used in eqs. 9 and 17, the trends in H_{rms} and H should be comparable.

In Figure 3a we plot the average degree of dissociation α of brush segments as a function of the salt concentration, for four values of the pH. The theoretical prediction (Figure 1a) shows a more or less constant $\alpha = \alpha^b$ in the QNB regime at high ϕ_s . With decreasing ϕ_s we enter the SB regime, where α is expected to remain constant down to the OsB/SB boundary. This boundary scales as $\sigma(\alpha^b)^{1/2}$, according to Eq. 16. If the numerical prefactors are assumed to be around unity, one would expect it to be situated at $\phi_s \approx 6 \times 10^{-4}$ for $pH = 6$ ($\alpha^b \approx 0.1$). The SCF calculations show indeed that the decrease of α sets in in this range; the transition is, however, rather broad. For very low ϕ_s , α decreases to low values, as expected. The NB regime (where $\alpha \approx 0$) is for the higher pH-values not reached in Figure 3a. Nevertheless, the general trends of Figure 1 are well reproduced.

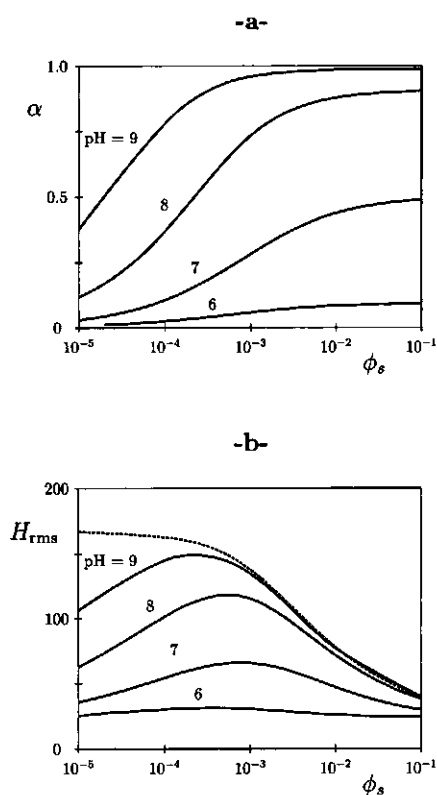


Figure 3 The degree of dissociation α , averaged over all brush segments, as a function of salt concentration ϕ_s at four different pH values (a) and the dependence of the root-mean-square layer thickness H_{rms} on ϕ_s (b). Parameters are the same as in Figure 2. The dashed curve in (b) represents the behaviour of an equivalent conventional (pH-independent) charged brush.

Figure 3b gives results for H_{rms} as a function of ϕ_s for four different values of the pH, at $N = 500$ and $\sigma = 0.002$ as before. All the curves show a maximum, as anticipated in Figure 1b. For comparison, the dotted curve in Figure 3b gives the equivalent results for a brush

with a constant degree of dissociation ($\alpha^b = 1$).

The maxima in this figure are predicted to be located at the OsB/SB boundary. We may derive this location from the curve for the constant-charge brush (dotted curve), for which the OsB/SB boundary can be recognized as the salt concentration where the brush thickness (constant at low ϕ_s) begins to decrease. From Figure 3b we read this boundary to be located at $\phi_s \approx 5 \times 10^{-4}$, and the brush thickness equals $H_{rms} \approx 155$ at this point.

At pH = 9 the maximum thickness should be found around this same salt concentration. This is indeed the case. The height of the maximum is only slightly lower than the thickness of the constant-charge brush, as expected. Thus, the curve at pH = 9 follows the scaling prediction for a brush of a weak polyacid.

Lower pH values lead to lower α^b values according to Eq. 4, so we expect the location of the maximum to shift to lower ϕ_s values. Also the height is expected to decrease. Surprisingly, we find the location of the maxima to shift to higher ϕ_s values instead. The thickness drops much faster than expected, i.e., faster than $(\alpha^b)^{1/2}$.

We may understand the shift of the maximum to higher ϕ_s by re-examining Eq. 7. In the SB regime we postulated $\alpha \approx \alpha^b$, which is equivalent to neglecting the factor e^{-y} in $\alpha = 1 / (1 + [H^+]e^{-y}/K_a)$. We note that both when $[H^+] \ll K_a$ and when $[H^+] \gg K_a$ this becomes a good approximation: in the first case we can safely neglect e^{-y} with respect to $[H^+]/K_a$ even when $-y$ is of order unity; the latter case leads to $\alpha^b \approx 0$ and y is vanishing. When $K_a \approx [H^+]$, however, even a moderate electrostatic potential will cause $\alpha < \alpha^b$. Consequently we expect for $pH \approx pK_a$ that α begins to decrease already in the SB regime.

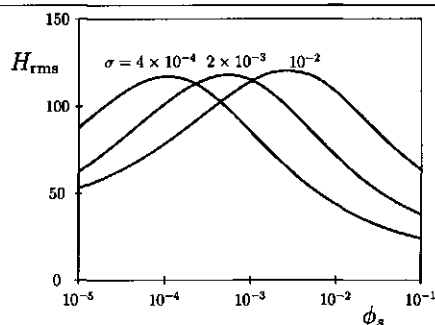


Figure 4 The root-mean-square layer thickness as a function of salt concentration at $pH = 8$ for three different anchoring densities (indicated). Other parameters as in Figure 2.

For e.g. the $pH = 8$ curve in Figure 3a we indeed find the salt concentration where α begins to decrease to be relatively high, clearly above the SB/OsB transition. The corresponding maximum in 3b follows this shift into the SB regime, where its height H^{\max} is no longer given by the OsB expression (Eq. 8). It is much lower due to the partial screening of electrostatic interactions in the SB regime.

The boundaries NB/OsB at low ϕ_s and SB/QNB at high ϕ_s cannot be read easily from Figure 3b, because the transitions are rather gradual. Moreover, it is clear that the NB/OsB boundary must be found at ϕ_s values lower than the plotted range. Nevertheless, the trend that the NB/OsB boundary shifts to lower ϕ_s , and the SB/QNB boundary to higher ϕ_s with increasing α^b is fully corroborated.

In Figure 4 we consider the effect of the anchoring density and plot H_{rms} vs. ϕ_s curves for three values of the brush density σ . The agreement with Figure 1b as to the location of the maximum is perfect: increasing the anchoring

density by a factor of 5 shifts the maximum to a 5 times lower salt concentration, but leaves its height unaffected.

In Figures 3 and 4 we focussed our comparison on the overall shape of the H vs. ϕ_s curve. Below we consider the variation of H as a function of σ and pH over a wide range of conditions. First we check Eq. 9, describing the thickness in the combined SB and QNB regimes. Subsequently we compare the SCF calculations with analytical predictions for the OsB regime (Eq. 15). We do not make a comparison in the NB regime, since it would require calculations at extremely low salt concentrations*.

In Figure 5 we present calculations on the RMS thickness of brushes at salt concentrations ranging from $\phi_s = 10^{-5}$ to 10^{-1} , at three different anchoring densities, and four different pH values. In the figure we plot the thickness as a function of σv_{eff} on a double-logarithmic scale, where v_{eff} depends on the salt concentration ϕ_s according to Eq. 10. Different shapes and orientations of the symbols refer to different combinations of σ and pH , as shown in the legend. Filled symbols represent systems in the SB or QNB regimes, whereas systems for which $\phi_s < \sigma(\alpha^b)^{1/2}$, corresponding to the NB and OsB regimes, are indicated by open symbols.

The filled symbols follow rather closely a straight line with slope $1/3$ (dashed line) as predicted by Eq. 9 for the SB and QNB regimes. The open symbols on the other hand, are scattered throughout the picture (and some are outside the boundaries of the picture). They strongly deviate from the linear behavior.

For a brush in the osmotic regime, we expect the thickness to scale as $\alpha^{1/2}$ (Eq. 8). For low values of α , its value may be approximated according to Eq. 15. Consequently, if we plot

*At low ionic strength, the Debye screening length becomes very large so that we are forced to take a huge number of layers into account. In this case the convergence of the numerical equations is very poor indeed.

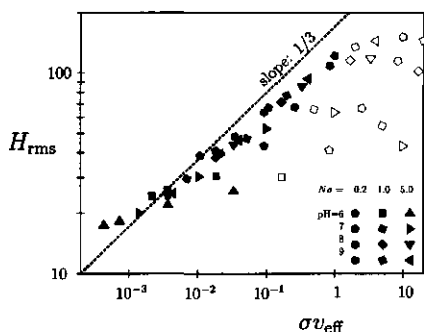


Figure 5 The RMS layer thickness as a function of σv_{eff} for systems at three different grafting densities and four different pH's, as indicated in the legend. Systems corresponding to the SB and QNB regimes are indicated by filled symbols, those in the NB and OsB regimes by open symbols. In the latter two regimes ($\phi_s > \sigma(\alpha^b)^{1/2}$) a straight line with slope 1/3 is expected according to Eq. 9.

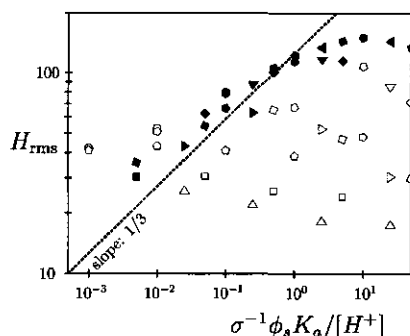


Figure 6 The RMS layer thickness as a function of $\sigma^{-1}\phi_s K_a/[H^+]$ for the same systems as in Figure 5. The filled symbols correspond now to the OsB regime, the open ones to the other regimes. In the OsB regime ($\sigma^2[H^+]/K_a < \phi_s < \sigma(\alpha^b)^{1/2}$) Eq. 8 predicts a straight line with slope 1/3.

H_{rms} as a function of the righthand side of Eq. 15 on a log-log plot, we expect a straight line with slope 1/3 for the data points corresponding to an osmotic brush with low α .

This is verified in Figure 6, where we present the same data as in Figure 5, now as a function of $\sigma^{-1}\phi_s K_a/[H^+]$. In this case the OsB symbols are filled, the open symbols represent now the SB/QNB, as well as the NB systems. At first sight the agreement is less good in this case than in Figure 5. Some points indeed follow the predicted straight line. However, at high thickness the breakdown of the assumption $\alpha \ll 1$ causes downward deviations. At the other end of the OsB regime, the onset of non-electrostatic excluded volume interactions causes a thickness which is higher than predicted by Eq. 8.

These two figures can be summarized as follows. Using the expressions derived in the theory section, data points in a wide range of parameters can be collected rather accurately onto two different master curves, one describing the behaviour in the OsB regime (Eq. 8), the other representing the combined SB/QNB behaviour (Eq. 9). The most noticeable deviations from the master curve are a higher than expected thickness around the NB/OsB boundary (especially at high σ) due to non-electrostatic excluded volume interactions, and a lower than expected thickness around the OsB/SB boundary (i.e., at the maximum thickness) due to an overestimation of the degree of dissociation at this point: both the assumption $\alpha(z) = \alpha^b$ (used in Figure 5) and the approximating ex-

pression 15 (used in Figure 6) overestimate α around the OsB/SB boundary.

3.5 Conclusions

We examined the thickness of a grafted polyacid, i.e., a polyelectrolyte brush where the charge of each segment is a function of the local pH, and discussed it in terms of the known behaviour of a constantly charged brush. The main conclusion of this study is that the thickness H of such a brush passes through a maximum as a function of the salt concentration ϕ_s , whereas the thickness of a "constant-charge" brush is a continuously decreasing function of (increasing) salt concentration.

Assuming a block profile for the grafted layer, and making first-order approximations for the degree of dissociation α , we derived analytical expressions for the position (Eq. 16), as

well as the height (Eq. 17) of this maximum. The dependence $H(\phi_s)$ on the right-hand-side of the maximum was found to be the same as that for a constant charge brush (Eq. 9). For the left-hand-side a new (albeit approximate) expression was derived.

These analytical expressions for the location and height of the maximum, as well as the evolution of the thickness on either side of it, were checked using a SCF numerical model. The predictions on the location of the maximum, as well as on the thickness at high salt concentrations, were qualitatively fully corroborated. However, as the SCF calculations showed, (over)simplifying assumptions on α around the maximum lead to an overestimation of the brush height. Furthermore, the thickness at low salt concentrations is only rather poorly described by the approximate scaling expression, due to the neglect of non-electrostatic excluded volume interactions.

Chapter 4

Adsorption of charged diblock copolymers

4.1 Introduction

Polymers are widely used to modify the properties of colloidal systems. They may act as flocculants, stabilizers or thickeners. Only in recent years, the synthesis of a variety of well-defined (di-)block copolymers has become feasible. They form a promising class of modifiers, wherein the characteristics of long polymers are combined with the amphiphilic character of surfactants. The length as well as the chemical composition of each of the blocks can be tailored to specific applications. Because of the high cost of developing new kinds of polymers, the ability to predict the behavior of a particular (class of) polymer would be very rewarding.

Several aspects of block copolymer adsorption have been addressed in the past few years. Two of them, although important, will not be dealt with in the present paper. Firstly, we shall consider equilibrium structures only, leaving aside all problems concerning the dynamics of polymer adsorption. Secondly, the formation of micelles in the solution is not taken into account, limiting our treatment to the case of a non-selective solvent or low solution concentrations.

The segment density profile of adsorbed uncharged block copolymers has been investigated theoretically by Evers et al.²⁵ and Whitmore and Noolandi.⁷³ When the surface is selective for one of the blocks, this anchor block is adsorbed in a relatively flat conformation. The free "buoy" block, on the other hand, protrudes far into the solution, and its profile is similar to that of a terminally attached chain. The profile has a maximum and extends over a relatively large distance.

The scaling behavior of the adsorbed amount and the layer thickness is interesting from both a theoretical and experimental point of view. This question has been addressed theoretically for uncharged block copolymers with an adsorbing A block (length N_A) and a non-adsorbing B block (length N_B) by Marques and Joanny⁴⁷ (MJ). Using a mean-field as well as a scaling approach, they found two regimes. Unless the A block is very short, the anchor density is always high, and a regime is found which we denote by HU (High density - Uncharged). In this regime the number of chains per surface area, σ , scales as

$$\sigma \propto 1/N_A \quad (HU) \quad (1)$$

independent of the value of N_B . The layer thickness L scales as:

$$L \propto N_B/N_A^{1/3} \quad (HU) \quad (2)$$

On the other hand, for highly asymmetric polymers with a short anchoring block the anchor density is low (LU regime) and the scaling relations are:

$$\sigma \propto (N_A/N_B)^{6/5} \quad (LU) \quad (3)$$

and

$$L \propto N_A^{2/5} N_B^{3/5} \quad (LU) \quad (4)$$

Munch and Gast⁵⁴ and, independently, Ligoure and Leibler⁴⁴ used a mean field analysis and obtained expressions that have to be solved numerically. Both groups described the highly asymmetric regime only and found a scaling of L with N_B that agrees roughly with the results of MJ: Ligoure and Leibler find $L \propto N_B^{0.55}$ whereas an exponent of 0.7 was found by Munch and Gast. Several experimental results confirm a scaling behavior with exponents that fall in the same range.^{42,46,55,67}

Evers et al.²⁵ have extended the self-consistent-field (SCF) lattice model, developed originally by Scheutjens and Fleer for the adsorption of homopolymers,^{61,62} to the adsorption of block copolymers at solid/liquid interfaces. Their results (interpreted in terms of the adsorbed amount θ , which can be related to the chain density σ through the relation $\theta = \sigma N$, where $N = N_A + N_B$) agree with the qualitative picture of MJ, showing a regime (LU) at low N_A/N_B where σ is an increasing function of N_A and a second regime (HU) at higher N_A/N_B where σ decreases with N_A . For the hydrodynamic layer thickness, an almost linear scaling with N_B was found if N_A is large enough (HU), whereas a clearly less-than-linear scaling with N_B was observed for smaller values of N_A (LU).

To modify systems that contain water as a solvent, polymers must be used that are (at least partly) soluble in water. In most practical cases this means that charged polymers are used. Recently, the first theoretical article on the adsorption of charged block copolymers appeared.² The article combines the results of Marques et al.⁴⁸ for the adsorption of uncharged copolymers from a selective solvent with those of Pincus⁵⁷ for a charged brush. Irrespective of the adsorbed amount, the anchor segments were assumed to form a molten layer of finite thickness. Consequently, only one regime was observed in which the chain density scales as

$$\sigma \propto N_A^{-6/11} N_B^{-3/11} (\phi_s^b)^{1/11} \quad (5)$$

where ϕ_s^b is the salt concentration in the solution. The thickness of the brush scales as $L_B \propto N_A^{-2/11} N_B^{10/11} (\phi_s^b)^{-7/11}$. In the present article we will show that the amount of A segments on the surface is below monolayer coverage for most practical situations, leading to a completely different scaling behavior.

In the past few years, there has been considerable progress on the related case of a charged brush. The papers of Pincus⁵⁷ and Borisov et al.⁹ agree on the main points: in the absence of salt the thickness of the brush is proportional to the polymer length N and the square root of the charge density on the chain. It is independent of the anchoring density σ . When the salt concentration in the bulk solution becomes comparable to the counterion concentration in the brush, a different scaling law applies:

$$L \propto N(\alpha_B^2 \sigma / \phi_s^b)^{1/3} \quad (6)$$

where α_B is the valency of brush segments, with $0 \leq \alpha_B \leq 1$.

Our present paper describes an extension of the work of Evers et al.²⁵ to the case of charged

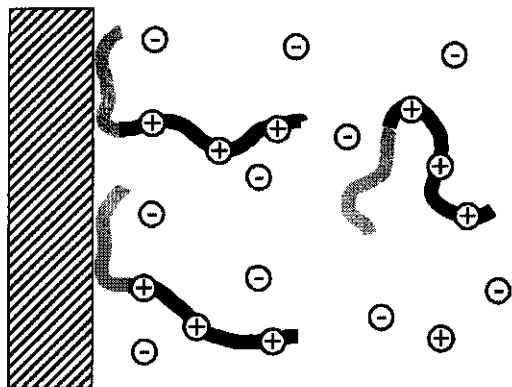


Figure 1 Schematic picture of ionic block copolymers adsorbing to a surface.

block copolymers. We apply the SCF model to the adsorption of charged block copolymers, where the A segments in the anchor block are still uncharged and adsorbing. The non-adsorbing B segments in the buoy block are charged now and have a valency α_B . For the present paper we restrict ourselves to an uncharged surface. The situation is depicted schematically in Figure 1, where the black part corresponds to A segments and the gray sections indicate the buoy (B) blocks. We compare our results to scaling predictions that are obtained by generalizing the charged brush model to the case of adsorbing block copolymers.

In Section 4.2 we review the basic assumptions of the lattice model, and subsequently we present the scaling model in Section 4.3. The choice of parameters is discussed in Section 4.4. Then, in Section 4.5, we present the results obtained by the lattice theory and compare them with the scaling predictions. These results are discussed in Section 4.6 and, finally, the main conclusions are summarized in Section 4.7.

4.2 Self-consistent-field lattice model

We use a self-consistent-field (SCF) lattice model to calculate the distribution of molecules near a surface. The mean field approximation implies the replacement of the local potential $u(x,y,z,t)$ of a segment at position (x,y,z) and time t by a time-independent potential $u(z)$, of a segment at a distance z from the surface. Hence, a pre-averaging over the variables x,y , and t is carried out. The introduction of a lattice is convenient to define and count conformations. A recent comparison between a lattice mean-field and a continuous mean-field model for the structure of an uncharged brush⁷⁵ shows that the use of a lattice does not introduce any error when the molecules are large compared to the size of one lattice cell. For the generation of conformations we use a first order Markov approximation: the position of any segment is determined only by the position of its immediate neighbours. The electrostatic interactions are handled using the multilayer Stern-model.⁸

We divide the halfspace next to a surface in parallel layers, numbered $z=1,2,\dots,M$ where M is sufficiently large so that bulk properties are reached at layer M . A conformation of a molecule is defined when for each of its segments the distance to the surface is specified. The (unnormalized) probability G^c of a conformation c is related to its potential energy u^c , which is the summation of the potential energies of its N segments:

$$\begin{aligned} G^c &= \Omega^c e^{-u^c/kT} = \Omega^c \prod_{s=1}^N e^{-u(z,s)/kT} \\ &= \Omega^c \prod_{s=1}^N G(z,s) \end{aligned} \quad (7)$$

In this equation Ω^c is the degeneracy of a conformation and depends on the type of lattice. The potential experienced by the s^{th} segment depends both on its position z and on the type of segment s . For example, for a diblock copolymer $A_{100}B_{200}$, $G(z, s) = G_A(z)$ for segments 1 to 100 and $G(z, s) = G_B(z)$ for segments 101 to 300. For later use we have defined here the weighting factor $G_A(z)$ for a segment A in layer z as $e^{-u_A(z)/kT}$. For a segment of type A the energy in layer z is given by^{8,25}

$$u_A(z) = u'(z) + e\alpha_A\psi(z) + kT \sum_B \chi_{AB}(\langle\phi_B(z)\rangle - \phi_B^b) \quad (8)$$

where $u'(z)$ is a Lagrange multiplier for layer z , introduced to meet the constraint that the lattice is completely filled:

$$\sum_A \phi_A(z) = 1 \quad [z = 1, \dots, M] \quad (9)$$

This summation is over all segment types in the system, including the solvent and salt molecules.

The second term in Eq. 8 takes into account the electrostatic contribution to the energy of a segment. In this term, e is the elementary charge, α_A the valence of a segment A and $\psi(z)$ is the electrostatic potential in layer z , obtained from the set of equations:

$$\frac{\partial^2 \psi(z)}{\partial z^2} = \frac{\rho(z)}{\epsilon(z)} d^2 \quad [z = 1, \dots, M] \quad (10)$$

In this equation the lattice spacing d is needed to keep z dimensionless; thus for charged systems the results of the lattice model are no longer invariant to a rescaling of this parameter. In our lattice calculations we use a discrete analogue of Eq. 10, taking into account the changes in dielectric permittivity between different layers.⁸ The space charge density $\rho(z)$ in layer z and the dielectric permittivity $\epsilon(z)$ of layer z are

obtained from the following mean field expressions, in which ϵ_A is the dielectric permittivity of pure A and $V_{\text{cell}} = \frac{3}{4}\sqrt{3}d^3$ (hexagonal lattice) is the volume of one lattice cell:

$$\rho(z) = \frac{\sum_A \alpha_A e \phi_A(z)}{V_{\text{cell}}} \quad (11)$$

$$\epsilon(z) = \sum_A \epsilon_A \phi_A(z) \quad (12)$$

The electroneutrality of the system is ensured by setting the field strength at the boundaries zero:

$$\left. \frac{\partial \psi}{\partial z} \right|_{z=0} = \left. \frac{\partial \psi}{\partial z} \right|_{z=M} = 0 \quad (13)$$

Again, in the lattice model a discrete version of these expressions is used.⁸

The last term of Eq. 8 represents the mixing energy (relative to the bulk solution). In this term χ_{AB} is the well known Flory-Huggins interaction parameter between segments A and B (with $\chi_{AA} = 0$), and $\langle\phi_B(z)\rangle$ is the volume fraction ϕ_B averaged over the neighbors of a lattice site in layer z . The summation index B runs over all monomer types in the system. In order to account for the adsorption energy in $u_A(z)$, we include in the summation of Eq. 8 also the surface, considering it as an additional component in the system with (fixed) volume fraction $\phi = 1$ in the layers $z \leq 0$ and $\phi = 0$ in solution ($z > 0$).

In order to calculate the volume fraction profile, we introduce a function $G(z, s|z', s')$, which is the combined statistical weight of all conformations of chain parts starting with segment s' in layer z' and ending with segment s in layer z . Summation of $G(z, s|z', 1)$ over all z' leads to the end-point distribution function $G(z, s|1)$ of a sequence $1, 2, \dots, s$. By definition we have:

$$G(z, 1|1) = G(z, 1) \quad (14)$$

and similarly :

$$G(z, N|N) = G(z, N) \quad (15)$$

where N is the number of segments of the molecule.

The first order Markov approximation allows us to obtain the distribution function $G(z, s+1|1)$ from its predecessor $G(z, s|1)$ by taking into account all possible steps from segment s to $s+1$, regardless of the positions of all segments 1 to $s-1$:

$$G(z, s+1|1) = G(z, s+1)\langle G(z, s|1) \rangle \quad (16)$$

where $\langle G(z, s|1) \rangle$ is again a shorthand notation for $G(z, s|1)$ averaged over the neighbors (in layers $z-1$, z , and $z+1$) of a lattice site in layer z . Applying expression 16 recursively ($N-1$) times to the starting relation 14 and also ($N-1$) times to expression 15, two sets of N distribution functions are generated. From these sets many characteristics of the adsorbed layer can be calculated. For example, in a system containing a diblock copolymer with block lengths N_A and N_B , respectively, and total length $N = N_A + N_B$, the volume fraction profile of monomer type A is given by:

$$\phi_A(z) = \frac{\phi_A^b}{N_A} \sum_{s=1}^{s=N_A} \frac{G(z, s|1)G(z, s|N)}{G(z, s)} \quad (17)$$

where ϕ_A^b/N_A is the proper normalization factor if we assume that the interface region is in full equilibrium with the solution far away from the surface (the bulk solution). For large z , where $G(z, s) = 1$ since this weighting factor is defined relative to the bulk solution, Eq. (17) gives $\phi_A(z) = \phi_A^b$, the concentration of A segments in the bulk solution.

We now have for any monomer type A in every layer z two unknowns $\phi_A(z)$ and $G_A(z) = e^{-u_A(z)/kT}$ and two corresponding equations: 8

and 17. Additionally we have for every layer two unknowns $\psi(z)$ and $u'(z)$ with corresponding equations 9 and 10. This set of equations can be solved numerically.

The excess amount of a monomer type A is defined as:

$$\theta_A^{ex} = \sum_{z=1}^M (\phi_A(z) - \phi_A^b) \quad (18)$$

In the remainder of the text we will drop the superscript "ex" and use θ_A instead of θ_A^{ex} .

For the thickness of the adsorbed layer, we will use two measures: the root-mean-square layer thickness δ_{rms} and the hydrodynamic layer thickness δ_h . The RMS layer thickness is given by:

$$\delta_{rms} = \sqrt{\frac{\sum_{z=1}^M z^2 \phi_A^a(z)}{\sum_{z=1}^M \phi_A^a(z)}} \quad (19)$$

where $\phi_A^a(z)$ is the volume fraction profile of adsorbed molecules, defined as the volume fraction of molecules that have at least one segment in direct contact with the surface.⁶² It can be obtained in a similar way as $\phi_A(z)$; for details we refer to the original papers.^{61,62} An expression for the hydrodynamic layer thickness was given by Evers.²⁵

There is no theoretical limit for the number of different types of molecules that may be included in a system. In the present paper we apply the model to a charged diblock adsorbing onto an uncharged surface from a salt solution. The distributions of salt and solvent molecules are calculated using exactly the same equations as for the polymer. Although in the above theory section we have used A and B to denote general variables, running over all monomer types in the system, in the remainder of the article A and B are specified to be the monomer types in the anchor and buoy block of the polymer respectively.

4.3 Scaling model

We start by briefly reviewing the main arguments of Pincus⁵⁷ and Borisov et al.,^{9,10,81} which lead to an expression for the thickness of a charged brush. Subsequently, we extend this model to the adsorption of charged block copolymers, deriving scaling relations for the layer thickness and adsorbed amount.

According to Flory²⁸ a chain of N_B segments, when stretched over a distance L , stores an amount of elastic energy that is proportional to L^2/N_B . Thus the elastic free energy stored in a (charged) brush containing σ chains per unit area scales as:

$$F^{el} \propto \frac{\sigma L^2}{N_B} \quad (20)$$

The elastic force tends to decrease the layer thickness. Its opposing force is the osmotic pressure of the polymer and counterions, which may be assumed to be trapped in the brush (if $\kappa^{-1} \ll L$). For this osmotic pressure Zhulina et al.⁸¹ derived $P^{osm} \propto (\alpha_B \phi / \kappa)^2$, where ϕ is the average segment volume fraction in the brush, $\kappa \propto \sqrt{\phi_s^b}$ is the inverse Debye screening length with ϕ_s^b the salt concentration in the bulk solution, and α_B is the valency of the buoy segments. Note that P^{osm} is proportional to ϕ^2 , similar to the excluded volume interaction in a dilute *uncharged* brush (good solvent). For the derivation of scaling relations, we may assume a block profile with $\phi \propto \sigma N_B / L$, leading to the following relation for the osmotic pressure in the brush:

$$P^{osm} \propto \frac{\alpha_B^2 \sigma^2 N_B^2}{\phi_s^b L^2} \quad (21)$$

A relation for the layer thickness may be obtained from equating the elastic force $\partial F^{el} / \partial L$ to the osmotic force:

$$\frac{\partial F^{el}}{\partial L} = P^{osm} \quad (22)$$

Substitution of relations (7) and (8) into Eq. (9) leads to Eq. (6). We write this expression as

$$L \propto N(\sigma v_e)^{1/3} \quad (23)$$

where we define an effective electrostatic excluded volume parameter

$$v_e \equiv \alpha_B^2 / \phi_s^b \quad (24)$$

There is an obvious analogy with the classical result $L \propto N(\sigma v_B)^{1/3}$ for an uncharged brush with excluded volume parameter v_B .⁷⁵ Typical values of α_B and ϕ_s^b lead to values for v_e of the order of 10 or higher. Consequently, if we wish to compare a neutral brush with an equally stretched charged brush, the brush density has to be lower by a factor ~ 10 or more for the charged brush.

For the adsorption of ionic diblock copolymers, we have a similar situation. Again osmotic and elastic forces are balancing each other, but additionally the interaction of anchoring A segments with the surface comes into play. Thus we have one extra degree of freedom, σ , which is fixed in the brush model. For copolymer adsorption it can be determined from the matching equation:

$$\frac{\partial F^{ads}}{\partial \sigma} = \frac{\partial F^{el}}{\partial \sigma} \quad (25)$$

For $\chi_{AS} N_A \gg 1$, the adsorption at any finite polymer concentration may be assumed to be in the plateau region of the adsorption isotherm. The translational entropy of polymer molecules upon adsorption (i.e. the effect of the chemical potential of polymer in solution) may be neglected then. The limited validity of this approximation will be discussed in the results section. Also the two-dimensional translational entropy of the adsorbed molecule, which is smaller than that of the free molecule, is neglected.

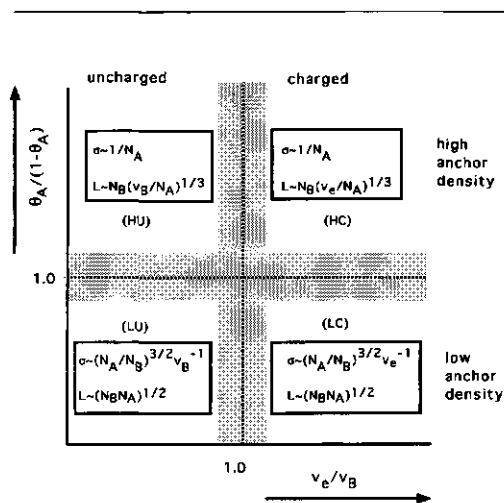


Figure 2 The four regimes for block copolymer adsorption, and the scaling relations for the chain density σ and the layer thickness L in each of them. N_A and N_B are the lengths of the anchoring and buoy block, respectively, v_B is the excluded volume parameter of uncharged B segments, and $v_e = \alpha_B^2/\phi_s^b$ is the effective excluded volume parameter of charged B segments, where α_B is the valence of B segments and ϕ_s^b is the salt solution concentration. The adsorbed amount (in equivalent monolayers) of anchoring A segments is given by θ_A .

An expression for the energy of the adsorbed anchor layer F^{ads} is not trivial, unless the density of anchor block segments is very low. In this "Low anchor density - Charged" (LC) regime, anchor blocks (consisting of N_A segments each) are adsorbed in a flat conformation and have no mutual interaction. F^{ads} may then be approximated as consisting of adsorption energy contributions only:

$$F^{ads} \propto N_A \sigma \chi_{AS} \quad (26)$$

In this equation χ_{AS} represents the Flory Hug-

gins interaction parameter between A segments and the adsorbent S . Equation (12) reads now $N_A \chi_{AS} \propto L^2/N_B$ or:

$$L \propto (N_A N_B)^{1/2} \quad (LC) \quad (27)$$

After substitution of (10) in this expression we find for the chain density:

$$\sigma \propto (N_A/N_B)^{3/2} v_e^{-1} \quad (LC) \quad (28)$$

There are a few interesting aspects in Eqs. 27 and 28. Firstly, we note that for uncharged diblock copolymers an analogous reasoning leads to the LU regime where the excluded volume parameter v_B of uncharged B segments is substituted for v_e :

$$L \propto (N_A N_B)^{1/2} \quad (LU) \quad (29)$$

$$\sigma \propto (N_A/N_B)^{3/2} v_B^{-1} \quad (LU) \quad (30)$$

Secondly, we note that these expressions are in strong contrast with the expressions found by Argillier et al.² (Eq. 5), who assume higher adsorbed amounts and consequently a completely different structure of the anchoring layer.²

Thirdly, σ turns out to be proportional to the salt concentration in the bulk through the dependence $v_e = \alpha_B^2/\phi_s^b$. We can understand this by realizing that, using the approximation of local electroneutrality,^{57,81} all electrostatic interactions in the adsorbed layer balance out exactly. Thus the only two opposing forces in the adsorption process are the adsorption energy on the one hand and the translation entropy loss of counterions on the other hand. When looked upon in this way, the process resembles a Henry-type adsorption of counterions, where the adsorbed amount is also linearly proportional to the bulk concentration of these ions.

At higher anchor density no simple relation can be derived, until the "high anchor density"

regime (HC) is reached, as described earlier by MJ for uncharged polymers. As indicated already by the name "anchor dominated regime" as used by MJ, it is expected to apply equally well to uncharged (HU) and charged (HC) polymers. Since the chain density σ is given by $\sigma \propto 1/N_A$ for HU and HC regimes alike, it would seem appropriate to merge both regimes into one (H) regime. The stretching of the B-block, however, and consequently the thickness of the brush, depends on v_e in the HC regime and to v_B in the HU regime.

The complete scaling picture is summarized in Figure 2, showing the regimes we expect as a function of $\theta_A/(1 - \theta_A)$ and of the ratio v_B/v_e . The quantity θ_A equals $N_A\sigma$, the latter ratio is determined by the buoy segment valency α_B and the salt concentration ϕ_s^b (Eq. 24). In Figure 2 the boundary between high and low coverage is taken to be located around $\theta_A/(1 - \theta_A) = 1$, and the boundary between charged and uncharged around $v_e/v_B = 1$. It should be stressed, however, that the transitions are not at all expected to be sharp, which is indicated by the shaded bands in Figure 2. As will be shown in the results section, deviations from the low coverage regime start already at $\theta_A/(1 - \theta_A) \simeq 0.1$ (i.e., above 10% of surface coverage for the anchor segments) and the scaling relations for the charged regime are found to apply if $v_e/v_B \gtrsim 10$ (e.g., $\phi_s^b < 10^{-3}$ if $\alpha_B = 0.1$, assuming $v_B \approx 1$).

4.4 Parameters

In this paper we apply the SCF model to the adsorption of a charged diblock copolymer p with an anchoring A-block and a buoy B-block with block lengths N_A and N_B , respectively, onto an uncharged surface S. The A segments are uncharged and adsorb to the surface ($\chi_{AS} = -4$).

The B segments differ from the A segments in only two aspects: they carry a charge α_{Be} and have no affinity for the surface ($\chi_{BS} = 0$). The effect of four different parameters on the adsorption is studied: the length of the A-block N_A , the length of the B-block N_B , the segment charge α_{Be} of the B-segments, and the salt concentration in the solution.

The charge of the B-block is defined by giving each B-segment a valency α_B , where α_B is constant throughout the system (acid-base equilibria are not considered). Different charge densities can be obtained by assigning a value between 0 and 1 to α_B . The charge is thus smeared out: a B-block in which 10% of the segments is charged is modelled as a B-block where every segment has a charge of 0.1e.

The salt concentration in the bulk solution, ϕ_s^b , is defined to be the bulk solution concentration of the co-ion (Co), the concentration of the counterion (Ct) being: $\phi_{Ct}^b = \phi_s^b + \phi_p^b \frac{N_B}{N_A + N_B} \alpha_B$, where ϕ_p^b is the polymer volume fraction in the bulk solution. In our computations we choose $\phi_p^b = 10^{-6}$. Salt concentrations are also given as volume fractions. The volume fraction ϕ can be converted to a molarity c through $\phi = cV_m$ where $V_m = N_A v_{cell}$ is the molar volume in litres/mole. The quantity V_{cell} follows from the lattice spacing d and the lattice type; for the hexagonal close-packed lattice³¹ used in all our calculations $V_{cell} = \frac{3}{4}\sqrt{3}d^3$. We choose $d = 0.6$ nm, giving $V_{cell} = 0.28$ nm³ and $V_m = 0.17$ l. Hence, the molarity is found from ϕ_s by multiplication by a factor of ~ 6 . A typical value $\phi_s^b = 10^{-3}$ of the volume fraction corresponds to a 6 mM salt solution.

All other parameters are kept constant throughout the paper. The solvent, water (W), is assumed to be a θ -solvent for both segment types ($\chi_{AW} = \chi_{BW} = 0.5$). For the charged B segments, this χ_{WB} parameter represents the

non-electrostatic interaction with the solvent (i.e., if there were no charge on the B segments). The *effective* solvency of charged B segments is much higher due to the electrostatic repulsion, which is automatically accounted for in the SCF model. For predicting the general behaviour of classes of polymers, we would have three typical choices for χ_{AW} and χ_{BW} : $\chi = 0$ (good solvent), $\chi = 0.5$ (bad solvent = θ -solvent), and $\chi > 0.5$ (non-solvent). In most practical polyelectrolyte/water systems, where the polymer is often insoluble when it is uncharged, the non-electrostatic interaction is unfavourable ($\chi \geq 0.5$). Therefore a choice $\chi = 0$ seems unrealistic. A very high value $\chi_{BW} \gg 0.5$, however, might lead to a first-order brush-collapse phase transition,^{9,60} a phenomenon we do not wish to investigate at present. For simplicity we prefer $\chi_{AW} = \chi_{BW} = 0.5$. We have to realize, however, that the scaling relations in section 4.3 were derived for the (unrealistic) case $\chi_{AW} = \chi_{BW} = 0$.

The solvent is modelled as a monomeric component with no charge ($\alpha_W = 0$) and a dielectric permittivity $\epsilon_W = 80\epsilon_0$. The dielectric permittivities of all other substances in the system, of which the precise values are of minor importance, are set equal to $5\epsilon_0$. Salt ions are considered to have only electrostatic interactions; consequently their χ -parameters are set equal to zero. Also χ_{AB} was chosen zero.

4.5 Results

In this section we present the results from calculations with the mean-field lattice model. First we show the volume fraction profiles for one specific set of parameters and then we focus on two more easily measurable quantities, viz. the ad-

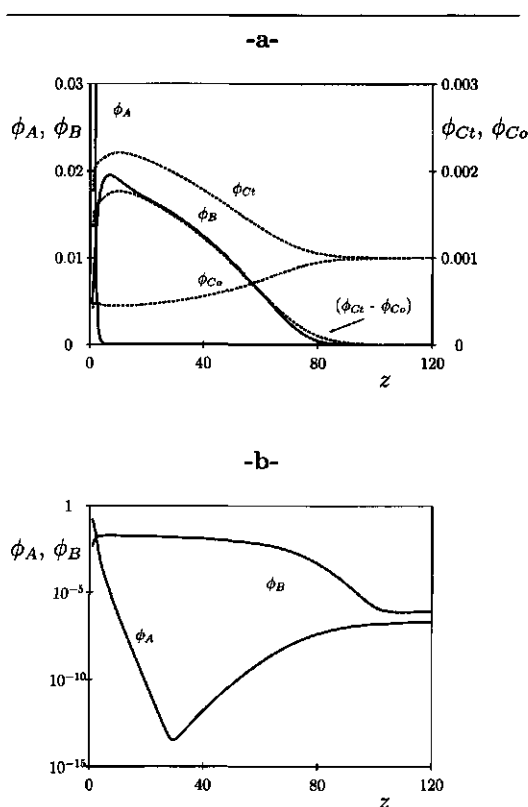


Figure 3 Volume fraction profiles for A segments and B segments (solid curves) and for coions (Co) and counterions (Ct) (dashed curves). Diagram (a) gives the profiles with a linear scale for ϕ , diagram (b) with a logarithmic scale for ϕ . Parameters: $N_A = 100$, $N_B = 400$, $\alpha_B = 0.1$, $\phi_s^b = 10^{-3}$.

sorbed amount and the layer thickness, for a range of parameters.

Profiles. In Figure 3 we show the volume fraction profiles of adsorbing A segments and of non-adsorbing B segments (with $\alpha_B = 0.1$) for a polymer $A_{100}B_{400}$ in a salt concentration of $\phi_s^b = 10^{-3}$ ($\phi_{Co}^b = 10^{-3}$, $\phi_{Ct}^b = 1.02 \times 10^{-3}$),

both on a linear scale (Figure 3a, solid curves) and on a logarithmic scale for ϕ (Figure 3b). Like for an uncharged diblock copolymer,²⁵ the A block adsorbs in a rather flat conformation on the surface, leading to an A profile that drops to a very low value after a few layers. The B profile has a maximum close to the surface and extends far into the solution (in this case ~ 80 layers): the B block is highly stretched.

In the logarithmic plot (Figure 3b) we notice that at large distances from the surface ($z > 100$) ϕ_A and ϕ_B reach constant values that equal their respective bulk volume fractions. Since the B block is four times longer than the A block, its bulk volume fraction is also four times higher. Another feature of the profiles is the fact that $\phi_A(z)$ in the "brush" region ($5 < z < 80$) is lower than ϕ_A^b . This is due to the fact that free molecules are repelled from this region by the electrostatic potential which is built up by the adsorbing chains. The adsorbed molecules have all their A segments close to the surface, and their B segments make up the brush.

The most important difference compared to the profiles of uncharged block copolymers is the density in the brush (and thus the adsorbed amount), which is lower by about a factor of 10 (in this example). Consequently, the average distance between the "anchoring" points is larger than the radius of gyration of the free polymer. In this sense the brush limit, as defined for uncharged terminally anchored chains, is not reached. Still we will consider the B layer to be a brush since the most important characteristic of a brush, i.e., the strong stretching of the chains, is retained. The stretching of the B block is due to the osmotic pressure of counterions, which increases the excluded volume interactions considerably.

Furthermore, an irregularity appears at the

maximum in the B profile, where (as seen most clearly in the linear plot, Figure 3a) an extra amount of B segments accumulates. For this effect we have the following explanation. Although to a first order approximation (i.e., the local electroneutrality concept as discussed in Section 4.3) the counterion profile is exactly proportional to the B profile, it is clear that it will never decay faster to zero than with the Debye screening length κ^{-1} , which in this case is of the order of 6 lattice layers. Thus, at the solution side of the brush, the counterion profile (or, more precisely, the difference between the profiles of counter- and coions) can almost exactly follow the slowly decaying polymer profile (Figure 3a, dashed curves, right-hand scale). Near the surface, however, $\phi_{Cl} - \phi_{Co}$ cannot follow the much sharper decrease of the B -profile. This leads to a surplus of (negative) counterion-charge in the depletion layer close to the surface, which slightly deforms the profile of positively charged B segments. A similar phenomenon is observed for nonadsorbing polyelectrolytes for which the profile shows a maximum next to the depletion layer.⁸

Adsorbed amount. We now turn to the results for the adsorbed amount and discuss them in terms of the four regimes defined in Section 4.3. First we consider the dependence on α_B , ϕ_s^b and N_B . In Figure 4a we show σ as a function of α_B on a log-log plot. All parameters in Figure 4 are the same as in Figure 3, unless mentioned otherwise. We note that σ is a continuously decreasing function of α_B . Moreover, when $\sigma < 10^{-3}$, corresponding to $\theta_A (= N_A \sigma) < 0.1$, the curve becomes a straight line, indicating a power law behavior $\sigma \propto \alpha_B^{-x}$. The exponent x in this LC-region is nearly -2, as predicted in Eq. 28: $\sigma \propto v_e^{-1} \propto \alpha_B^{-2}$.

Also in line with Eq. 28, we see in Figure

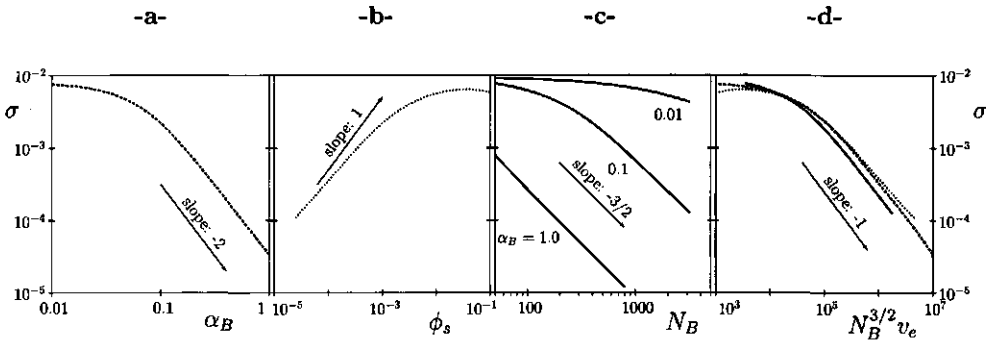


Figure 4 The chain density σ as a function of α_B (a), as a function of ϕ_s^b (b), and as a function of N_B for three different values of α_B (c). The arrows indicate slopes that correspond to the low anchor density power law behavior (Eq. 28). Diagram (d) gives the curves (a), (b), and the middle curve of (c) plotted as a function of $N_B^{3/2} v_e$. Parameters are the same as in Figure 3, unless indicated otherwise.

4b that σ is a continuously increasing function of ϕ_s , and in Figure 4c that it is a continuously decreasing function of N_B (the three curves correspond to an uncharged B block, an intermediately charged and a highly charged B block). In all cases shown, we find in the LC regime ($\theta_A < 0.1$) the predicted power law behavior. The slopes corresponding to the exponents of Eq. 28 are indicated by arrows. In Figure 4d we plot a compilation of Figures 4a, b and c ($\alpha_B = 0.1$), using $N_B^{3/2} v_e$ as the parameter along the abscissa. The curves fall essentially on one master curve, demonstrating the validity of using an effective excluded volume parameter $v_e = \alpha_B^2 / \phi_s^b$. Moreover, when $\theta_A < 0.1$ the power law Eq. 28, which was derived for the LC-regime in Section 4.3, is confirmed. Although in Figure 2 the boundary between the LC and HC regime is taken to be around $\theta_A / (1 - \theta_A) = 1$, Figure 4 clearly shows that deviations from the

LC power law start already at a five times lower anchor density. Consequently, there must be a rather wide intermediate "regime", obeying neither LC nor HC power laws.

We ascribe the small difference between the dotted curve in Figure 4d (where ϕ_s^b is varied) and the other two curves to the fact that the lattice model incorporates the volume of the salt ions. Because of this volume occupied by the ions, the effect of salt addition is expected to be weaker than on the basis of screening by point charges only.

At high θ_A we would expect to find a "high anchor density" (HC) regime, where σ is independent of N_B , α_B and ϕ_s^b . We do find a regime where the dependence is much weaker than in the LC regime, but θ_A (proportional to σ) is

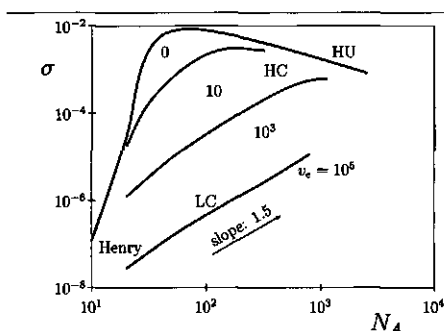


Figure 5 The chain density σ as a function of N_A for various values of the electrostatic excluded volume parameter $v_e = \alpha_B/\phi_s^b$ (indicated). For the curves for $v_e = 10$ and 10^3 the salt concentration is $\phi_s^b = 10^{-3}$, for $v_e = 10^5$ this parameter was chosen as $\phi_s^b = 10^{-5}$. Other parameters are the same as in Figure 3. The long arrow corresponds to the slope as predicted by Eq. 28 (LC), the short arrow to the slope as predicted by Eq. 1 (HU).

certainly not constant: with the molecular weights used in this study ($N < 2000$) and with the present choice of χ parameters, the HC regime can not be reached.

The effect of N_A on the adsorbed amount is somewhat more complicated. In Figure 5 we show σ as a function of N_A for different values of $v_e = \alpha_B^2/\phi_s^b$, which is a measure for the importance of electrostatic interactions. In the top curve ($v_e = 0$) we have the uncharged diblock where electrostatic interactions are absent, in the bottom curve ($v_e = 10^5$) electrostatic interactions are very strong and, consequently, the adsorbed amount is very low.

The curve for uncharged molecules shows a maximum as discussed earlier by Evers et al.²⁵ For high N_A the coverage is high and $\sigma \propto N_A^{-1}$ as predicted for the HU-regime (Eq. 1). Left of the maximum σ increases with N_A , but there is no extended region where $\sigma \propto N_A^{3/2}$ as expected according to Eq. 30 for the LU regime.

For small N_A (< 20 in this example) the dependence of σ on N_A is very strong and σ becomes too small for the brush regime to be valid. We have here essentially an unsaturated surface and approach the Henry regime where σ depends strongly on N_A because this parameter determines the adsorption energy per molecule. Moreover, in this regime the adsorbed amount (and σ) depends on the polymer solution concentration: it is far below the (pseudo) plateau of the adsorption isotherm.

The curves for the charged molecules in Figure 5 lie entirely below that of uncharged molecules due to the strong electrostatic repulsion. For $v_e = 10$ ($\alpha_B = 0.1$, $\phi_s^b = 10^{-3}$) the adsorbed amount approaches that of uncharged polymer in the Henry regime (low N_A) and in the HC regime (high N_A). In the intermediate range of N_A there is still a maximum, and to the left of it the variation of σ with N_A is not too far from the LC-prediction $\sigma \propto N_A^{3/2}$ (Eq. 28), although also here there is no extended region with a constant exponent. As v_e increases σ becomes smaller: at $v_e = 10^5$ a nearly straight line is obtained with slope 1.5-1.7, which is very close to the predicted LC power law $\sigma \propto N_A^{3/2}$ (Eq. 28).

We thus find three limiting regimes, where we can understand and predict what is happening: the Henry regime, the high coverage regime (which turns out to be relevant for uncharged molecules only (HU)), and low coverage regime (relevant for charged molecules only (LC)). However, for intermediate values of v_e ($10 \lesssim v_e \lesssim 10^3$) the regimes are not well separated, leading to wide intermediate regions where no simple power law applies.

Layer thickness. The other interesting quantity of an adsorbed layer is its thickness, for which we use two different definitions. The

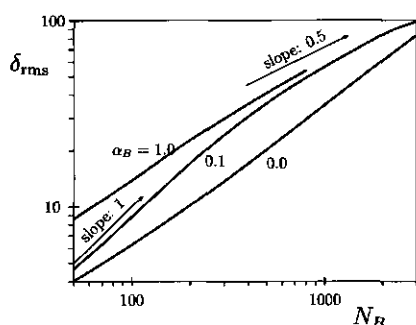


Figure 6 The root-mean-square layer thickness δ_{rms} (in lattice layers) as a function of N_B for three different values of α_B (indicated). Other parameters are the same as in Figure 3, the long arrow corresponds to the slope predicted in Eq. 27, the short arrow to the slope in Eq. 2.

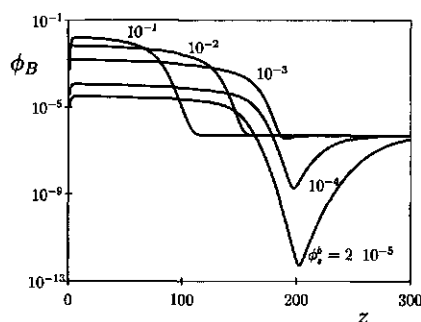


Figure 7 Volume fraction profiles for B segments on a semi-logarithmic scale for five salt concentrations (indicated). Other parameters: $N_A = 400$, $N_B = 400$, $\alpha_B = 1$.

root mean square layer thickness δ_{rms} (which is related to, e.g., the ellipsometric thickness) is weighted by the density of the brush (Eq. 19). It is therefore rather insensitive to the adsorbed amount and depends mainly on the stretching of individual chains. On the other hand the hydrodynamic layer thickness δ_h (measured by hydrodynamic methods, including dynamic light scattering) is insensitive to the brush density only when the volume fractions are well above 1%.⁶³ In our calculations, however, we find very low volume fractions and the density has a considerable effect on δ_h .

In Figure 6 we show δ_{rms} as a function of N_B for an uncharged diblock ($\alpha_B = 0$) and for two charged diblock copolymers ($\alpha_B = 0.1$, $\alpha_B = 1.0$). If we compare this figure with Figure 4c we see that in all three cases the thickness is an increasing function of the length of the B

block, while at the same time the chain density σ decreases with N_B . The charged chains are in the LC regime with $\theta_A (= N_A \sigma) \lesssim 0.1$ (compare Figure 4c) and the layer thickness for long chains more or less follows Eq. 27, predicting $L \propto N_B^{1/2}$ (the corresponding slope is indicated by the long arrow). Two other regimes can be recognized in this figure. For the lowly charged diblock copolymer we find for $N_B < 200$ a regime where δ_{rms} is almost proportional to N_B , corresponding to the HC regime where, according to Figure 2, $L \propto N_B$. At intermediate values for N_B we find a crossover to the LC regime. For the uncharged diblock copolymer at $N_B < 100$ we recognize a "mushroom" regime where B blocks do not interact and $\delta_{rms} \propto N_B^{0.5}$. At higher block lengths, chains begin to overlap and this inter-chain interaction leads to an exponent greater than $1/2$. We expect that even-

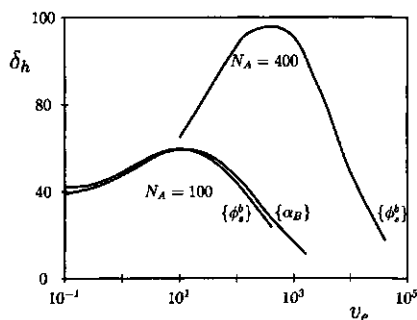


Figure 8 The hydrodynamic layer thickness (in lattice layers) as a function of $v_e = \alpha_B^2 / \phi_s^b$ at varying salt concentration (denoted by $\{\phi_s^b\}$) and at varying segment charge (denoted by $\{\alpha_B\}$). The value of N_A is indicated, N_B equals 400.

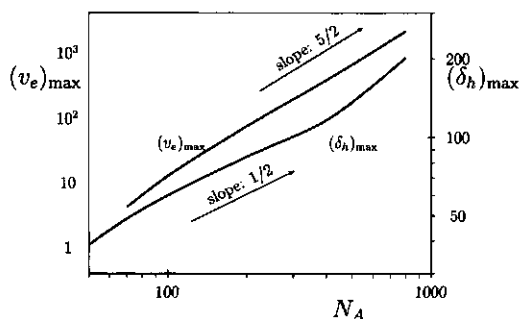


Figure 9 The location (left-hand scale, upper curve) and the height (right-hand scale, lower curve) of the maximum in a curve δ_h vs. v_e (like in Figure 8), as a function of N_A . The upper arrow corresponds to $(v_e)_{\max} \propto N_A^{5/2}$, the lower arrow to $(\delta_h)_{\max} \propto N_A^{1/2}$. Parameters: $N_B = 400$, $\phi_s^b = 10^{-3}$.

tually (at $N \gg 10,000$) the *LU* regime will be reached and the exponent will decrease again to $1/2$.

The effect of increasing the electrostatic interactions on the thickness of the layer is analyzed in Figures 7, 8 and 9. First we show in Figure 7 that, from inspection of the profiles of *B* segments, we can distinguish two kinds of behaviour. In this figure the *B* segment volume fraction profiles of an $A_{400}B_{400}$ polymer are plotted for $\alpha_B = 1.0$ at different salt concentrations. At high salt concentrations a decrease in ϕ_s leads to a stretching of the profile and a concomitant decrease in density. For $\phi_s < 10^{-3}$ we still see a decrease in density with decreasing ϕ_s , but now a minimum develops at $z \approx 200$ and the stretching of the chain (as measured by the distance between the surface and the minimum)

remains constant. These low salt concentrations correspond to the *LC* power law regime (Eq. 28). The minimum (not to be confused with the minimum in the *A* profile shown in Figure 3b) results from the interplay between electrostatic forces acting over a (variable) distance $\sim \kappa^{-1}$ and conformational restrictions (depending on the chain length).

The change in the shape of the profile makes a comparison of RMS layer thicknesses problematic. Instead, we show in Figure 8 the hydrodynamic layer thicknesses corresponding to the profiles in Figure 7. In this figure we plot δ_h as a function of the electrostatic excluded volume v_e , varying either α_B at constant salt concentration (curves marked with $\{\alpha_B\}$), or varying ϕ_s^b at constant charge density (denoted with $\{\phi_s^b\}$). The length of the *A* block is indicated, and the

other parameters are the same as in Figure 3. We find in all three cases a maximum. The increase in δ_h (at low v_e) is a result of the stretching of the chain, the decrease (at high v_e) is caused by chain desorption.

As Figure 8 illustrates, the effects of increasing α_B and decreasing ϕ_s are very similar. Using again the parameter $v_e = \alpha_B^2/\phi_s$ the two curves for $N_A = 100$ overlap nearly completely. The curve for $N_A = 400$, on the other hand, has a distinctly different shape from the curves for $N_A = 100$: it cannot be rescaled in such a way that it overlaps the other two. What we can do, however, is try to predict the location of the maximum $[(v_e)_{max}, (\delta_h)_{max}]$ in the curve. This is shown in Figure 9, where we plot $(v_e)_{max}$ (upper curve) and $(\delta_h)_{max}$ (lower curve) as a function of N_A . Since δ_h is an increasing function of v_e in the HC regime and a decreasing function of v_e in the LC regime, this maximum is located at the upper boundary of the LC regime. Thus the amount of adsorbed A segments at the maximum equals the (constant) boundary value. Using Eq. 28, which is valid in the LC regime:

$$cN_A^{5/2}N_B^{-3/2}/(v_e)_{max} = \text{constant} \quad (31)$$

This expression leads immediately to $(v_e)_{max} \propto N_A^{5/2}$ and (with Eq. 27) to $(\delta_h)_{max} \propto N_A^{0.5}$. If we compare the curves to the arrows indicating these theoretical predictions, we find indeed an approximate agreement, although two remarks must be made. Firstly, at low N_A no maximum in δ_h is found and, consequently, the curves end. This is due to the fact that (with the current selection of parameters) for $N_A < 50$ adsorbed amounts never get high enough to leave the LC regime (compare Figure 5). Consequently, the high/low coverage boundary, where the maximum is located, is never reached. Secondly, we find at high N_A

deviations that point to the onset of yet another regime. In this regime the A block is no longer flatly adsorbed, leading to an increased total thickness and a stronger dependence on N_A .

4.6 Discussion

In this paper we compare a scaling model (Section 4.3) describing the adsorption of ionic diblock copolymers with numerical calculations using a SCF model (4.2). A first conclusion of our results is that adsorbed amounts are low, typically about a factor of 10 or more lower than for uncharged block copolymers. This has a number of consequences. Firstly, the adsorbing density is lower than the overlapping density. Thus, for this type of polymers, using a reasonable value for the surface affinity, a real brush will never be formed. Still, the adsorbed layer does show brush-like behaviour, as a result of the long distance electrostatic repulsion among B segments.

Secondly, the adsorbed amounts are so low that it may be difficult to measure them experimentally. We expect that experiments aimed at measuring the layer thickness will be more successful than those measuring adsorbed amounts only.

Finally, in the SCF calculations the HC regime, where σ should be inversely proportional to N_A and independent of N_B , α_B and ϕ_s , did not show up. From theoretical considerations⁴⁷ such a regime should exist. Possibly, using a longer A block ($N_A \gg 1000$) might lead to this regime. We could not investigate this limit because of our limited computer capacity. What we do reach is a kind of inter-regime, where σ is still an increasing function of N_A and dependent on the other parameters, even though the dependencies are much weaker than in the low coverage regime.

In the LC regime, the agreement with the simple scaling predictions is surprisingly good, even when $\chi_{BW} = \chi_{AW} = 0.5$, whereas the scaling picture was based upon an athermal solvent. It turns out that the arguments in Section 4.3 leading to Eq. 28 offer a good description of the low coverage regime: with the numerical calculations, we do indeed find a power law behaviour; the exponents do not differ more than 15% from the predicted values.

A relation similar to our expression for σ in the LU regime (Eq. 30) was also derived by Marquez and Joanny⁴⁷ (MJ). For the free energy of a brush (Eq. 7) they used an alternative expression given by Alexander: $F^B \propto N_B \sigma^{11/6}$ arriving at the slightly different result $\sigma \propto (N_A/N_B)^{6/5}$ instead of $(N_A/N_B)^{3/2}$. Neither of these relations could be confirmed by the SCF calculations (Figure 4c and 5, $\alpha_B = 0$). The assumption that the translational entropy loss of polymers may be neglected is valid only when N_A is sufficiently large ($\chi_{AS} N_A > 100$). Using such a strong anchor block, a low adsorbed amount (typical for the LU regime), can only be found using an extremely long B block, typically of the order ($N_B > 10,000$). Such chain lengths are beyond our present computer capacity.

From Figure 3 we conclude that the boundary of the low coverage regime is located at an adsorbed amount for the A block around 10% of monolayer coverage. This result can be reformulated using Eq. 28 and $\theta_A = \sigma N_A$ as:

$$(N_B/N_A)^{1/2} > (c N_A v_e^{-1})^{1/3} \quad (32)$$

where $c \approx 0.28$ is a numerical constant. The equivalent relation for an uncharged polymer $(N_B/N_A)^{1/2} > (c N_A)^{1/3}$ has already been given by MJ, assuming $v_B = 1$.

In the numerical calculations we encountered one type of behaviour that is not included

in the scaling relations depicted in Figure 2. If N_A is smaller than some critical length (in our calculations around 50 segments), the adsorbed amount increases exponentially with N_A . In contrast with the other regimes mentioned so far, calculations show σ to depend on the polymer concentration here. Ultimately (for very short B-blocks), the Henry regime will be reached:

$$\sigma \propto \phi_p^b e^{a N_A / kT} \quad (33)$$

where a is a positive numerical constant related to the segmental adsorption energy. The fact that σ depends on ϕ_p^b for short chains only is in agreement with the results of MJ, who argue that the polymer solution concentration has no effect on the adsorption of diblock copolymers, as long as it is higher than (in their case an extremely low) critical concentration of the order of e^{-N_A} .

4.7 Conclusions

Charged block copolymers with an uncharged anchoring block and a charged buoy block adsorb in low amounts on an uncharged surface, forming a very extended brush of a low density. These charged block copolymers behave qualitatively similar to uncharged block copolymers. In principle, relations valid for uncharged molecules may be applied to the charged ones if an effective excluded volume parameter of charged buoy segments $v_e = \alpha_B^2 / \phi_s^b$ is substituted for v_B , the excluded volume parameter of uncharged buoy segments. Here α_B is the valency of the charged segments and ϕ_s^b the volume fraction of salt.

If the length of the buoy block is equal to or larger than the length of the anchor and carries a moderate charge, the adsorbed amount decreases even at intermediate salt concentrations

($v_e > 10$) to extremely low values. This regime can be described very accurately by a simple scaling law: the thickness of the brush (which is measurable) is proportional to the geometric mean of the two block lengths and independent of the charge on the buoy block or of the salt concentration.

If the anchor block is much longer than the buoy block, the adsorbed amount can become

of the order of one equivalent monolayer, like for adsorbing homopolymers. In this regime no simple scaling law is found. In particular, an inverse proportionality between the chain density and anchor block length N_A , as found for uncharged block copolymers, is not observed: in all relevant cases the chain density is an increasing function of N_A .

Chapter 5

Stabilization by charged diblock copolymers

5.1 Introduction

It is now well established that homopolymers can induce attractive as well as repulsive interactions in colloidal suspensions. Colloidal stability may be enhanced when thick adsorbed layers give rise to steric repulsion forces. On the other hand, attraction is found when a chain can adsorb simultaneously onto two or more particles, thereby forming so-called bridges. Different situations may be distinguished. If the two surfaces are only partially covered, bridges are easily formed and the interaction is attractive. When the surfaces are fully covered by polymer, flocculation may occur if chains can desorb quickly enough. This can only be realized when the timescale of particle encounters is longer than the average polymer desorption time. If this time is shorter than the desorption time, however, all polymers remain bound to the surface and the interaction is repulsive.

In the remainder of the text we will refer to the fast desorption as a "free" system: the polymer is free to leave the gap between the particles. To the slow desorption (or fast collision) we will refer as a "restricted" system: the polymers are not allowed to exit from the gap.

Because of the possibility of bridge formation, homopolymer adsorption is not expected to be the optimal way to stabilize colloidal systems. An obvious way to improve the stabilizing capacity of a polymer is to graft the chains chemically onto the surface. In this way high adsorbed amounts can be achieved, whilst desorption is completely prevented. If a non-adsorbing polymer is end-grafted and the grafting density is high enough, a so-called brush is formed. Such a brush could be very effective in stabilizing suspensions: bridging is impossible. The interaction between two brushes is often described by the Alexander-de Gennes theory.^{1,18,21} If the separation M between the particles is smaller than twice the thickness H of an isolated brush, the repulsive pressure $P(M)$ scales as:

$$P(M) \approx \frac{kT}{\sigma^{3/2}} \left[\left(\frac{2H}{M} \right)^{9/4} - \left(\frac{M}{2H} \right)^{3/4} \right] \quad (1)$$

where σ is the grafting density. The first term within the brackets gives the osmotic repulsion between the brush molecules, whereas the second term represents the gain in elastic energy when the brush is compressed. For $M/2H$ in the range 0.2 – 0.8, the above expression is

roughly exponential: $P(M) \sim e^{-\pi M/H}$.

Another class of promising stabilizers is formed by $A_x B_y$ diblock copolymers of which the anchor block A adsorbs to the surface, and the buoy block B extends into the solution. If the anchor is strong, desorption is virtually impossible and the properties of the adsorbed layer are similar to those of a brush of B segments. It was shown by Evers et al.²⁶ that such an $A_x B_y$ diblock copolymer can prevent flocculation also when the adsorbed molecules are in full equilibrium with dissolved ones (a free system).

In the above only short-range interactions were considered. In water-based systems, however, also long-range electrostatic interactions generally play an important role. There are two reasons to study water based systems. Firstly, for environmental reasons, in many commercial products organic solvents will have to be substituted by water in the near future. Secondly, this class of systems is relevant in a biological context, where colloidal stability is an important issue.

Recently, there has been considerably theoretical progress on the charged counterparts of two systems mentioned above: brushes, and diblock copolymer adsorption.

In a paper by Pincus,⁵⁷ which was followed by a series of papers by Zhulina et al.,^{9,10,33,79-81} the structure of charged brushes was analysed. Depending on the salt concentration ϕ_s , on the average charge α per segment, and on the anchoring density σ , at least three brush regimes may be distinguished. We may summarize the results as follows: at high ϕ_s electrostatic interactions are fully screened and the brush behaves as a neutral one, with a parabolic density profile. At low ϕ_s electrostatic interactions dominate: the profile changes from a parabola to a quadratic exponential and the thickness becomes independent of the grafting density. This

regime has been called the Osmotic Brush. At intermediate ϕ_s , the Salted Brush regime may be found, in which external salt penetrates into the brush; the profile is still parabolic and the electrostatic interactions can be incorporated into an effective exclude volume parameter:

$$v_{\text{eff}} = v + \alpha^2 / \phi_s \quad (2)$$

where v is the excluded volume parameter of uncharged segments. The brush thickness H is given by:

$$H \sim N(v_{\text{eff}}\sigma)^{1/3} \quad (3)$$

The adsorption of ionic diblock copolymers, $A_x B_y$ molecules of which the buoy block B carries a charge, is the main subject of the present contribution. Only very recently, three theoretical studies of this system were published. A first route was followed independently by two groups,^{2,76} who combined the results of Pincus on charged brushes⁵⁷ with those of Marques, Joanny and Leibler⁴⁸ on uncharged diblock copolymers adsorbing from a selective solvent. They find a regime which we will refer to as the charged brush (CB) regime, where the ionic diblock adsorbs in relatively high amounts. The A segments, being exposed to a non-solvent, form a molten layer at the surface, whereas a charged brush is formed by the B segments. A central result, as put by Wittmer et al.,⁷⁶ is that the CB regime can only be found for not too highly charged B -blocks. Specifically, if the following requirement:

$$\alpha < N_A^{4/5} N_B^{-6/5} (\gamma_A)^{6/5} (l_B/d)^{2/5} \quad (4)$$

is not fulfilled, the adsorbed amount is expected to be very low. In this equation, α is again the average charge per B segment, N_A and N_B are the respective block lengths, d is the size of one segment, l_B is the Bjerrum length (which roughly equals 7 Å in water) and γ_A gives the

free energy (expressed in units kT per area d^2) of an interface between A and solvent segments.

We followed an alternative route to analyse ionic block copolymer adsorption⁴⁰ and combined the model developed by Evers et al.²⁴ for the adsorption of uncharged diblock copolymers with the polyelectrolyte adsorption model of Böhmer et al.⁸ We studied adsorption from a non-selective solvent and concluded that low adsorbed amounts are to be expected for a wide range of parameters. At low ϕ_s or high α ($\alpha^2/\phi_s \gg v$), electrostatic interactions dominate the scaling behaviour, and the adsorbed amounts are very low indeed, below the detection limit of conventional methods. Our results are different from those of Argillier et al.² or Wittmer et al.,⁷⁶ but there is no contradiction: we chose our parameters in such a way that electrostatic interactions can be expected to be important and found low adsorbed amounts; they chose to describe a regime with high adsorbed amounts and concluded that it exists only when electrostatic interactions are not too strong.

In this paper we demonstrate that our model can also be used to study ionic block copolymers adsorbing from selective solvents. We will give a typical example of a system in the CB regime. The main goal of the paper, however, is to investigate and prove the relevance of the low coverage (LC) regime. As stated by Wittmer et al., the extremely low adsorbed amounts in this regime should, in principle, preclude a big effect on stability. We will evaluate this expectation quantitatively and calculate the interaction between two surfaces covered with ionic diblock copolymers. Specifically, we investigate the effect of N_A , N_B , α , and ϕ_s on the magnitude of the interaction and on the shape of the interaction curve.

The remaining part of this paper is organized as follows. In Section 5.2 we describe

the SCF model and we derive an analytical expression for the force profile in Section 5.3. We present results from the SCF model in Section 5.4. The main conclusions are drawn in Section 5.5.

5.2 SCF model

In the following we summarise the main points of our theory. The self-consistent-field (SCF) theory rests on four approximations: (I) The space between two flat interfaces (representing colloidal particles) is discretised using a lattice, which serves as a system of coordinates on which segments and solvent molecules are positioned. The lattice cells are organized in layers of L lattice sites, each numbered $z = 1, \dots, M$. Layers 0 and $M + 1$ are occupied by the solid substrate S . (II) Chain conformations are generated with a first order Markov approximation, equivalent to a freely jointed chain model. (III) The many-chain problem is reduced to that of a test chain in an external field generated by all the chains in the system. (IV) The system is assumed to be incompressible, which means that each layer is exactly filled by segments, solvent, or ion species: no vacancies are allowed. Below we will give a concise elaboration of these four points. For a full derivation of the model, as well as a discussion of its approximations, we refer to a recent review by Fleer et al.²⁷

In the lattice theory, molecular details on length scales smaller than monomers are neglected. All segment types are taken to be of equal size. They are indicated by the subscript A, B, \dots , representing buoy block segments, anchor block segments, water molecules, positively or negatively charged ions, and surface segments. Components are indicated by the subscript i, j, \dots . Polymeric molecules may consist of several segment types; the ranking

number of their segments is $s = 1, 2, \dots, N_i$, where N_i is the chain length of component i . The composition is very important. In this paper we discuss diblock copolymers $A_x B_y$ where segments $s = 1, \dots, x$ are of type A and segments $s = x + 1, \dots, N$ are of type B .

In a Markov approximation the segment density is found by:

$$\phi_i(z, s) = C_i \frac{G_i(z, s|1)G_i(z, s|N)}{G_i(z, s)} \quad (5)$$

Here $G_i(z, s|1)$ is the statistical weight to find in layer z the end-segment of a sequence of s segments, of which the composition is dictated by the molecular architecture of component i . Analogously, the quantity $G_i(z, s|N)$ is defined as the overall statistical weight for the chain part $s' = N, N-1, \dots, s$ to be in the system with the only constraint that segment s , the endpoint of this sequence, is in layer z . In the composition law Eq. 5 a correction for the double counting of segment s is included by the division by the free segment distribution function $G_i(z, s)$.

The normalization constant C_i is, for molecules which are in equilibrium with the bulk solution, given by $C_i = \phi_i^b/N_i$, where the bulk concentration ϕ_i^b is an input quantity. For a restricted equilibrium, when the number of molecules between the surfaces is fixed, C_i follows from the condition $\theta_i/N_i = \sum_z \phi_i(z, s)$; now θ_i is the input quantity. Defining $G_i(1|N)$ as the overall statistical weight to find a chain i in the system, according to $G_i(1|N) = \sum_z G_i(z, 1|N)$, we find: $C_i = \theta_i/[N_i G_i(1|N)]$.

The chain end distribution functions follow from a recurrence type relation which is a discrete version of the Edwards diffusion equation:

$$G_i(z, s|1) = \langle G_i(z, s-1|1) \rangle G_i(z, s) \quad (6)$$

and

$$G_i(z, s|N) = \langle G_i(z, s+1|N) \rangle G_i(z, s) \quad (7)$$

where the angular brackets indicate an averaging over the neighbors of a site in layer z . For a cubic lattice, such an average is defined by:

$$\langle f(z) \rangle = \frac{f(z-1) + 4f(z) + f(z+1)}{6} \quad (8)$$

The function $f(z)$ may be any function, such as a chain end distribution function or a volume fraction.

In Eqs. 5 - 7 the free segment distribution function $G_i(z, s)$ is a central quantity. It is defined as the Boltzmann factor of the local segment potential. When segment s of molecule i is of type A , then $G_i(z, s) = G_A(z) = \exp(-u_A(z))$. The dimensionless potential $u_A(z)$ is expressed in units of kT , as we will do for all potentials and energies from here on. Thus, Eq. 5 can be evaluated once the segment potentials are known. The key ingredient of an SCF theory is that the potentials themselves are again a function of the local densities. In this paper we include three terms in the local potential:

$$u_A(z) = u'(z) + u_A^{\text{mix}}(z) + u_A^{\text{el}}(z) \quad (9)$$

The first term originates from the incompressibility constraint and is in fact a Lagrange parameter. The second term accounts for short-range interactions:

$$u_A^{\text{mix}}(z) = \sum_B \chi_{AB} (\langle \phi_B(z) \rangle - \phi_B^b) \quad (10)$$

and the third term in Eq. 9 represents the long-range electrostatic interactions:

$$u_A^{\text{el}}(z) = \alpha_A y(z) \quad (11)$$

In Eq. 10 the summation index B runs over all segment types in the system, including the surface segments. The parameter χ_{AB} is the

familiar Flory-Huggins interaction parameter, defined as the free energy associated with the process of transferring an A segment from an A environment to a B environment. In Eq. 11, α_A represents the valency of the segment type A , and $y(z)$ is the dimensionless electrostatic potential, in units kT per elementary charge e . The reference point of the potentials (including $y(z)$) is the bulk solution. This results in a free segment distribution function $G_A(z) = 1$ in the bulk, which implies ideal chain statistics in this part of the system.

The evaluation of the local electrostatic potential, under the constraint that the system is electroneutral, can conveniently be performed once in each layer the effective charge density $\sigma(z)$ and the local dielectric permittivity are known. Both quantities are computed from the segment distributions. Obviously, the charge density can be calculated as $\sigma(z) = (e/d^2) \sum_A \alpha_A \phi_A(z)$, where e is the elementary charge, and d the lattice spacing. We approximate the dielectric permittivity in a layer by the mean field expression $\epsilon(z) = \sum_A \epsilon_A \phi_A(z)$.

Gauss' law couples the charge distribution to the distribution of electrostatic potentials. It states generally that the integral of the field strength E across a closed area surrounding a given volume equals the ratio of the charge and the dielectric constant in this volume. In the present case, we take layer z as this volume, and write E as $-(kT/d) \partial y / \partial z$, where the lattice spacing d is needed to convert the dimensionless distance z into a real distance. If ϵ is taken to be a constant, the discrete version of Gauss' law becomes:

$$\frac{y(z) - y(z-1)}{d} + \frac{y(z) - y(z+1)}{d} = \frac{e}{kT} \frac{\sigma(z)}{\epsilon} \quad (12)$$

This equation can also be written as $C\{y(z) -$

$y(z-1) + y(z) - y(z+1)\} = e\sigma(z)/kT$, where $C = \epsilon/d$ is the capacitance per unit area. If $C(z) = \epsilon(z)/d$ is a function of z , we have to modify this expression, taking into account that ϵ changes discontinuously half-way the charge planes. The average capacitance $C(z, z')$ between neighboring planes z and z' is given by:

$$C^{-1}(z, z') = \frac{1}{2} \{C^{-1}(z) + C^{-1}(z')\} \quad (13)$$

The corrected version of Eq. 12 is now:

$$C(z, z-1)\{y(z) - y(z-1)\} + C(z, z+1)\{y(z) - y(z+1)\} = \frac{e\sigma(z)}{kT} \quad (14)$$

It is easily seen that Eq. 14 reduces to Eq. 12 if C is constant.

The electroneutrality of the system is ensured by setting the field strength at the boundaries to zero:

$$\left. \frac{\partial y}{\partial z} \right|_{z=0} = \left. \frac{\partial y}{\partial z} \right|_{z=M} = 0 \quad (15)$$

We use a discrete version, analogous to Eq. 14.

All told the set of equations (5 - 15) can be solved numerically. The SCF solution is characterized by the fact that the set of local potentials $\{u_A(z)\}$ (Eqs. 9 - 11) must be consistent with $\{\phi_A(z)\}$ (Eq. 5). The solution is only accepted when the incompressibility constraint is obeyed. This solution is routinely obtained numerically; analytical solutions can, in general, not be found.

We now turn our attention to the evaluation of the free energy of interaction between two interfaces. As explained in the introduction, we distinguish full and restricted equilibrium. These two situations are controlled by the choice for C_i , as discussed below Eq. 5. The free energy of the system (in units kT per lattice site) at an interplate separation M is given

by:

$$A(M) = \sum_i \frac{\theta_i}{N_i} \ln(N_i C_i) - \sum_{z,A} \phi_A(z) \ln G_A(z) + U^{\text{mix}} + U^{\text{el}} \quad (16)$$

In Eq. 16 the last two terms represent the energetic contributions to the free energy: U^{mix} is the contact energy and U^{el} the electrostatic energy. These terms are given by:

$$U^{\text{mix}} = U^* + \frac{1}{2} \sum_{z,A,B} \chi_{AB} \langle \phi_A(z) \rangle \phi_B(z) \quad (17)$$

and

$$U^{\text{el}} = \sum_z \frac{1}{2} \sigma(z) y(z) \quad (18)$$

U^* is the mixing energy in the reference state which we take here as the pure amorphous phase of each individual component. This reference state is not important for calculating the interaction free energy. The Flory-Huggins parameter χ_{AB} is the mixing energy per $A-B$ contact.

Free molecules are in full equilibrium with the bulk solution: their chemical potential equals the chemical potential of molecules in the bulk solution:²⁴

$$\mu_j = \ln \phi_j^b + 1 - N_j \sum_i \frac{\phi_i^b}{N_i} + \frac{1}{2} N_j \sum_{A,B} \chi_{AB} (\phi_{Aj}^* - \phi_A^b) (\phi_B^b - \phi_{Bj}^*) \quad (19)$$

where ϕ_{Aj}^* is the volume fraction of segments A in the reference state of pure component j . We define the excess free energy $A^\sigma(M)$ as:

$$A^\sigma(M) = A(M) - \sum_i \frac{\theta_i \mu_i}{N_i} \quad (20)$$

where the prime indicates that the summation runs over the free components only. The interaction free energy at separation M is the difference between the excess free energy (as calculated from Eq. 20) at separation M and that at infinite separation:

$$A^{\text{int}}(M) = A^\sigma(M) - A^\sigma(\infty) \quad (21)$$

In the actual calculations this "infinite separation" is taken to be finite, but large enough so that it does not effect the results as found by Eq. 21.

5.3 Scaling

As shown before,⁴⁰ the adsorbed amount and layer thickness in the low coverage (LC) regime can be interpreted in terms of a simple analytical model: the total free energy of the system can be approximated by a summation of elastic, osmotic, and adsorption free energy contributions. We use the Gaussian approximation for the elastic free energy, which gives $\frac{\sigma H^2}{N_B}$. The osmotic contribution is the same as that for charged brushes in the Salted Brush regime, resulting in a contribution $\frac{v_{\text{eff}} \sigma^2 N_B^2}{H}$. Furthermore, it is assumed that the A block is adsorbed in a flat conformation, so that the adsorption energy is proportional to $N_A \sigma$. Hence,

$$A = \frac{\sigma H^2}{N_B} + \frac{v_{\text{eff}} \sigma^2 N_B^2}{H} - N_A \sigma \quad (22)$$

Note that the translational entropy for the adsorbed molecule is neglected. Disregarding the effects of interactions in the bulk, we set the partial derivatives $\partial A / \partial \sigma$ and $\partial A / \partial H$ to zero. This immediately leads to:

$$\sigma \sim (N_A / N_B)^{3/2} (v_{\text{eff}})^{-1} \quad (23)$$

and:

$$H \sim (N_A N_B)^{1/2} \quad (24)$$

These results were obtained already in a previous publication.⁴⁰ We now continue and derive expressions for the repulsive force between two of these adsorbed layers. If we ignore interpenetration of the two brushes, the energetic effect of squeezing the brush for $0 < M < 2H$ is simply obtained by inserting $H = M/2$ in Eq. 22. We assume restricted equilibrium and take σ to remain constant, given by eq 23. Furthermore, we leave out the adsorption energy term, which is constant anyway, and the elastic contribution since it becomes negligible with respect to the rapidly increasing osmotic pressure. The interaction sets in when the outer parts of the brushes meet, i.e., at $M = 2H$. Defining the interaction with respect to this point, the interaction energy A^{int} is found as:

$$A^{\text{int}}(M) \approx \frac{N_A^3}{N_B} (v_{\text{eff}})^{-1} (1/M - 1/2H) \quad (25)$$

This expression approaches infinity when M goes to zero. The central part of a curve $A(M)$ vs. M is again roughly exponential: if $A(M)$ is plotted on a log-lin scale, we find a straight part. The slope of this exponential part is affected only by the last factor within brackets: it is inversely proportional to the brush thickness H . The prefactor $N_A^3/(N_B v_{\text{eff}})$ determines the offset of the line and is a measure for colloidal stability. If we want to make a prediction on the stability of a suspension of spherical particles, we have to convert A^{int} , an interaction energy between two infinitely large flat surfaces, to the interaction between two spheres. A very rough estimate can be obtained from the Langbein approximation,³⁷ stating that two spheres interact with an effective contact area that scales with the radius of the particles. This leads to the following prediction: a colloidal system is stable when:

$$\frac{N_A^3}{N_B v_{\text{eff}}} \gg \frac{a}{R} \quad (26)$$

where R is the radius of the particles, v_{eff} is given by Eq. 2, and a is an undetermined numerical constant.

5.4 Results

Parameters In the calculations we use a cubic lattice, with lattice spacing $d = 0.6$ nm, leading to a number concentration of lattice sites equal to $(0.6 \times 10^{-9})^{-3} \text{m}^{-3}$, or a molar concentration of 7.7 moles/l. This value is important, since it is the concentration of pure monomers and provides the conversion factor from a volume fraction to a molarity. As explained in the introduction, we choose selective solvent conditions for the A-B diblock copolymer in the Charged Brush (CB) regime. The following values are used for the Flory-Huggins exchange parameters, with O referring to the solvent: $\chi_{AO} = 1.0$ (non-solvent) and $\chi_{BO} = 0$ (good solvent). In the Low coverage - high Charge (LC) regime the solvency has very little effect on the adsorption behaviour. As before,⁴⁰ we choose Θ conditions for both segment types in the polymer: $\chi_{AO} = \chi_{BO} = 0.5$. Furthermore, the uncharged A segments adsorb to the surface with an adsorption energy of 1 kT per segment ($\chi_s = 1$), whereas the B segments of the buoy block have no affinity for the surface. The charge of the B segments is expressed through α , the average valence of one B segment. In this way the charges on the chain are smeared out: we model a chain of which every tenth B segment is charged as a chain in which each segment has a charge of 0.1 e . The relative dielectric constant of the solvent is set to 80, that of all other species equals 5.

Volume fraction profiles Before turning to the main section of our results, i.e., the description of force curves in the LC regime, we briefly review the characteristics of the adsorbed layer in this regime. As a comparison, we also present volume fraction profiles for the CB regime.

In Figure 1 typical volume fraction profiles in the LC regime are presented for anchoring *A* and buoy-block *B* segments. The inset shows the same profiles on a logarithmic scale for ϕ . As discussed before,⁴⁰ the most prominent features of these profiles are: (I) An almost absolute confinement of *A* segments to the first layer in contact with the surface. The concentration in this layer, $\phi_A(1) = 0.038$, is outside the range plotted in Figure 1. (II) The "brush" region composed of *B* segments is extremely dilute. The density in this region is below the brush-limit for uncharged molecules, defined as the density above which *B* blocks start to overlap physically. (III) Despite the low density of the brush, the *B*-tails are highly stretched due to inter-chain electrostatic interactions.

These features may be compared with those of the adsorbed layer in the CB regime, for which two typical profiles are plotted in Figure 2. These were obtained by choosing selective-solvent conditions for the diblock copolymer, and a moderate charge ($\alpha_B = 0.2$) for the segments of the buoy block. Combined with a salt concentration $\phi_s = 10^{-2}$, this leads to rather weak electrostatic interactions. The electrostatic part ($v_{el} = \alpha^2/4\phi_s$) of the total excluded volume interaction $v_{eff} = v + v_{el}$ is only twice the uncharged contribution $v = 1/2$. The length of

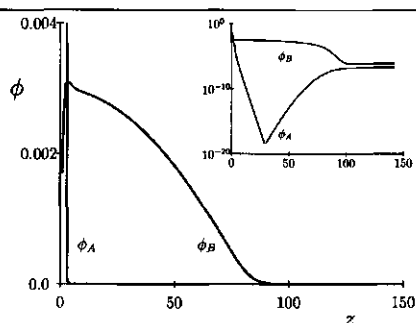


Figure 1 Volume fraction profiles of adsorbing *A* segments and buoy *B* segments in the LC regime: Low coverage – high Charge. The curves are plotted on a lin-lin, as well as on a log-lin (inset) scale. Parameters: $N_A = 100$, $N_B = 400$, $\phi_s = 10^{-2}$, $\phi_p = 10^{-6}$, $\alpha_B = 1.0$, $\chi_{AO} = \chi_{BO} = 0.5$, $\chi_s = 1$, cubic lattice with $d = 0.6$ nm at a separation $M = 300$ layers.

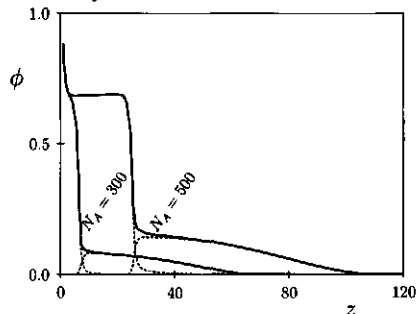


Figure 2 Volume fraction profiles in the Charged Brush regime of diblock copolymers $A_{300}B_{200}$ and $A_{500}B_{200}$ (solid curves) and the individual contributions of *A* and *B* segments (dashed curves). Parameters: $\chi_{AO} = 1.0$, $\chi_{BO} = 0.0$, $\alpha_B = 0.2$, $\phi_s = 0.01$, other parameters as in Figure 1

the buoy block equals 200, whereas two different values for the anchor block length were chosen (indicated in the figure). The solid curves in Figure 2 represent the total volume fraction of polymer; in the shape of these curves the individual contributions of the *A* and *B* block,

shown as dashed curves, can easily be recognized.

The general structure of the adsorbed layer is in agreement with the results of Wittmer and Joanny:⁷⁶ the anchoring block forms a molten layer of A segments, the density of which is of order unity. Furthermore, the segment density in the B region is clearly high enough to give rise to significant excluded volume interactions, and a true brush is formed. Obviously, since the length of the B block is constant, the area under the B profile is proportional to the number of adsorbed molecules. The figure shows it to increase with N_A , which contrasts the results of Wittmer et al. It should be noted, however, that the formation of micelles in the bulk is completely neglected in our present calculation, which precludes a full interpretation of this result.

Interaction curves in free and restricted equilibrium In the previous subsection we discussed the structure of the adsorbed layer in two regimes. From now on we focus on the LC regime, and study how the adsorbed polymer effects the interaction between two surfaces. As explained in the introduction, we distinguish two different cases. In the "full equilibrium" case the polymer is free to adjust its adsorbed amount during the approach of the two surfaces. Alternatively, in the "restricted equilibrium" we stipulate the amount of polymer between the two surfaces to remain constant.

In Figure 3 we plot the free energy of interaction A^{int} as computed from Eq. 21 for the same system as in Figure 1, both for full equilibrium (Figure 3a), and for restricted equilibrium (Figure 3b). In both figures, A^{int} is plotted on a linear scale in the main figure; the inset shows the shape of the curves on a log-lin plot.

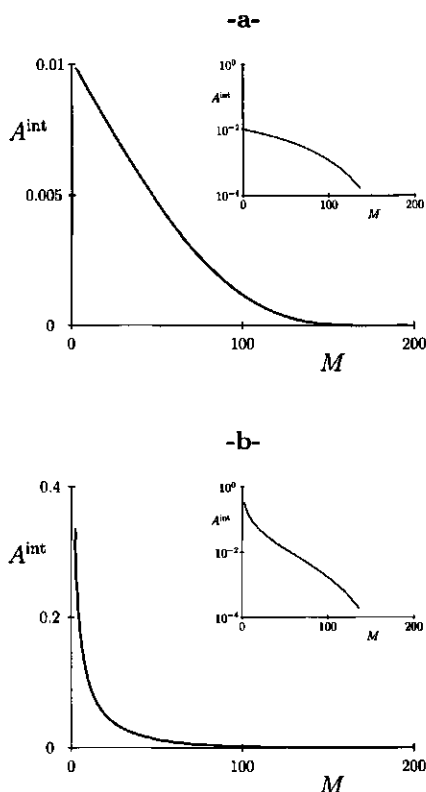


Figure 3 The free energy of interaction A^{int} (in units kT per lattice site) as a function of plate separation M , for full equilibrium (a), and restricted equilibrium (b). The insets show the same data on a logarithmic scale for A^{int} . The parameters for both (a) and (b) are the same as in Figure 1.

For restricted and free equilibrium alike, A^{int} increases monotonically with decreasing separation. Thus, the interaction between the adsorbed layers is purely repulsive, as expected. Comparing Figures 3a and 3b, we notice that there is a big difference in the magnitude of the interaction, as well as in the shape of the curve.

For the free case depicted in Figure 3a,

the repulsive interaction is necessarily lower than for the restricted case in 3b: in any non-equilibrium situation the free energy should be higher than in full equilibrium. For the present system, the two curves are almost identical down to a separation of ~ 80 layers. Upon a further decrease of M , the two curves diverge, indicating the onset of desorption in the free system. Upon a further decrease of M the repulsive interaction increases nearly linearly in the free system, whereas it increases exponentially (and much stronger) in the restricted case. Thus, the latter follows the prediction for the interaction between uncharged brushes by de Gennes (Eq. 1). In fact, all our calculations show that the free case leads to a linearly increasing repulsion, whereas for a restricted equilibrium the repulsive interaction increases exponentially. If plotted on a log-lin scale, the two cases may easily be distinguished: only the restricted interaction curve has an inflection point, whereas the slope of the curve representing full equilibrium decreases monotonically with decreasing M .

We believe the restricted case to be the more relevant one for most experimental situations. In order to obtain a more detailed insight in the interaction of two ionic block copolymer layers, we show the volume fraction profiles for three surface separations in Figure 4. In this figure the B profiles of polymer adsorbed on the left-hand-side surface (located at $z = 0$) are plotted as thick lines. The thin mirror images of these curves represent the B profiles of polymers adsorbed to the opposite surface, which is located at $M = 50, 100$, and 150 , respectively.

From a comparison of Figures 3 and 4 we observe that the repulsive interaction is negligible when the two profiles do not yet overlap, at $M \gtrsim 150$. One might expect that the electrostatic long range interactions would lead to

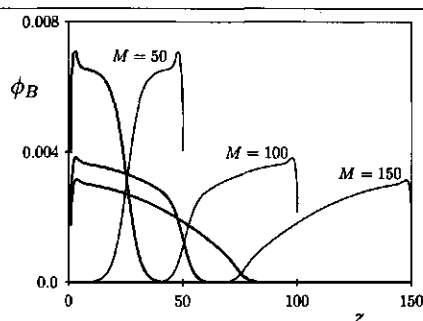


Figure 4 Volume fraction profiles of B segments at different plate separations. Thick curves give the profiles of polymers adsorbed on the lefthand surface. The thin mirror images are the profiles of polymers adsorbed onto surfaces at the indicated separation. Parameters as in Figure 1.

an onset of repulsion at separations $M > 2H$. Generally, this is expected to be the case when $\kappa^{-1} > H$: when the decay length of the electrostatic potential, i.e., the Debye screening length, is larger than the thickness of the adsorbed layer. Such a regime has been described for anchored brushes.⁵⁷ However, in our case $\kappa^{-1} \ll H$ and the repulsion sets in at $M = 2H$, as it would for an uncharged brush. This observation is related to the "local electroneutrality assumption" which applies for charged brushes in the Osmotic Brush and Salted Brush regimes:^{9,38,81} if the brush thickness is larger than the length scale on which charges are neutralized, the system behaves essentially as an uncharged system. As explained in Ref. 36, in this case the electrostatic interactions can be described as resulting from only the translational entropy of counterions. The segment density profile of the latter follows closely the profile of the charged polymer segments.

A second observation we can make from an inspection of Figure 4 is that interpenetration of the chains, although it does take place, is

not very prominent. When the two layers are brought in close proximity, they respond by changing their individual conformations, while avoiding mutual interpenetration. This feature has also been described for uncharged brushes.^{1,18,21} It does not imply that the chains would not mix favourably. The correct explanation follows from the fact that chains in an isolated brush are highly stretched (deformed). Compression of the brushes restores the chains to a more natural conformation. This is more favourable than mixing chains of opposite surfaces whereby the chains remain stretched.

The absence of interpenetration is a crucial assumption in the Alexander-deGennes model^{1,18,21} for the interaction between uncharged brushes. It allows one to express the total repulsion between two brushes as a combination of an increased osmotic force, and a decreased elastic force, leading to Eq. 1. The local electroneutrality condition permits us to use a slightly modified form of this expression for our charged system. In contrast with Eq. 1, we used the Gaussian expression for the chain elasticity; for the osmotic force we applied the expression derived for the SB regime⁸¹ to arrive at Eq. 25. Below we compare this analytical, but approximate, expression with mean field calculations.

The relation between segment density profiles and interaction curves In Figure 5 we have collected interaction curves and volume fraction profiles for a variety of systems, all of them located in the LC regime, for restricted equilibrium conditions. In the four upper frames (a-d), interaction curves are displayed on a log-lin scale. The left-hand scale gives the free energy of interaction in units kT per lattice site (Eq. 21), as in Figure 3. This may be converted to a force between two curved

surfaces using the Deryaguin approximation,¹⁴ which leads to a "force-over-radius" value, expressed in $\mu N/m$, as used for the righthand scale. Thus, the terms "interaction curve" and "force profile" have an identical meaning with respect to Figure 5; in the remainder of this text we will use both terms. Segment density profiles for the corresponding isolated brushes are presented in the four bottom figures (e-h), again on a log-lin scale. Each of the four bottom figures corresponds to its top counterpart: we consider the effect of the buoy block charge density α in Figures 5a and 5e, of the salt concentration ϕ_s in 5b and 5f, of the buoy block length N_B in 5c and 5g, and of the anchor block length N_A in 5d and 5h.

As explained in section 3, the central part of the force profile is roughly exponential. Two features of this exponential part may be distinguished: the offset, which is determined by the prefactor in Eq. 25, and the slope, which is inversely proportional to the thickness H of an isolated adsorbed layer.

We start with discussing the effect of the charge density α on the buoy block. As shown in Figure 5e, and as discussed before,⁴⁰ an increase of the charge density leads to a decreased segment density in the brush, while its thickness remains the same. We would expect also the force profile in Figure 5a to reflect this constant thickness. At first sight this does not seem to be the case. However, inspection of Eq. 25 reveals that the constancy of the brush thickness should be reflected in a constant slope of the exponential part of the force profile on a log-lin plot, its offset decreasing with $(2 \log \alpha)$. This is indeed what we see in Figure 5a.

According to Eq. 2, electrostatic effects can be accounted for in terms of an effective excluded volume parameter $v_{\text{eff}} = v + \alpha^2/4\phi_s$. Thus we expect the effect of the salt concentra-

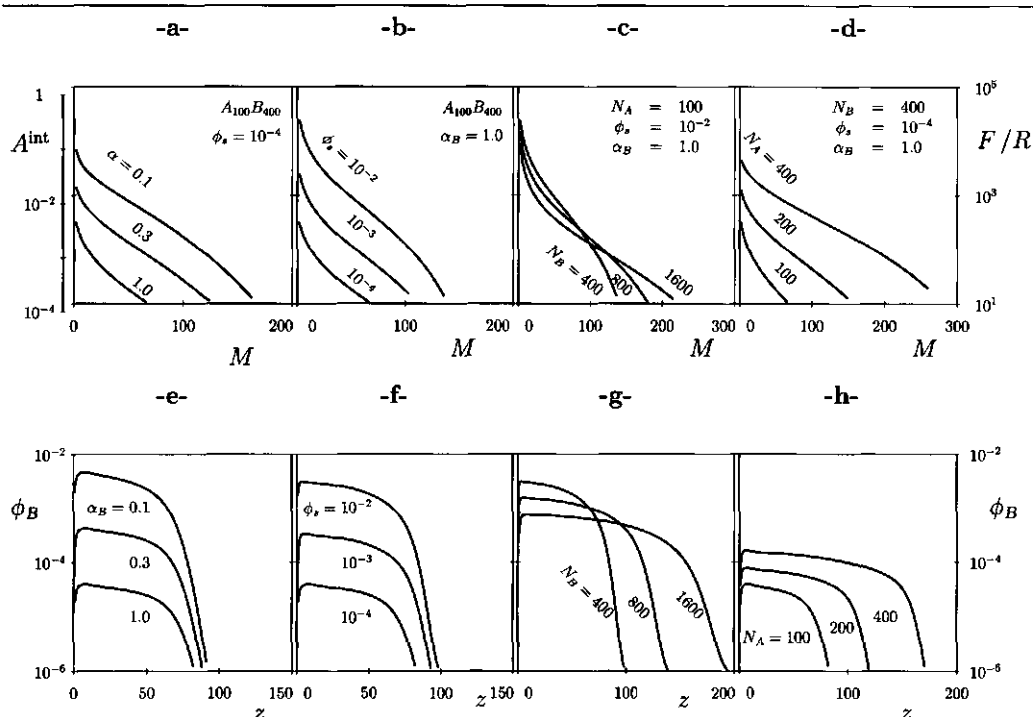


Figure 5 Interaction curves for different parameters as indicated (top row) and corresponding volume fraction profiles of the B units (bottom row). From left to right the effect of charge density (a,e); salt concentration (b,f), buoy block length (c,g), and anchor block length (d,h) is considered. Both the interaction curves and the density profiles are plotted on a log-lin scale. The interaction energy, which is calculated for the restricted case, is expressed in units kT per site (left-hand scale). The right-hand scale gives the force-over-radius in $\mu N/m$, as obtained from the Deryaguin approximation.¹⁴

tion ϕ_s , displayed in Figures 5b and f, to be opposite to that of the charge density α , discussed above. The brush density should increase linearly with the salt concentration (while the thickness remains constant again), resulting in an upward shift of the force profile. This expectation is quantitatively corroborated: a ten-fold increase in the charge density α has roughly the same effect as a hundred-fold decrease in the salt concentration ϕ_s . The slightly higher repulsion at low separations for the upper interaction curve in 5b as compared to the upper one in 5a must be attributed to the effect of the own volume of salt ions, which is neglected in the scaling analysis.

Variation of the block lengths N_A or N_B leads to a slightly more complex behaviour, due to the fact that these parameters *do* have an effect on the thickness H . A higher anchor block length causes the density as well as thickness of the adsorbed layer to increase (5h), the latter one scaling with the square root of the block length. Increasing the buoy block length also leads to a more extended layer, which is accompanied, however, by a diminished density (5g).

As mentioned above, the slope of the exponential part in the force profile should be inversely proportional to the thickness H . This is indeed confirmed by Figures 5c and 5d: the twofold increase in H observed in either Figure 5g (going from $N_B = 400$ to 1600), or in Figure 5h (going from $N_A = 100$ to 400), leads to a roughly two times lower slope in the force profiles 5c, and 5d, respectively.

The variation of the magnitude of the interaction is more interesting. From the prefactor of Eq. 25 we read that the repulsive interaction increases with N_A , and decreases with N_B . This effect is explained from the increasing and decreasing density resulting from making these blocks longer. Again, the agreement is semi-

quantitative: the effect of doubling the anchor block length, which increases $(N_A)^3$ by a factor eight, is comparable to that of a ten-fold increase in the salt concentration. The effect of the buoy block length, on the other hand, is much weaker.

The trends found for the effects of N_A and N_B are easy to understand once the density profiles are known but would perhaps be less trivially explained in the absence of this information. For example, increasing the B tail does not automatically increase stability, as one might have guessed intuitively.

In the above we presented both segment density profiles and interaction curves. The density profiles are very dilute, as anticipated. Nevertheless, the magnitude of the force is well within the range that can be measured by the surface force apparatus. Another point of discussion is whether or not the interaction force can induce colloidal stability. In general, this will depend on the particle size. The total energy of interaction between two particles should exceed their average kinetic energy which is independent of the particle size and of order 1 kT. Moreover, also the attractive Van der Waals interaction should be compensated for. At least some of the interaction energies presented in Figure 5 are, for not too small particles, high enough to ensure stability. On the other hand, the calculations show clearly that the repulsive interactions approach zero when the electrostatic interactions become too strong (high α , low ϕ_s). The exact point where a system begins to flocculate cannot be predicted with our model, since neither the particle entropy, nor the Van der Waals attraction is taken into account. Nevertheless, we can predict how this critical point scales with the four parameters we investigated, as shown in Eq. 26. We wish to stress that this expression is counter-intuitive:

although the stability arises primarily from electrostatic interactions, any increase in the relative importance of those interactions (i.e., either increasing N_B/N_A^3 or α^2/ϕ_s) leads to a *lower* stability. As shown above, this is explained by the lower adsorbed amounts resulting from stronger electrostatic interactions.

5.5 Conclusion

Using an SCF model, we calculated the interaction between two surfaces covered with an adsorbed layer of charged diblock copolymers. At low salt concentration and/or high charge density on the buoy block, the adsorbed amount for these molecules is very low. The calculations show, however, that despite this low adsorbed amount the repulsive interaction should be measurable with a surface force apparatus.

Although the Van der Waals attraction is strong at short separations, it falls off very rapidly. Therefore, the calculated repulsive interaction might induce at least kinetic stability. We estimate that it may be strong enough to do so, provided the radius of the particles is sufficiently large.

We investigated the effect of the anchor block length N_A , of the length N_B of the charged buoy block, of the charge density α on this buoy block, and of the salt concentration ϕ_s on the strength of the repulsion. Intuitively, one might expect the repulsion to increase when electrostatic interactions become more important. However, we show the effect to be exactly opposite: the repulsive interaction scales as $N_A^3\phi_s/N_B\alpha^2$. This is attributed to the fact that increasing electrostatic interactions lead to a decreased adsorbed amount.

Chapter 6

Summary

In this thesis we present Scheutjens-Fleer (SF) calculations on the adsorption of diblock copolymers. More specifically, we restrict ourselves to adsorption at uncharged surfaces, while the specific type of block copolymers we consider have one uncharged adsorbing "anchor" block and one non-adsorbing charged "buoy" block. We compare these systems with a more simple one, that of the charged brushes. A polymer brush is the structure that is formed when polymer molecules are attached by one end to a surface, with a density high enough so that the chains are obliged to stretch away from the interface. Complementary to the numerical computations, the scaling behaviour of these systems is discussed. We study the structure of the adsorbed layer, and try to answer ultimately the question what the effect of the adsorption is on colloidal stability.

In the introductory Chapter 1 we explain the most important terms and discuss the relevance of this study. Furthermore, we introduce the SF model and compare it to two other approaches: Monte Carlo and Scaling. Finally, we briefly present the available information on the two systems under consideration, and compare them to a number of related systems.

The body of this work is divided in two parts. In Chapters 2 and 3 we discuss charged

brushes, systems that are simpler than diblock copolymer adsorption, but still exhibit similar characteristics. In the subsequent two chapters we then proceed to the adsorption of diblock copolymers (Chapter 4) and its effect on colloidal stability (Chapter 5).

In Chapter 2 we present numerical results from the SF model for the structure and scaling behaviour of charged brushes and compare these with predictions of an analytical model on the same system. The relevant parameters are the chain length N , the average anchoring density σ , the average segmental charge α on the chains, and the salt concentration ϕ_s .

At high anchoring densities, three regimes of brush behaviour may be distinguished. In the salt-free case, the behaviour of the brush is dominated by electrostatic interactions if the charges are high (the so-called *Osmotic Brush*) or by non-electrostatic excluded volume interactions if the charges are low (the *quasi-Neutral Brush* regime). Upon adding salt a third regime can be found: the *Salted Brush*. The behaviour in this regime, although resulting from electrostatic interactions, is very similar to that in a neutral brush and can effectively be described using an electrostatic excluded volume parameter $v_{ei} \sim \phi_s^{-1} \alpha^2$. We find excellent agreement regarding structure as well as scaling relations

between the two theories in these three (high anchoring density) regimes. At extremely low anchoring densities, the agreement with the analytical theory is less good. This is due to the breakdown at low densities of the mean-field approximation presently used in the numerical model.

In between, at intermediate anchoring densities, the analytical theory predicts a very peculiar regime, where the thickness H scales as $H \sim N^3 \sigma^{-1} \alpha^2$. This so-called "*Pincus Brush*", named after the author who originally described it, is not recovered with the numerical theory. For the wide range of parameters used, we find the *Pincus regime* is too small to be detected. This is probably true for any reasonable set of parameters.

In Chapter 3 we consider the acid-base equilibrium of the charged brush segments, so that grafted weak polyacids may be studied. For these systems the charge of a brush segment depends on its local environment and on the pH in the solution. The scaling dependence of the thickness H on the salt concentration ϕ_s for such a brush is very different from that for a conventional charged brush with constant charge density.

At high ϕ_s the electrostatic interactions are screened and the brush behaves like a neutral one. As ϕ_s is decreased, the brush reaches the Salted Brush regime, where the charge density on the chain is independent of ϕ_s . Consequently, in this regime the polyacid brush behaves as a constant-charge brush: its thickness is an increasing function of decreasing ϕ_s . At still lower ϕ_s , a constant-charge brush enters the Osmotic Brush regime and its thickness becomes independent of ϕ_s . However, for a grafted polyacid the degree of dissociation decreases to zero with decreasing ϕ_s in this Osmotic Brush regime, until the brush is virtually uncharged.

Its thickness decreases along with the decreasing charge density. Hence, the thickness of a grafted polyacid layer passes a maximum as a function of the salt concentration. We study this maximum in the brush thickness as a function of pH and grafting density.

This scaling analysis is based on the assumption of a constant degree of dissociation throughout the brush. It is checked with the numerical SF model. The acid-base equilibrium of the brush segments is accounted for in a so-called two-state model, in which segments can either be charged or uncharged, depending on their dissociation constant and the local pH. Detailed segment density profiles are obtained that qualitatively confirm the scaling results. However, they show that polymer brushes generally have inhomogeneous degrees of dissociation. This leads to small deviations from the scaling predictions.

In Chapter 4 we proceed to the adsorption of ionic diblock copolymers. One block, the "anchor", consists of N_A uncharged adsorbing A segments, whereas the "buoy" block has N_B segments which carry a fixed charge and are non-adsorbing. Upon adsorption these molecules form a layer that resembles a brush of B segments. In contrast with the brushes discussed in the previous two chapters, the molecules in the adsorbed layer are in equilibrium with those in solution. Consequently, the chain density of the brush is not fixed; its value is determined by the dynamic equilibrium between polymer adsorption and desorption.

We interpret the results in terms of the limiting behavior in four regimes, indicated as HU, HC, LU, and LC. The system is classified to have either a high (H) or a low (L) anchor density and, irrespective of the anchor density, to be either in the charged (C) or uncharged (U) regime. We find scaling relations for the ad-

sorbed amount and layer thickness as a function of the block lengths N_A and N_B , the charge αe on the B segments, and the salt concentration ϕ_s in each of the four regimes. The scaling relations are checked using SF calculations.

The existence of two regimes for uncharged diblock copolymer adsorption has been reported previously. We argue that those HU and LU regimes are closely related to the two regimes HC and LC we find for charged molecules. Scaling relations can be translated from the uncharged to the corresponding charged regimes by replacing the excluded volume parameter v of the buoy segments by an effective electrostatic excluded volume parameter $v_e = \alpha^2/\phi_s$.

In the LC regime the chain density σ scales as $\sigma \propto (N_A/N_B)^{3/2} v_e^{-1}$ and the layer thickness H as $H \propto (N_A N_B)^{1/2}$. The latter scaling is independent of v_e . Using the SF model, these relations are found to be valid for an adsorbed amount of A segments below 10% of monolayer coverage.

In the HC regime the adsorption is dominated by the anchoring block and the scaling relation $\sigma \propto 1/N_A$ for the chain density is identical to that for uncharged molecules. The SF calculations show that this regime will not be reached in practical situations.

Finally, we address in Chapter 5 the effect of the adsorption of charged diblock copolymers on colloidal stability. Using again a sca-

ling as well as the SF approach, we focus on the LC regime and find that the adsorbed layer may cause a significant repulsive interaction between two surfaces, despite the very low adsorbed amounts. The magnitude of this repulsion is well within the range that could be measured using a surface force apparatus. Moreover, we estimate that the repulsive interaction may be strong enough to induce kinetic stability, provided the particle radius is large enough. Upon lowering the salt concentration, however, a critical concentration ϕ_s^* is reached eventually, below which the repulsion is no longer strong enough to effect colloidal stability. The scaling analysis predicts that this critical concentration scales as:

$$\phi_s^* \sim N_B \alpha^2 / R N_A^3$$

where R is the radius of the particles and the other parameters have been defined above. Thus the repulsive interaction decreases when the relative importance of charge effects increases, i.e., with decreasing salt concentration, and increasing buoy block length or buoy block charge. This counterintuitive behaviour can be explained from the effect that electrostatic interactions have on the adsorbed amount: stronger interactions lead to a lower adsorbed amount, which, in turn, leads to a weaker repulsion. The SF calculations confirm these scaling predictions.

Chapter 7

Samenvatting

In dit proefschrift bestuderen we twee gerelateerde systemen. Centraal staat de adsorptie van "anker-boei"-diblokcopolymeren met een electrostatisch geladen boeiblok. Deze moleculen adsorberen in een specifieke conformatie aan ongeladen oppervlakken: het ankerblok hecht aan het oppervlak, het boeiblok steekt in de oplossing. De uiteindelijke vraag waar het om gaat is hoe de adsorptie van dit type moleculen de kolloïdale stabiliteit kan beïnvloeden. Daartoe bestuderen we eerst de structuur van de geadsorbeerde laag.

Ter vergelijking beschouwen we ook een tweede systeem: electrostatisch geladen brushes. De oorspronkelijk uit het engels afkomstige term "brush" (borstel) wordt ook in het nederlands gebruikt om de systemen aan te duiden waarin polymeren eindstandig verankerd worden op een oppervlak, met een dichtheid die zo hoog is dat een borstelachtige structuur ontstaat. Dit systeem is relatief simpel te beschrijven, omdat het evenwicht tussen adsorptie en desorptie hier geen rol speelt. Desondanks vertoont het veel gelijkenis met de adsorptie van geladen diblokcopolymeren en is dus een goed model-systeem. De methode die we gebruiken om beide systemen te beschrijven is steeds een combinatie van twee modellen. We maken numerieke berekeningen met het model

van Scheutjens en Flee (SF-model), en rekenen zo volledig mogelijk de parameter-ruimte van een systeem door. Vervolgens vatten we de uitkomsten van deze berekeningen samen in eenvoudige analytische vergelijkingen.

In hoofdstuk 1 worden de belangrijkste termen toegelicht en bespreken we een mogelijke toepassing van het beschreven onderzoek. Verder introduceren we er het SF model, dat we onder andere vergelijken met twee andere mogelijke methodes van aanpak: schaling en Monte Carlo. Tenslotte geven we de belangrijkste eigenschappen van een aantal systemen waarvan we verwachten dat ze (soms slechts gedeeltelijk) verwant zijn aan de door ons bestudeerde systemen.

In hoofdstuk 2 presenteren we numerieke berekeningen met het SF-model voor de structuur van geladen brushes. We vergelijken deze berekeningen met voorspellingen van een analytisch model. De relevante parameters zijn de ketenlengte N , de gemiddelde verankeringsdichtheid σ , de gemiddelde segmentlading α en de zoutconcentratie ϕ_s .

Alleen als de verankeringsdichtheid hoog genoeg is, wordt een echte brush gevormd, waarin de moleculen elkaar sterk beïnvloeden en een gestrekte conformatie aannemen (in de richting loodrecht op het oppervlak). We onderschei-

den drie verschillende brush-types (regimes). In de afwezigheid van zout vinden we òf een regime dat we met een engelse naam aanduiden als *Osmotic Brush*, òf we vinden een zogenaamde *quasi Neutral Brush*. In het *Osmotic Brush*-regime worden de eigenschappen van de brush gedomineerd door de electrostatistische interacties. Dit regime wordt alleen gevonden als de ladingsdichtheid op de ketens relatief hoog is. Als dat niet het geval is vinden we het *quasi-Neutral Brush*-regime, waar het uitgesloten volume de belangrijkste rol speelt. In de aanwezigheid van zout kan een derde regime gevonden worden, het zogenaamde *Salted Brush*-regime. Het gedrag in dit regime wordt weliswaar bepaald door electrostatistische krachten, maar lijkt sterk op het gedrag van een quasi-neutral brush. Het blijkt dat de electrostatistische interacties beschreven kunnen worden in termen van een effectieve uitgesloten volume parameter $v_{el} = \phi_s^{-1} \alpha^2$.

In deze drie regimes is de overeenkomst tussen de numerieke en analytische berekeningen zeer goed. Dit geldt niet voor een aantal andere regimes waarin de verankeringsdichtheid veel lager is en de verankerde polyelectrolyten zich meer als geïsoleerde ketens gedragen. De door ons gebruikte een-dimensionale versie van het model van Scheutjens en Fleer is niet geschikt voor een beschrijving van zulke systemen. Een interessant tussengebied wordt gevormd door de brushes met een dichtheid die niet al te hoog maar ook niet al te laag is. De analytische theorie voorspelt in dit gebied een zeer opmerkelijk regime, waar de dikte H van de polymeerlaag zou moeten schalen als $H \sim N^3 \sigma^{-1} \alpha^2$. Deze zogenaamde *Pincus Brush*, genaamd naar de auteur die een dergelijk systeem als eerste beschreef, hebben we niet kunnen vinden met onze modelberekeningen. Met onze parameterkeuze blijkt dit regime te

klein te zijn om waar te nemen. Waarschijnlijk geldt dit voor elke fysisch relevante keuze van parameters.

In hoofdstuk 3 gaan we een stap verder: we bestuderen een brush van verankerde zwakke polyzuren, waartoe het effect van het zuurbase-evenwicht in het model wordt ingebracht. De lading op de verankerde ketens wordt nu beïnvloed door de electrostatistische interacties. We verwachten dat met name het effect van zout op deze systemen hierdoor sterk verschilt van het effect op de hierboven beschreven brush, waar de grootte van de lading op de ketens een vast gegeven is.

Bij hoge zoutsterkte verdwijnen alle electrostatistische interacties en gedragen beide typen zich als een ongeladen brush. Bij een verlaging van de zoutconcentratie bereiken we het *Salted Brush* regime. Ook hier gedragen beide brushes zich nog identiek: de electrostatistische potentiaal in de brush is relatief laag en de dissociatie van brush segmenten wordt er niet door beïnvloed. Het gevolg is dat voor beide types de dikte van de brush toeneemt met afnemende zoutsterkte. Echter, als de zoutsterkte laag genoeg wordt, bereiken we het *Osmotic Brush* regime. Hier is de maximale dikte bereikt en voor een brush met constante lading verandert de dikte niet meer in dit regime bij een verdere verlaging van ϕ_s . Echter, een eenvoudige analyse laat zien dat voor een verankerd polyzuur met zwakke groepen de dissociatiegraad begint af te nemen in dit regime. Daarmee neemt ook de dikte van de brush af. Dit betekent dat de dikte van een laag van verankerd poly-zuren een maximum kent als functie van de zoutconcentratie. We bestuderen de ligging en de hoogte van dit maximum als functie van de pH en de verankeringsdichtheid.

Bovenstaande analyse is gebaseerd op de aanname dat de dissociatiegraad onafhanke-

lijk is van de lokatie van segmenten in de brush. We gaan de geldigheid van deze aanname na door middel van SF-berekeningen. We gebruiken een zogenaamde "two-state"-theorie om het evenwicht tussen geladen en ongeladen brushsegmenten te modelleren. Deze theorie is oorspronkelijk ontwikkeld door Björling et al.⁷ voor een beschrijving van een brush van Poly(ethyleenoxide) polymeren. De berekende volume fractie profielen bevestigen grotendeels het hierboven beschreven gedrag. Kleine afwijkingen worden veroorzaakt door het feit dat de dissociatiegraad inderdaad niet de hele brush door constant is.

In hoofdstuk 4 beschrijven we de adsorptie van geladen diblok copolymeren. Het ankerblok bestaat uit N_A ongeladen adsorberende A-segmenten, het boeiblok heeft N_B segmenten die geen affiniteit voor het oppervlak maar wel een (vaste) lading hebben. Als deze moleculen adsorberen vormen ze een laag die veel weg heeft van een brush van geladen B-segmenten. Het verschil met de hierboven beschreven brushes is dat de moleculen in de geadsorbeerde laag in evenwicht zijn met de moleculen in de oplossing. Dit betekent dat de geadsorbeerde hoeveelheid niet een vast gegeven is, maar bepaald wordt door een dynamisch evenwicht tussen polymeeradsorptie en -desorptie.

Voor een interpretatie van de gevonden resultaten onderscheiden we vier regimes, aangeduid als HU, HC, LU and LC. De indicatie H of L heeft betrekking op de dichtheid van A-segmenten op het oppervlak: hoog (H) of laag (L). Onafhankelijk hiervan onderscheiden we geladen en ongeladen systemen, waarvoor we de letters C ("Charged") en U ("Uncharged") gebruiken. We leiden schalingsrelaties af voor de geadsorbeerde hoeveelheid en de laagdikte als functie van de lengtes van de beide blokken,

van de zoutsterkte en van de lading op het boeiblok. Deze schaalwetten worden gecontroleerd door middel van SF berekeningen.

De regimes voor hoge en lage dichtheid zijn al eerder beschreven voor ongeladen systemen. Een eenvoudige argumentatie laat zien dat de LC- en HC-regimes die wij voor geladen moleculen vinden rechtstreeks gerelateerd zijn aan deze LU- en HU-regimes. Schaalwetten voor ongeladen systemen kunnen vertaald worden van de ongeladen, naar de corresponderende geladen regimes door de uitgesloten volume parameter v van de boeibloksegmenten te vervangen door een effectieve parameter van electrostatistische origine: $v_{el} = \phi_s^{-1} \alpha^2$. In het LC regime vinden we de volgend schaalwet voor het aantal adsorberende moleculen per eenheid van oppervlakte: $\sigma \propto (N_A/N_B)^{3/2} v_{el}^{-1}$. De laagdikte H is onafhankelijk van v_{el} en schaalt als $H \propto (N_A N_B)^{1/2}$.

Uit een vergelijking met SF berekeningen blijkt dat de beide L-regimes gevonden worden wanneer het oppervlak voor minder dan 10 % bezet is met A-segmenten. Voor geladen systemen, in het LC-regime dus, is er een kwantitatieve overeenkomst tussen de schaalwetten en uitkomsten van de numerieke berekeningen.

In het HC-regime wordt de adsorptie gedomineerd door het ankerblok. De verwachte schaalwet $\sigma \propto 1/N_A$ is onafhankelijk van (de lading op) het boeiblok en dus gelijk aan die voor het HU regime. De berekeningen tonen aan dat dit regime voor een redelijke keuze van parameters niet relevant is.

Tenslotte bekijken we in hoofdstuk 5 het effect van de adsorptie van deze geladen blokcopolymeren op de kolloïdale stabiliteit. We gebruiken weer SF-berekeningen en schalingsrelaties en stellen het LC regime centraal. Ondanks de zeer lage geadsorbeerde hoeveelheid in dit regime vinden we een significante repulsie

tussen twee met geadsorbeerd polymeer bedekte oppervlakken. Deze repulsie is zeker van een grootte-orde die gemeten zou kunnen worden met een "surface-force"-apparaat. Bovendien schatten we dat de repulsie sterk genoeg zou kunnen zijn om een kolloïdaal systeem te stabiliseren, indien de kolloïdale deeltjes groot genoeg zijn. Onze analyse laat zien dat de grootte van de repulsie afneemt bij verlaging van de zoutconcentratie. We kunnen een kritische concentratie ϕ_s^* definiëren, beneden welke de repulsie te klein wordt om nog een stabiliserend effect te hebben. Deze kritische concentratie schaaft als volgt:

$$\phi_s^* \sim N_B \alpha^2 / R N_A^3$$

In deze vergelijking is R de straal van de deeltjes, de andere grootheden zijn hierboven gedefinieerd. Bij de afleiding is de Van der Waals-interactie buiten beschouwing gelaten. Uit deze vergelijking blijkt dat de stabiliserende repulsie groter is, naarmate het belang van electrostatische interacties afneemt: met toenemende zoutconcentratie, met afnemende ladingsdichtheid, en met afnemende boei-bloklengte. Dit onverwachte resultaat is een gevolg van het effect dat deze interacties hebben op de geadsorbeerde hoeveelheid: sterkere electrostatische interacties geven een lagere geadsorbeerde hoeveelheid, en daardoor indirect een zwakkere repulsie. De SF berekeningen bevestigen dit beeld.

Appendix A

Parabolic potential profile

The potential profile of a brush has to a good approximation a parabolic shape. This was derived in 1975 by Semenov⁶⁴ for the case of brushes without solvent and extended to include solvent independently by Milner et al.⁵¹ and Skvortsov et al.⁶⁵ We use the assumption of a parabolic potential profile in Chapter 2. In this appendix we present a straightforward derivation along the lines of a publication by Zhulina et al.⁸²

Let us consider a brush of chains with chain length N , anchoring density σ . We split the free energy of a brush molecule in two parts: the stretching free energy F_{str} and concentration dependent contributions F_{conc} :

$$F = F_{\text{str}} + F_{\text{conc}} \quad (1)$$

To keep the treatment general, this latter contribution will not be specified. Using the Gaussian expression $\int_0^{x'} \frac{3}{2} E(x, x') dx'$ for the elastic free energy of one conformation, the total elastic free energy for the brush is given by:

$$F_{\text{str}} = \frac{3}{2} \int_0^H g(x') dx' \int_0^{x'} E(x, x') dx \quad (2)$$

where $g(x')$ is the probability density to find the chain end at position $x = x'$. The quantity $E(x, x')$ gives the average stretching at position x of chains having their end-segment at x' . Note

that expression 2 implies a simplification: all chain conformations having an endsegment at $x = x'$ are replaced by one most probable conformation. This approximation is reasonably good for highly stretched chains: $x' \gg a\sqrt{N}$, where N is the total number of chain segments.

We have to minimize this free energy, taking into account the following two boundary conditions:

$$\int_0^{x'} \frac{dx}{E(x, x')} = N \quad \text{for all } 0 < x' < H \quad (3)$$

and

$$\int_0^H \phi(x) dx = N/\sigma \quad (4)$$

Only conformations that have their endsegment at a distance $x' > x$ can contribute to the segment density $\phi(x)$ at distance x . This contribution is inversely proportional to the stretching of the conformation at x . Thus, $\phi(x)$ is given by:

$$\phi(x) = \frac{1}{\sigma} \int_x^H \frac{g(x') dx'}{E(x, x')} \quad (5)$$

We use the Lagrange method of undetermined multipliers λ_1 and $\lambda_2(x')$ and define a

new function that is to be minimized:

$$\begin{aligned} \mathcal{Y} = & F_{\text{str}} + F_{\text{conc}} + \lambda_1 \int_0^H \phi(x) dx \\ & + \int_0^H \lambda_2(x') dx' \int_0^{x'} \frac{dx}{E(x, x')} \end{aligned} \quad (6)$$

We obtain from Eqn. 5:

$$\begin{aligned} \delta\phi(x) = & \frac{1}{\sigma} \int_x^H dx' \left\{ \frac{\delta g(x')}{E(x, x')} \times \right. \\ & \left. \frac{-g(x')\delta E(x, x')}{E(x, x')^2} \right\} \end{aligned} \quad (7)$$

which can be used to calculate the variation of \mathcal{Y} with respect to the unknown functions $E(x, x')$ and $g(x')$. The terms in δE and δg are collected separately:

$$\begin{aligned} \delta\mathcal{Y} = & \int_0^H \int_0^{x'} dx' dx \delta E \left\{ \right. \\ & \frac{3}{2} g(x') - \frac{\lambda_2(x')}{E(x, x')} \\ & \left. - \left(\frac{df(x)}{d\phi(x)} + \lambda_1 \right) \frac{g(x')}{E(x, x')^2} \right\} \\ & + \int_0^{x'} dx' \delta g \left\{ \int_0^{x'} \left[\frac{3E(x, x')}{2} + \right. \right. \\ & \left. \left. \frac{1}{E(x, x')} \left(\frac{df(x)}{d\phi(x)} + \lambda_1 \right) \right] dx \right\} \end{aligned} \quad (8)$$

Both terms must be zero for all δE and δg , which for the δE term leads to:

$$\frac{3}{2} E^2(x, x') = \left[\frac{df(x)}{d\phi(x)} + \lambda_1 \right] + \frac{\lambda_2(x')}{g(x')} \quad (9)$$

Realizing that the stretching $E(x, x')$ is zero at the endsegment, i.e., for any $x = x'$, we can rewrite the two terms on the righthand side of Eqn. 9 using an unknown function $\Psi(x)$ as:

$$E^2(x, x') = \Psi(x') - \Psi(x) \quad (10)$$

If we substitute this equation once again in the boundary condition 3 we arrive at a standard integral equation for $\Psi(x)$, the solution of which can easily be checked to be:

$$\Psi(x) = \frac{\pi^2}{4N^2} x^2 \quad (11)$$

Combination of this result with Eqn. 9 leads to:

$$\Psi(x) = \left[\frac{df(x)}{d\phi(x)} + \lambda_1 \right] = \frac{\pi^2}{4N^2} x^2 \quad (12)$$

or, introducing a new constant Λ :

$$\frac{df(\phi(x))}{d\phi(x)} = \Lambda - \frac{3}{8N^2} x^2 \quad (13)$$

Q.E.D.

Appendix B

Twostate model for monomers

The statistical thermodynamics of chain molecules in inhomogeneous systems, wherein the polymer units can be in more than one state, was derived by Björling et al.,^{7,45} and simplified considerably by Hurter et al.³⁶ In both cases, this so-called two-state model was used to describe the behaviour of poly(ethylene oxide) polymers in water. We apply it to the acid-base equilibrium of (weak) polyacids. In this appendix we present yet another (even more simple) derivation of the two-state model.

We consider the following system: a monomer (of type *A*) that can be in either one of two states (*A1* and *A2*). For this case, Eqs. 1 and 5 in Chapter 3 can easily be obtained, as we show below. The key point in our derivation is that we may view upon this system in two ways.

(1) We may treat the monomer *A* as one type of monomer (that can be in several states). In this case we may define the (free) segment weighting factor as:

$$\begin{aligned} G_A(z) &= \phi_A(z) / \phi_A^b \\ &= \sum_{j=1,2} \phi_{Aj}(z) / \sum_{j=1,2} \phi_{Aj}^b \end{aligned} \quad (1)$$

where $\phi(z)$ denotes a concentration in layer *z*

and ϕ^b denotes a bulk concentration.

(2) Alternatively, we may consider the states *A1* and *A2* to be individual molecules that happen to be in chemical equilibrium (*A1* \rightleftharpoons *A2*). Then we define individual weighting factors as:

$$G_{Aj}(z) = \phi_{Aj}(z) / \phi_{Aj}^b \quad (2)$$

with *j* = 1, 2. Inserting Eq. 2 in 1 and introducing the degree of dissociation α_i^b in the bulk solution:

$$\alpha_{Ai}^b = \phi_{Ai}^b / \sum_{j=1,2} \phi_{Aj}^b \quad (3)$$

we immediately arrive at:

$$G_A(z) = \sum_{j=1,2} \alpha_{Aj}^b G_{Aj}(z) \quad (4)$$

and the degree of dissociation in layer *z* (defined analogously to α^b) is found as:

$$\alpha_{Aj}(z) = \phi_{Aj}^b G_{Aj}(z) / G_A(z) \quad (5)$$

It is easy to see that Eq. 4 is a general form of Eq. 1 as used in the chapter 3. Similarly, Eq. 5 can easily be brought in the form of Eq. 5. Both equations are identical to the ones derived by Hurter for polymeric systems.

Appendix C

curriculum vitae

De auteur van dit proefschrift werd geboren op 20 februari 1965 te Groningen. Aldaar behaalde hij in 1983 het VWO diploma aan het Praedinius Gymnasium en begon vervolgens in Wageningen aan de studie Moleculaire Wetenschappen. Deze studie sloot hij in 1989 cum laude af met hoofdvakken in de biochemie, moleculaire biologie en fysische chemie, alsmede een stage aan de Eidgenössische Technische Hochschule in Zürich.

Het in dit proefschrift beschreven onderzoek werd uitgevoerd bij de vakgroep Fysische en Kolloïdchemie van de Landbouwuniversiteit Wageningen in de jaren 1989 tot en met 1993. Vanaf januari 1994 is de auteur als postdoc in dienst van de Pittsburgh University in de Verenigde Staten.

Bibliography

- 1 Alexander, S.; *J. Phys. (Paris)* **1977**, 38, 983.
- 2 Argillier, J. F.; Tirrell, M. *Theor. Chim. Acta* **1992**, 82, 343.
- 3 Barneveld, P. A.; Hesselink, D. E.; Leermakers, F. A. M.; Scheutjens, J. M. H. M.; Lyklema, J. *Langmuir* submitted.
- 4 Bell, G. M.; Levine, S. in: *Chemical Physics of Ionic Solutions*, B. E. Conway et al., Eds, Wiley, NY, 1966.
- 5 Beltran, S.; Hooper, H. H.; Blanch, H. W.; Prausnitz, J. M. *Macromolecules* **1991**, 24, 3178.
- 6 Birshtein, T. M.; Liatskaya, Yu. V.; Zhulina, E. B. *Polymer* **1990**, 31, 2185.
- 7 Björling, M.; Linse, P.; Karlström, G. *J. Phys. Chem.* **1990**, 94, 471.
- 8 Böhmer, M. R.; Evers, O. A.; Scheutjens, J. M. H. M. *Macromolecules* **1990**, 23, 2288.
- 9 Borisov, O. V.; Birshtein, T. M.; Zhulina, E. B. *J. Phys. II* **1991**, 1, 521.
- 10 Borisov, O. V.; Priamitsin, V. A.; Birshtein, T. M. *Macromolecules* **1991**, 24, 140.
- 11 Borisov, O. V.; Zhulina, E. B.; Birshtein, T. M. **preprint**.
- 12 Cohen Stuart, M. A.; *J. Phys. France* **1988**, 49, 1001.
- 13 Cosgrove, T.; Heath, T.; van Lent, B.; Leermakers, F. A. M.; Scheutjens, J. M. H. M. *Macromolecules* **1987**, 20, 1692.
- 14 Deryaguin, B. V.; *Kolloid Zeits.* **1934**, 69, 155.
- 15 Dan, N.; Tirrell, M. *Macromolecules* **1993**, 26, 4310.
- 16 Dijt J. C. **1993** PhD Thesis, Wageningen Agricultural University.
- 17 Edwards, S. F. *Proc. Phys. Soc.* **1966**, 88, 265.
- 18 de Gennes, P. G.; *C. R. Acad. Sci (Paris)* **1985**, 300, 839.

- 19 de Gennes, P. G.; *Macromolecules* **1981**, *14*, 1637.
- 20 de Gennes, P. G.; *Macromolecules* **1982**, *15*, 492.
- 21 de Gennes, P. G.; *Adv. Colloid Interface Sci.* **1987**, *27*, 189.
- 22 de Gennes, P. G. *Scaling Concepts in Polymer Physics*, Cornell University Press, Ithaca, NY 1985 (2nd ed.).
- 23 Eisenriegler, E.; Kremer, K.; Binder, K. *J. Chem. Phys.* **1983**, *77*, 6296.
- 24 Evers, O. A.; Scheutjens, J. M. H. M.; Fleer, G. J. *J. Chem. Soc. Faraday Trans.* **1990**, *86*, 1333.
- 25 Evers, O. A.; Fleer, G. J.; Scheutjens, J. M. H. M.; Lyklema, J. *J. Colloid Interface Sci.* **1986**, *111*, 446.
- 26 Evers, O. A.; Scheutjens, J. M. H. M.; Fleer, G. J. *Macromolecules* **1991** *24*, 5558.
- 27 Fleer, G. J.; Cohen Stuart, M. A.; Scheutjens, J. M. H. M.; Cosgrove, T.; Vincent, B. *Polymers at Interfaces*; Chapman & Hall, 1993.
- 28 Flory, P. J. *Principles of Polymer Chemistry*; Cornell University Press: Ithaca, NY, 1953.
- 29 Halperin, A.; Tirrell, M.; Lodge, T. P. *Adv. Polym. Sci.* **1991**, *100*, 31.
- 30 Guenoun, P.; Tirrell, M. In preparation.
- 31 Hart-Davis, A. *Solids: an Introduction*; McGraw-Hill, 1975.
- 32 Hesselink, F. Th. *J. Colloid Interface Sci.* **1977**, *60*, 448.
- 33 see e.g., Hill, T. L. *Introduction to Statistical Thermodynamics*; Addison-Wesley, 1962.
- 34 Hirz, S. **1987** M.Sc. Thesis, University of Minnesota.
- 35 Huinink, H. **1992** M.Sc. Thesis, Wageningen Agricultural University.
- 36 Hurter, P. N.; Scheutjens, J. M. H. M.; Hatton, T. A.; *Macromolecules* **1993**, *26*, 5030.
- 37 Israelachvili, J. *Intermolecular & surface forces*; Academic Press, 1991 (2nd ed.).
- 38 Israëls, R.; Fleer, G. J.; Leermakers, F. A. M.; Zhulina, E. B. *Macromolecules* submitted (chapter 2 of this thesis).
- 39 Israëls, R.; Fleer, G. J.; Leermakers, F. A. M.; *Macromolecules* submitted (chapter 3 of this thesis).

- 40 Israëls, R.; Scheutjens, J. M. H. M.; Fleer, G. J.; *Macromolecules* **1993**, 26, 5404 (chapter 4 of this thesis).
- 41 Kawaguchi, M.; Takahashi, A. *Adv. Colloid Interface Sci.* **1992**, 37, 219.
- 42 Killman, E.; Maier, H.; Baker, J. A. *Colloids Surf.* **1988**, 31, 51.
- 43 Lal M.; CLark, A. T. *J. Chem. Soc. Faraday Trans. II* **1982**, 74, 1857.
- 44 Ligoure, C.; Leibler, L. *J. Phys. France* **1990**, 51, 1313.
- 45 Linse, P.; Björling M.; *Macromolecules* **1991**, 24, 6700.
- 46 Luckham, P. F.; Ansarifar, A. *Chem. Eng. Sci.* **1987**, 42, 799.
- 47 Marques, C. M.; Joanny, J. F. *Macromolecules* **1989**, 22, 1454.
- 48 Marques, C. M.; Joanny, J. F.; Leibler, L. *Macromolecules* **1988**, 21, 1051.
- 49 Metropolis, N.; Rosenbluth, A. W.; Rosenbluth, M. N.; Teller, A. H. *J. Chem. Phys.* **1953**, 24, 1087.
- 50 Miklavic, S. J.; Marcelja, S. J. *J. Phys. Chem.* **1988**, 92, 6718.
- 51 Milner, S. T.; Witten, T. A.; Cates, M. E. *Macromolecules* **1988**, 21, 2610.
- 52 Milner, S. T. *Science* **1991**, 251, 905.
- 53 Misra, S.; Varanasi, S.; Varanasi, P. P. *Macromolecules* **1989**, 22, 4173.
- 54 Munch, M. R.; Gast, A. P. *Macromolecules* **1988**, 21, 1366.
- 55 Munch, M. R.; Gast, A. P. *Macromolecules* **1990**, 23, 2313.
- 56 Muthukumar, M. *J. Chem. Phys.* **1987**, 86, 7230.
- 57 Pincus, P. *Macromolecules* **1991**, 24, 2912.
- 58 Podgornik, R. *J. Phys. Chem.* **1992**, 96, 884.
- 59 Ploehn, H. J.; Russel, W. B.; Hall, C. K. *Macromolecules* **1988**, 21, 1075; Ploehn, H. J.; Russel, W. B. *Macromolecules* **1989**, 22, 266.
- 60 Ross, R. S.; Pincus, P. *Macromolecules* **1990**, 25, 2177.
- 61 Scheutjens, J. M. H. M.; Fleer, G. J. *J. Phys. Chem.* **1979**, 83, 1619.
- 62 Scheutjens, J. M. H. M.; Fleer, G. J. *J. Phys. Chem.* **1983**, 84, 178.
- 63 Scheutjens, J. M. H. M.; Fleer, G. J.; Cohen Stuart M. A. *Colloids Surf.* **1986**, 21, 285.

- 64 Semenov, A. N. *Sov. Phys. JETP* **1975**, 61, 733.
- 65 Skvortsov, A. M.; Parlushvov, I. V.; Gorbunov, A. A.; Zhulina, E. B.; Priamitsyn, V. A.; Borisov, O. V. *Polymer Science USSR* **1988**, 30, 1706.
- 66 Stamm, M.; Dorgan, J. R. *Colloids Surf.* submitted.
- 67 Taunton, H. J.; Toprakcioglu, C.; Klein, J. *Macromolecules* **1988**, 21, 3333.
- 68 Van Lent, B.; Scheutjens, J. M. H. M. *J. Phys. Chem.* **1990**, 94, 5033.
- 69 Varoqui R.; *J. Physique* **1993**, 7, 1097.
- 70 Van de Steeg, H. G. M.; Cohen Stuart, M. A.; de Keizer, A.; Bijsterbosch, B. H. *Langmuir* **1992**, 8, 2538.
- 71 Van der Linden, C. C.; Leermakers, F. A. M. *Macromolecules* **1992**, 25, 3449.
- 72 Van der Schee, H. A.; Lyklema, J. *J. Phys. Chem.* **1984**, 88, 6661.
- 73 Whitmore, M. D.; Noolandi, J. *Macromolecules* **1990**, 23, 3321.
- 74 Wiegel, F. W.; *J. Phys. A* **1977**, 10, 299.
- 75 Wijmans, C. M.; Scheutjens, J. M. H. M.; Zhulina, E. B. *Macromolecules* **1992**, 25, 2657.
- 76 Wittmer, J.; Joanny, J. F. *Macromolecules* **1993**, 26, 2691.
- 77 Zhan, Y.; Mattice, L. W.; Napper, D. H. *Macromolecules* **1993**, 98, 7502.
- 78 Zhan, Y.; Mattice, L. W.; Napper, D. H. *Macromolecules* **1993**, 98, 7508.
- 79 Zhulina, E. B.; Borisov, O. V.; Priamitsin, V. A. *J. Colloid Interface Sci.* **1990**, 137, 495.
- 80 Zhulina, E. B.; Borisov, O. V.; Priamitsin, V. A.; Birshtein, T. M. *Macromolecules* **1991**, 24, 140.
- 81 Zhulina, E. B.; Birshtein, T. M.; Borisov, O. V. *J. Phys. II* **1992**, 2, 63.
- 82 Zhulina, E. B.; Borisov, O. V.; Brombacher, L. *Macromolecules* **1991**, 24, 4679.

Dankwoord

De oplettende lezer heeft mogelijk bemerkt dat dit proefschrift geen dankwoord bevat. Daarvoor zijn verschillende redenen. De meest direkte aanleiding was tijdgebrek; de meer fundamentele was enige persoonlijke aversie tegen dankwoorden, waarin volgens traditie op humoristische wijze zoveel mogelijk begeleiders, vrienden, kennissen, ooms en tantes worden opgesomd. Soms wordt de indruk gewekt dat een dankwoord meer dient om de populariteit van de auteur te illustreren, dan om aan te geven wie werkelijk aan het proefschrift hebben bijgedragen. Wat ik me niet heb gerealiseerd is, dat nu de indruk gewekt wordt dat ik alles alleen heb gedaan, dat ik geen waardering heb voor mijn beide promotoren, of dat ik een onplezierige tijd gehad zou hebben op de vakgroep fysische en kolloidchemie. Dat is geenszins het geval; vandaar dit dankwoord – alsnog.

Degenen die op meest direkte wijze aan dit proefschrift hebben bijgedragen zijn mijn beide promotoren Gerard Fler en Frans Leermakers, en de co-auteurs van respectievelijk hoofdstuk 2 en 4: Katja Zhulina en Jan Scheutjens. Zo verschillend als deze vier mensen zijn, hebben ze een ding gemeenschappelijk: het zijn allen zeer goede wetenschappers. Ik ben er trots op met hen samengewerkt te hebben en wil ze vanaf deze plaats bedanken voor hun bijdrage aan dit proefschrift.

Daarnaast is er een groot aantal mensen die mij de afgelopen vier jaar direct dan wel indirect hebben gesteund bij het doen van dit onderzoek. In mijn hokjesgeest wil ik ze nog wel eens indelen in: **polymeerclan**: Cas, Katinka, Klaas, Peter, Chris, **mede-AIO's**: Bert, Martin, en de rest **TAP-ers**: Willy, Ronald, Ben, Puc en Max, **wetenschappers**: Luuk, Martien, Herman, **relatiedeskundigen**: Jose, Janet, Marc, Frans **gasten**: Andrew, Patricia, Yannis, Arpad, Curro, Mikael, Raquel **hardlopers**: Leontine, Ronald, Marcel, Bernard, Jennifer, Carl, Ingrid, Maud, Fred, Maarten, Foske, Erik, Hans, Jan, Jelle **Groningers**: Frank, Gijs, **familie**: Jette, Harry, Trijn, Kees, Han, Peter, mijn ouders **huisgenoten**: Michiel, Milou, Sasja, Edward “**dat conservatieve clubje**”: Huub, Jacques, Dick, Aad **SNP-ers**: Femmy, Gerard, Anneke, Paul, Lisenka **Trans-ers**: Frans, Siewert **copel-fans**: Nynke, Ali, Douglas, Wilco, Henk, Heleen ...

..., maar zo'n indeling is kunstmatig: het zijn vaak de TAP-ers die de wetenschap bedrijven; de hardlopgroep is soms vertrouwder dan familie, terwijl de familie verbazend hard kan lopen; de CL-ers bleken progressiever dan menig mede-AIO; de drie wetenschappers hebben elk zeer verhelderende ideeën over relaties en als je lang genoeg in de kelder “woont” worden de clan-leden als huisgenoten. Wat een copel-fan al niet vermag, zal ik hier maar niet beschrijven.

Gelukkig zijn ze niet allen grote wetenschappers, maar trots ben ik zeker wel op ze. Ook hen wil ik graag bedanken voor hun steun in de afgelopen vier jaar.